Urban Biosolar Roof Design at Scale:
Assessing Their Benefits and Trade-offs

by

Yeongseo Yu

A dissertation accepted and approved in partial fulfillment of the

requirements for the degree of

Doctor of Philosophy

in Landscape Architecture

Dissertation Committee:

Dr. Yekang Ko, Chair

Dr. Rob Ribe, Core Member

Dr. Junhak Lee, Core Member

Dr. Ihab Elzeyadi, Institutional Representative

University of Oregon

Spring 2025

© 2025 Yeongseo Yu

DISSERTATION ABSTRACT

Yeongseo Yu

Doctor of Philosophy in Landscape Architecture

Title: Urban Biosolar Roof Design at Scale: Assessing Their Benefits and Trade-Offs

This dissertation investigates the environmental performance of biosolar roofs—rooftop systems that integrate vegetation with photovoltaic (PV) panels—to assess their multifunctional benefits and trade-offs across diverse climatic contexts. While biosolar roofs offer the potential for microclimate cooling, stormwater retention, renewable energy production, and building energy savings, their real-world performance remains underexplored and highly dependent on localized design conditions. This research combines computational modeling, parametric simulations, and empirical field validation to quantify how design configurations and climate shape biosolar roof effectiveness.

Chapter 1 provides a comprehensive review of existing literature, highlighting the environmental potential and practical barriers of biosolar roofs, along with critical gaps in standardized design guidance. Chapter 2 evaluates the influence of key design parameters—PV density, height, layout, and planting density—on cooling performance using ENVI-met simulations, supported by field-measured temperature data. apter 3 expands the analysis across three contrasting U.S. climate zones—Eugene (marine), Tucson (hot-arid), and Buffalo (cold-humid)—and compares biosolar roofs with conventional green, PV, and concrete roofs through four key environmental performances: cooling effect, stormwater runoff decrease, solar energy yield potential, and building energy load decrease. Chapter 4 presents field experiments that validate prior simulations, further revealing the significance of shade conditions in improving

soil moisture persistence and surface temperature, while also confirming modest PV yield improvements.

The findings emphasize that biosolar roofs do not passively provide multifunctional benefits—they require deliberate, climate-responsive design to reconcile trade-offs between energy, water, and thermal performance. Design strategies must be tailored to rooftop accessibility, functional goals, and regional environmental constraints. This dissertation ultimately proposes a flexible design framework for adaptive rooftop infrastructure, by integrating simulation and validation. In doing so, it contributes to the broader landscape architecture discourse on urban multifunctionality, resource-efficient land use, and climate-adaptive urban design.

ACKNOWLEDGMENTS

I would like to express my sincere and deep appreciation to my committee members—Dr. Yekang Ko, Dr. Rob Ribe, Dr. Junhak Lee, and Dr. Ihab Elzeyadi—for their invaluable guidance and support throughout the completion of this dissertation. I am especially grateful to Dr. Yekang Ko and Dr. Junhak Lee for their unwavering mentorship, insightful feedback, and encouragement at every stage of my research journey. Their guidance has been truly instrumental in shaping the direction and success of this work. My sincere thanks also go to Dr. Josh Peterson of the UO Solar Monitoring Lab and Mac's Batteries for their consultation and technical advice on solar system installations. I am also thankful to Dr. Makena Coffman, Prof. Lopez Buson, and Prof Eischeid for their mentorship and thoughtful guidance during a pivotal time in my research, especially in helping me refine and focus my topic. Special thanks to Feni, Tamana, Joseph, Dr. Anupam Satumane, and Dr. Dimas Wicaksono, for their friendship and emotional support throughout this journey. This research was made possible with funding from the University of Oregon David S. Easly Memorial Award.

For my father, mother, sister, and my love Yeji

TABLE OF CONTENTS

Chapter Page

TABLE OF CONTENTS 7
LIST OF FIGURES 10
LIST OF TABLES 12
DISSERTATION OVERVIEW 13
Introduction of Dissertation 13
Dissertation Framework 15
Dissertation documentation 17
References 18
CHAPTER 1 20
COMPREHENSIVE REVIEW OF BIOSOLAR ROOF'S BENEFITS, CHALLENGES, AND DESIGN PARAMETERS 20
1.Introduction 20
1.1 Background 20
1.2 Purpose 21
2. Method 22
3. Reviews 22
3.1 Typology of Biosolar Roofs 22
3.2 Multifunctional Benefits of Biosolar Roofs 23
3.3 Challenges of Biosolar Roof Implementation 28
3.3 Design Parameters for The Biosolar Roof Design 31
4. Discussion 37
4.1 Place-based Biosolar Design Considering Trade-offs 37
4.2 Potential to Being Coupled with Urban Agriculture as Rooftop Agrivoltaics 38
4.3 East–West Bifacial PV: a Strategy to Flatten the *Duck Curve* 38
4.4 Enhancing Understanding at the City-wide Scale 39
4.5 Criteria for Biosolar roof Placement 40
5. Conclusion 43
References 44
CHAPTER 2 48
EXPLORING IDEAL DESIGN PARAMETERS TO ENHANCE COOLING PERFORMANCE OF BIOSOLAR ROOF 48
1. Introduction 48
1.1 Background and Purpose 48

1.2 Research Frameworks....51
2. Methods....53
2.1. Biosolar Roof Modeling and Composing 28 Different Design Scenarios....53
2.2 ENVI-met Simulation....54
2.3 Simulation Data Processing and Visualization....55
2.4 Validating the Simulation Results with Field Measurements....55
3. Results....57
3.1 Air Temperature Simulation Results at Near-Vegetation Under PV Array....57
3.2 Air Temperature Simulation Results Above PV Panel....62
3.3 Simulation Validation....64
4. Discussion....67
5. Conclusion....71
References....72
CHAPTER 3....74
COMPARATIVE ENVIRONMENTAL PERFORMANCE OF BIOSOLAR ROOF ACROSS THREE CLIMATE ZONES....74
1.Introduction....74
1.1. Background....74
1.2 Research Framework....76
2. Methodology....78
2.1 ENVI-met Simulation for Evaluating Cooling Performance....78
2.2 SWMM Simulation for Evaluating Stormwater Management....81
2.3 Solar Energy Potential Evaluation....86
2.4 OpenStudio-EnergyPlus for Evaluating the Impact on Building Energy Load....88
3. Results....92
3.1 Impact on Cooling Performance (ENVI-met Results)....92
3.2 Impact on Stormwater Management (SWMM Results)....95
3.3 Impact on Solar Energy Yields (Rhino-Grasshopper Analysis Results)....97
4. Discussion....104
5. Conclusion....108
References....110
CHAPTER 4....113
EMPIRICAL AND COMPARATIVE PERFORMANCE ASSESSMENT FOR BIOSOLAR ROOF....113
1. Introduction....113
2. Method....115
2.1 Field Experiment Design and Installation....115
2.2 Experiment Modules Description....115

2.3 Environmental Sensors Installations and Data Collection 118
2.4 Off-grid Solar PV System and Real-time Solar PV Yield Monitoring System 119
2.5 Bifacial East-West Facing Solar PV Installations 121
3. Results 122
3.1 Near-Surface Air Temperature Comparisons in Autumn 122
3.2 Near-Surface Air Temperature Comparisons in Spring 124
3.3 Soil Moisture Dynamics Under Dry Conditions and Manual Irrigation 125
3.4 Soil Moisture Dynamics During Rainy Season 126
3.5 Solar Yield Comparison Between the Biosolar Roof and The PV Roof Modules 128
3.6 Bifacial Solar Yield Enhancement on Reflective Film 129
3.7 Comparison of Surface Temperature Across the Modules 131
4. Discussion 133
5. Conclusion 139
References 140
DISSERTATION CONCLUSION 142

LIST OF FIGURES

Figure Page

Figure 1.1 Dissertation framework 16
Figure 1.2 Schematic drawings for possible installation of biosolar roof, adopted from Zluwa and Pitha (2021) and modified 23
Figure 2.1 Chapter 2 research framework....52
Figure 2.2 Validation process....56
Figure 2.3 Boxplot comparison of near-vegetation air temperature under different PV heights (1.0 m–3.0 m) 57
Figure 2.4 Boxplot comparison of near-vegetation air temperature under full (100%) versus half (50%) PV coverage conditions 58
Figure 2.5 Boxplot comparison of biosolar roof designs (Designs 8A–10C) with varying vegetation heights under consistent PV settings (full PV density and fixed configuration) 59
Figure 2.6 Comparison of additional design variations (Designs 20–28) that combine changes in vegetation height with different PV array configurations (row spacing and East–West orientation) under half PV density 60
Figure 2.7 Boxplot comparison of near-vegetation air temperature under various PV configuration patterns....61
Figure 2.8 Potential air temperature tendency comparison over PV array....62
Figure 2.9 Heatmaps in both under and above PV array 63
Figure 2.10 Comparison between field measurement and ENVI-met simulation and their statistical significance. Red lines mean field measured temperature, blue line means the predicted temperature 66
Figure 3.1 Rooftop energy balance comparison between plain rooftop, PV rooftop, and biosolar roof (adopted from Ogali & Sailor (2016) and improved)....76
Figure 3.2 Chapter 3 research framework....77
Figure 3.3 Subcatchment Configuration for Biosolar Roof in SWMM Simulation....83
Figure 3.4 Four modules' settings in OpenStudio....90
Figure 3.5 Annual Average of Potential Air Temperature Differences (°C) at Two Heights by Roof Typology and Climate Zone; positive value means cooler than concrete roof; negative value means hotter than concrete roof....93
Figure 3.6 Example snapshots of ENVI-met simulations at near-vegetation level in Eugene, OR (z=0.25m)....94
Figure 3.7 Simulated stormwater runoff reduction by vegetated roofs (green/biosolar) under 24-hour rain events in Eugene, Tucson, and Buffalo. 97
Figure 3.8 Annual simulated AC energy yield (kWh) for half PV density of Biosolar roof and PV roof across climatic zones (Full PV density is added for the comparison with Half density)....98
Figure 3.9 The boxplot of cooling load (kBtu/h) by roof typology across three climate zones 101
Figure 3.10 The boxplot of heating load (kBtu/h) by roof typology across three climate zones 103
Figure 4.1 Top: experimental setup on the rooftop (south-facing biosolar roof, PV roof, and green roof modules); bottom: East-West facing bifacial biosolar and PV roof setup on the rooftops 117
Figure 4.2 Weight estimation and environmental sensor installation scheme (air temperature sensors at 0.25m) ...118

Figure 4.3 Off-grid solar PV system composition 120
Figure 4.4 Internet of Things (IoT) Realtime monitoring system with Raspberry Pi and BMS 120
Figure 4.5 Bifacial East-West facing solar PV experiment setup over vegetation (Left) and high-albedo reflective film (Right) 121
Figure 4.6 Comparison of air temperature across different roof types (autumn); Colored boxes represent the inter-quartile range (IQR, 25th–75th percentiles). 123
Figure 4.7 Near-surface air temperature comparisons in spring 124
Figure 4.8 (Top) Boxplot comparing soil moisture levels among biosolar shaded, biosolar non-shaded, and green roof modules, during manual irrigation periods. (Bottom) Line graph showing temporal soil moisture dynamics, during manual irrigation periods. 126
Figure 4.9 (Top) Boxplot comparing soil moisture levels among Biosolar shaded, Biosolar non-shaded, and green roof modules during rainy season. (Bottom) Line graph showing temporal soil moisture dynamics, during rainy season. 127
Figure 4.10 A box plot comparing PV energy yield between biosolar and standard PV roofs (unit: Watts)..... 128
Figure 4.11 Left: Boxplot showing higher mean yield for bifacial PV on reflective film (78.2 W) than on concrete (68.1 W). Right**:** Diurnal yield curve indicating consistently greater performance on reflective film, especially during early and late hours..... 130
Figure 4.12 (Top) Diurnal surface temperature patterns and daily maxima across five roof types (Apr 12–16, 2025), and (Bottom) Box plot comparison of surface temperature distributions. 132
Figure 4.13 (Right) Advantage of bifacial panels in mitigating snow accumulation compared to tilted modules, and (Left) Scatter plot showing daily accumulated solar yield for bifacial PV panels (east–west facing) and conventional PV panels (south-facing tilt)..... 135

LIST OF TABLES

Table Page

Table 1.1 Overview of biosolar roof studies with reported PV height and performance outcomes 32
Table 1.2 Preferred plant characteristics against PV shade 35
Table 1.3 Biosolar roof plant species choice evaluation criteria (Lamnatou & Chemisana, 2015).....36
Table 2.1 28 Different biosolar roof design scenarios.....53
Table 3.1 ENVI-met 3D model configurations 79
Table 3.2 EPA-SWMM analysis process at each model.....84
Table 3.3 EPA-SWMM green roof configuration: input settings and simulation parameters (Hörnschemeyer et al., 2023; Huber et al., 1975; Jeffers et al., 2022; Tolderlund, 2010).....84
Table 3.4 Comparison of Solar Potential Estimation Software 87
Table 3.5 The common parameter settings in OpenStudio across four modules.....90
Table 3.6 Additional parameter settings for green roof and biosolar roof in OpenStudio.....90
Table 3.7 Cooling and heating design loads and reduction rates (%) of alternative roof types under peak design conditions compared to conventional concrete roof sacross three climate zones (Eugene, OR; Tucson, AZ; Buffalo, NY).....100
Table 3.8 Monthly cooling load trends and distribution by roof typology across three climate zones 101
Table 3.9 Monthly heating load trends and distribution by roof typology across three climate zones.....103
Table 4.1 Summary of experimental module configurations 116
Table 4.2 Paired t-test results comparing PV energy yield between biosolar and standard PV roofs 129
T**able 4.3** Comparison of bifacial PV solar yield on concrete vs high-reflective film surfaces 130

DISSERTATION OVERVIEW

Introduction of Dissertation

Cities now face unprecedented extreme weather events, which increasingly exceed the adaptive capacity of urban infrastructures. To address both climate change mitigation and adaptation, scholars have applied the urban metabolism lens to streamline the flows of energy, materials, and other resources in an urban area (Kennedy et al., 2011; Newell & Cousins, 2015). This perspective has brought more attention to the Food–Water–Energy nexus (Arthur et al., 2019; Barron-Gafford et al., 2019) and multifunctional land-use (Hernandez et al., 2015, 2019; Kammen & Sunter, 2016; Lovell & Johnston, 2009; Lovell & Taylor, 2013), all of which emphasize transforming limited urban spaces into more efficient and multifunctional places with less conflicts (Kammen & Sunter, 2016; Kennedy et al., 2011).

Urban rooftops are a representative example showing a land-use tension among sustainable roofing solutions, covered with environment-friendly materials such as vegetation for stormwater management (Green roofs), solar photovoltaics for energy production (PV roofs), and light-colored coating that lowers the roof surface temperature (Cool roofs). Each roofing solution has been implemented in a mono-functional manner, and such single-purposed deployments limit multifunctional land use and may hinder synergistic and climate-resilient urban strategies (Kammen & Sunter, 2016).

Biosolar roofs, which stack solar photovoltaic (PV) panels over a vegetated substrate, offer a powerful multifunctional strategy (Shafique et al., 2020). By collocating PV array and green roof, they can deliver clean energy and ecosystem services within the same footprint (Abdalazeem et al., 2022; Talwar et al., 2023). Moreover, this colocation generates synergistic gains—plants help moderate panel temperatures and retain soil moisture longer, which in turn enhances PV efficiency (Jahanfar et al., 2020; Schindler et al., 2018; Shafique et al., 2020). These combined benefits not only can enhance rooftop productivity but

also support the shift to decentralized energy systems, thereby strengthening local grid resilience (Hoicka et al., 2021; Shafique et al., 2020).

The biosolar roof also aligns with recent discourses regarding place-based renewable energy landscape approach : an approach designed to minimize ecological disruption and deliver more community-centered benefits, rather than merely focusing on technical metrics (Jasiūnas et al., 2021; Parra et al., 2017; Pasqualetti & Stremke, 2018; Stremke & Koh, 2011; Wolsink, 2018). Reflecting on this, a recent article (Pevzner et al., 2021) published in the Landscape Architecture Magazine and an white paper (O'Neil et al., 2022) from the Pacific Northwest National Laboratory outlined rational a multifunctional and place-based renewable energy landscapes conceptual framework, proposing six key pathways for advancing place-based renewable energy landscapes: *Multifunctionality, Decentralization, Generating Local Value, Natural Capital, Resilience to Climate Disruption, and Energy Justice*. Among these pathways, biosolar roofs could embody multifunctionality and demonstrate how renewable energy and vegetation can be seamlessly integrated to create resilient, productive urban landscapes.

Although biosolar roofs promise to deliver the dual benefits of renewable energy and green-infrastructure, our quantitative understanding of their performance remains limited (Abdalazeem et al., 2022; Shafique et al., 2020). To date, only a few biosolar roof studies have measured its environmental impacts (Bousselot et al., 2017; Jahanfar et al., 2019). No research has yet provided a side-by-side quantitative comparison of biosolar roof performance with conventional alternatives— standalone concrete, green, and PV roofs. This lack of comparative knowledge makes it difficult for urban policymakers to establish effective climate action goals and make informed decisions about urban rooftop strategies.

Therefore, in my dissertation, I evaluate the environmental performance of biosolar roofs by benchmarking them against three conventional alternatives—concrete roofs, green roofs, and PV roofs. To capture both climatic influences and design-parameter effects, I developed idealized models in Rhino–Grasshopper and ran simulations using ENVI-Met (CFD), EPA-SWMM (stormwater), and OpenStudio–

EnergyPlus (building energy) across three distinct climate datasets. I also validate these simulations with field experiments on the Pacific Hall rooftop at the University of Oregon, where I collected air and surface temperature, humidity, runoff, and energy-yield data. By integrating empirical measurements with simulation results, I quantify how biosolar roofs influence energy generation, microclimate regulation, stormwater retention, and overall building energy load. I demonstrate their multifunctional advantages over single-purpose roof systems. Finally, I translate these insights into evidence-based biosolar roof design guidelines and policy recommendations for planners, designers and policymakers. In doing so, I aim to support more effective climate change mitigation and adaptation strategies in the era of climate emergency.

Dissertation Framework

In my work, I propose comprehensive research of benefits and tradeoffs of urban biosolar roofs. First, I conduct a comprehensive literature review to organize its benefits and challenges and identify key design parameters of biosolar roofs. Next, I evaluate how key design parameters influence the biosolar roof's environmental performance, focusing on cooling performance for mitigating urban heat island effects. Third, I perform a comparative analysis of biosolar roofs against conventional roofing solutions—concrete, green, and PV roofs—across three distinct climate zones. I assess how their environmental performance varies with three different climatic conditions: Marine, Hot-dry, and Cool-humid. Finally, as a field experiment, I designed four scaled-down concrete roof, green roof, PV roof, and biosolar roof, and collect their environmental data to validate the simulation results and reveal real-world performance differences among the four roofing strategies.

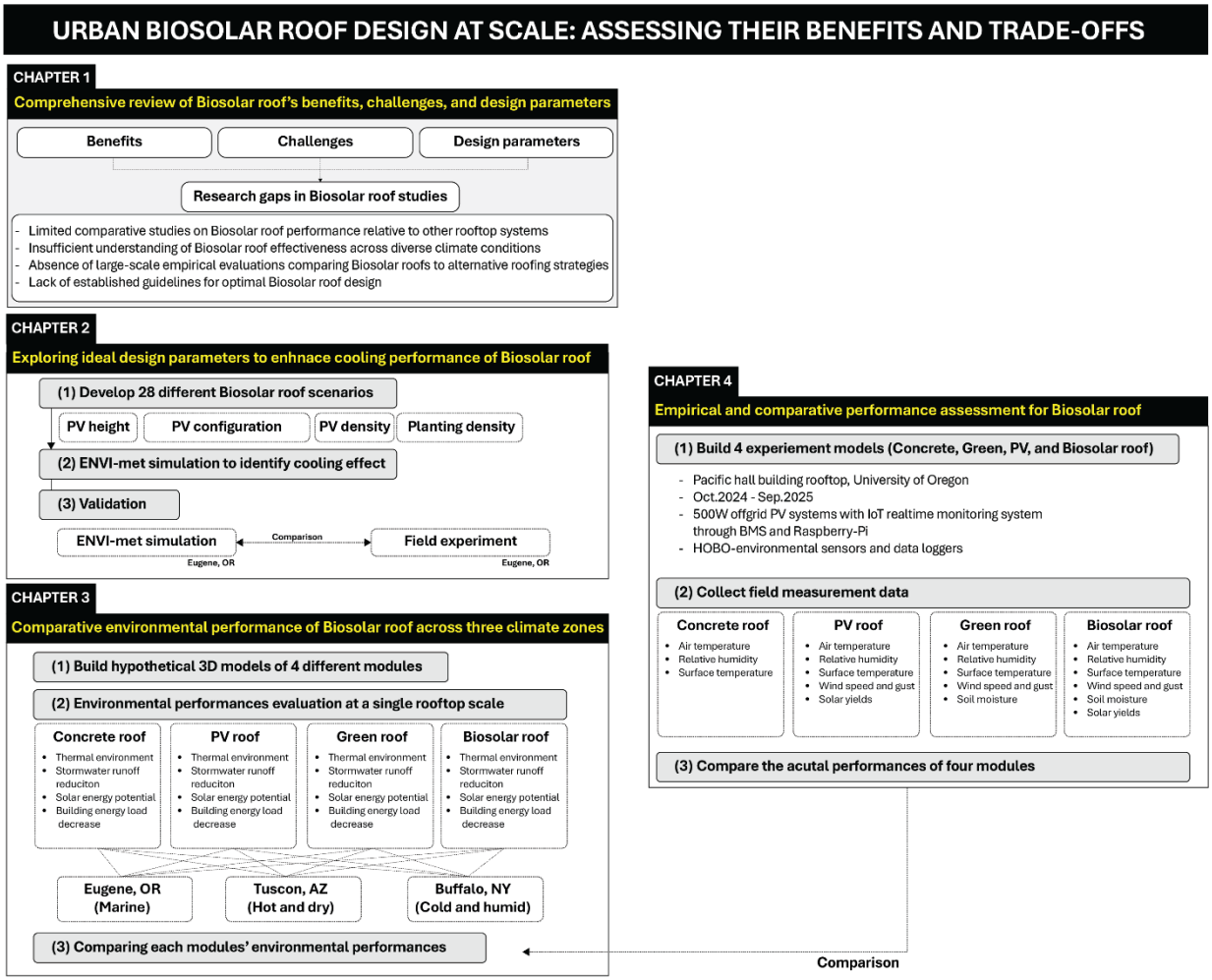


Figure 1.1 Dissertation framework

Dissertation documentation

This dissertation is organized into four chapters.

- Chapter 1 comprehensive review biosolar roofs' benefits, challenges, key design parameters, and reveal existing knowledge gaps.
- Chapter 2 studies the impact of varying design settings on biosolar roof cooling performance.
- Chapter 3 broadly evaluate multiple co-benefits of biosolar roof—(1) microclimate cooling, (2) stormwater management, (3) solar energy yield, and (4) building energy savings—using relevant simulation tools, under three climate scenarios. It then quantitatively compares the overall performance of biosolar roofs against single-function alternatives: concrete, green, and PV roofs.
- Chapter 4 presents a field experiment with four scaled-down roof modules—concrete, green, PV, and biosolar—both to validate our simulations against on-site environmental measurements and to quantify their real-world performance differences.

References

Abdalazeem, M. E., Hassan, H., Asawa, T., & Mahmoud, H. (2022). Review on integrated photovoltaic-green roof solutions on urban and energy-efficient buildings in hot climate. *Sustainable Cities and Society*, *82*(April), 103919. https://doi.org/10.1016/j.scs.2022.103919

Arthur, M., Liu, G., Hao, Y., Zhang, L., Liang, S., Asamoah, E. F., & Lombardi, G. V. (2019). Urban food-energy-water nexus indicators: A review. *Resources, Conservation and Recycling*, *151*(September), 104481. https://doi.org/10.1016/j.resconrec.2019.104481

Barron-Gafford, G. A., Pavao-Zuckerman, M. A., Minor, R. L., Sutter, L. F., Barnett-Moreno, I., Blackett, D. T., Thompson, M., Dimond, K., Gerlak, A. K., Nabhan, G. P., & Macknick, J. E. (2019). Agrivoltaics provide mutual benefits across the food–energy–water nexus in drylands. *Nature Sustainability*, *2*(9), 848–855. https://doi.org/10.1038/s41893-019-0364-5

Bousselot, J., Slabe, T., Klett, J., & Koski, R. (2017). Photovoltaic Array Influences the Growth of Green Roof Plants. *Journal of Living Architecture*, *4*(3), 9–18. https://doi.org/10.46534/jliv.2017.04.03.009

Hernandez, R. R., Armstrong, A., Burney, J., Ryan, G., Moore-O'Leary, K., Diédhiou, I., Grodsky, S. M., Saul-Gershenz, L., Davis, R., Macknick, J., Mulvaney, D., Heath, G. A., Easter, S. B., Hoffacker, M. K., Allen, M. F., & Kammen, D. M. (2019). Techno–ecological synergies of solar energy for global sustainability. *Nature Sustainability*, *2*(7), 560–568. https://doi.org/10.1038/s41893-019-0309-z

Hernandez, R. R., Hoffacker, M. K., & Field, C. B. (2015). Efficient use of land to meet sustainable energy needs. *Nature Climate Change*, *5*(4), 353–358. https://doi.org/10.1038/nclimate2556

Hoicka, C. E., Conroy, J., & Berka, A. L. (2021). Reconfiguring actors and infrastructure in city renewable energy transitions: A regional perspective. *Energy Policy*, *158*. https://doi.org/10.1016/J.ENPOL.2021.112544

Jahanfar, A., Drake, J., Gharabaghi, B., & Sleep, B. (2020). An experimental and modeling study of evapotranspiration from integrated green roof photovoltaic systems. *Ecological Engineering*, *152*. https://doi.org/10.1016/J.ECOLENG.2020.105767

Jahanfar, A., Drake, J., Sleep, B., & Margolis, L. (2019). Evaluating the shading effect of photovoltaic panels on green roof discharge reduction and plant growth. *Journal of Hydrology*, *568*(October 2018), 919–928. https://doi.org/10.1016/j.jhydrol.2018.11.019

Jasiūnas, J., Lund, P. D., & Mikkola, J. (2021). Energy system resilience – A review. *Renewable and Sustainable Energy Reviews*, *150*(July). https://doi.org/10.1016/j.rser.2021.111476

Kammen, D. M., & Sunter, D. A. (2016). City-integrated renewable energy for urban sustainability. *Science*, *352*(6288), 922–928. https://doi.org/10.1126/science.aad9302

Kennedy, C., Pincetl, S., & Bunje, P. (2011). The study of urban metabolism and its applications to urban planning and design. *Environmental Pollution*, *159*(8–9), 1965–1973. https://doi.org/10.1016/j.envpol.2010.10.022

Lovell, S. T., & Johnston, D. M. (2009). Creating multifunctional landscapes: How can the field of

ecology inform the design of the landscape? *Frontiers in Ecology and the Environment*, *7*(4), 212–220. https://doi.org/10.1890/070178

Lovell, S. T., & Taylor, J. R. (2013). Supplying urban ecosystem services through multifunctional green infrastructure in the United States. *Landscape Ecology*, *28*(8), 1447–1463. https://doi.org/10.1007/s10980-013-9912-y

Newell, J. P., & Cousins, J. J. (2015). The boundaries of urban metabolism: Towards a political–industrial ecology. *Progress in Human Geography*, *39*(6), 702–728. https://doi.org/10.1177/0309132514558442

O'Neil, R. S., Preziuso, D. C., Arkema, K. K., Ko, Y., Pevzner, N., Diamond, K., Gore, S., Morrice, K., Henderson, C. D., & Powell, D. W. (2022). *Renewable Energy Landscapes: Designing Place-Based Infrastructure for Scale*. Pacific Northwest National Laboratory (PNNL), Richland, WA (United States).

Parra, D., Swierczynski, M., Stroe, D. I., Norman, S. A., Abdon, A., Worlitschek, J., O'Doherty, T., Rodrigues, L., Gillott, M., Zhang, X., Bauer, C., & Patel, M. K. (2017). An interdisciplinary review of energy storage for communities: Challenges and perspectives. *Renewable and Sustainable Energy Reviews*, *79*(May), 730–749. https://doi.org/10.1016/j.rser.2017.05.003

Pasqualetti, M., & Stremke, S. (2018). Energy landscapes in a crowded world: A first typology of origins and expressions. *Energy Research and Social Science*, *36*(October 2017), 94–105. https://doi.org/10.1016/j.erss.2017.09.030

Pevzner, N., Ko, Y., & Dimond, K. (2021). Power Player. *Landscape Architecture Magazine*. https://landscapearchitecturemagazine.org/2021/06/08/power-player/

Schindler, B. Y., Blaustein, L., Lotan, R., Shalom, H., Kadas, G. J., & Seifan, M. (2018). Green roof and photovoltaic panel integration: Effects on plant and arthropod diversity and electricity production. *Journal of Environmental Management*, *225*(August), 288–299. https://doi.org/10.1016/j.jenvman.2018.08.017

Shafique, M., Luo, X., & Zuo, J. (2020). Photovoltaic-green roofs: A review of benefits, limitations, and trends. *Solar Energy*, *202*(February), 485–497. https://doi.org/10.1016/j.solener.2020.02.101

Stremke, S., & Koh, J. (2011). Integration of ecological and thermodynamic concepts in the design of sustainable energy landscapes. *Landscape Journal*, *30*(2), 194–213. https://doi.org/10.3368/lj.30.2.194

Talwar, P., Verma, N., Khatri, H., Ahire, P. D., Chaudhary, G., Lindenberger, C., & Vivekanand, V. (2023). A systematic review of photovoltaic-green roof systems in different climatic conditions focusing on sustainable cities and societies. *Sustainable Cities and Society*, *98*(July), 104813. https://doi.org/10.1016/j.scs.2023.104813

Wolsink, M. (2018). Co-production in distributed generation: renewable energy and creating space for fitting infrastructure within landscapes. *Landscape Research*, *43*(4), 542–561. https://doi.org/10.1080/01426397.2017.1358360

CHAPTER 1

COMPREHENSIVE REVIEW OF BIOSOLAR ROOF'S BENEFITS, CHALLENGES, AND DESIGN PARAMETERS

1.Introduction

1.1 Background

Biosolar roofs refer to a system that vertically installs PV arrays above green roof systems. It has emerged as an innovative solution to reconcile the traditional land-use competition between Green and PV roof, while provide the dual benefit of Green roof and PV roof (Abdalazeem et al., 2022). Heretofore, various terms have been used to describe this concept such as *PV green colocation, PV green roof, Green PV roof, and Building greenery and Photovoltaic system*, and unfortunately, there has not yet been determined common term indicating this concept (Abdalazeem et al., 2022; Shafique et al., 2020; Talwar et al., 2023). However, in this study, I adopt the term biosolar roof based on earlier references (Ciriminna et al., 2019; P. J. Irga et al., 2022; Schindler et al., 2018). This choice is made for clarity and consistency, as alternative terms such as PV-Green roof, because it could cause confusion when discussing PV roofs and green roofs as separate typologies in the later analysis chapter. Thus, I expect that the use of biosolar roof ensures clearer distinction and improved readability throughout the manuscript.

A nascent body of biosolar roof research largely concentrated on solar engineering perspectives with a primary focus on optimizing PV yields and its improvement (Chemisana & Lamnatou, 2014; Scherba et al., 2011). They revealed how existence of vegetation under PV array affects solar panel temperature and output, comparing it to gravel or bare concrete surface (Chemisana & Lamnatou, 2014; Nagengast et al., 2013). In contrast, relatively few studies had been grounded in fields like landscape architecture or urban planning (Scherba et al., 2011). As a result, aspects such as biodiversity increase, microclimate regulation,

and aesthetics aspects of biosolar roofs are barely discussed in empirical literature. To date, scholars started paying attention to the interdisciplinary nature of biosolar roofs, expanding to multiple environmental benefits that biosolar roof can offer, in addition to the PV yields (Bousselot et al., 2017; Jahanfar et al., 2019; Talwar et al., 2023).

However, as these studies were conducted independently, the fragmented state of current research limits the ability to derive meaningful insights for biosolar roof installations, optimal configurations, or ideal locations. (Shafique et al., 2020). To be more specific, it remains unclear what the ideal spacing or tilt of panels should be to balance sunlight for plants and energy generation, or which building types and roof structures are best suited for these systems (Pan et al., 2024). Likewise, no standardized planning or building codes specifically address biosolar roofs, and existing green roof or solar roof guidelines do not fully cover the integrated case. This lack of established standards and best practices can make it challenging for decision-makers to justify and implement biosolar roof projects, even when the concept is appealing in principle (Kelly et al., 2020; Pan et al., 2024). Therefore, a comprehensive review of biosolar roofs is both timely and necessary.

1.2 Purpose

This review aims to assess the benefits and challenges associated with biosolar roofs, identify key design parameters, and highlight practical synergies and trade-offs. Such a synthesis will not only fill critical knowledge gaps but also help guide future practice – offering architects, engineers, and urban planners' clearer evidence-based guidance for optimizing biosolar roof designs in different scenarios. Ultimately, consolidating these insights now will help ensure that the growing interest in biosolar roofs translates into effective real-world applications, with improved designs and policies that maximize their environmental benefits.

2. Method

I conducted a systematic, multi-stage literature search of both peer-reviewed papers and government-agency research reports using Google Scholar, ScienceDirect, and SpringerLink. First, I queried the terms "biosolar roof" and "PV-green roof," each paired with the sub-keywords "design", "planning", "benefits", "tradeoffs", "challenges", and "policies". I then added "agrivoltaic design" to capture insights from that related field.

This initial search returned 104 sources (21 on "biosolar roof", 52 on "PV-green roof", 31 on "agrivoltaic design"). I screened titles and abstracts to identify the 43 most relevant peer-reviewed papers and agency reports and reviewed them in depth—extracting each study's strengths, weaknesses, opportunities, and challenges—to structure my comprehensive review.

3. Reviews

3.1 Typology of Biosolar Roofs

The typology of biosolar roofs can be broadly divided into two configurations based on the arrangement of PV panels and vegetation: abreast and vertical. In the abreast layout, PV arrays and green-roof modules occupy adjacent but discrete zones on the same rooftop; because they do not share a footprint, this pattern essentially behaves as two mono-functional systems side by side—providing little shading synergy and only modest gains in space efficiency. By contrast, the vertical configuration elevates PV panels above the vegetated surface, integrating both functions within the same footprint. This arrangement unlocks the distinctive synergies of biosolar roofs: PV canopies shade the substrate, reducing solar radiation and prolonging moisture retention, while the cooler microclimate beneath panels boosts PV efficiency. This streamlined interaction—absent in the abreast pattern—arises directly from the vertical stacking of panels and vegetation. **Figure 1.2** (Zluwa & Pitha, 2021) illustrates several biosolar sub-typologies, differentiated by panel type and physical configuration. The most common is the canopy style, in which

panels are mounted 0.3–2.4 m above the roof deck as Figure 1.2 Coverage ratios and orientations (south-facing, east–west) vary, and both monofacial and bifacial modules may be employed.

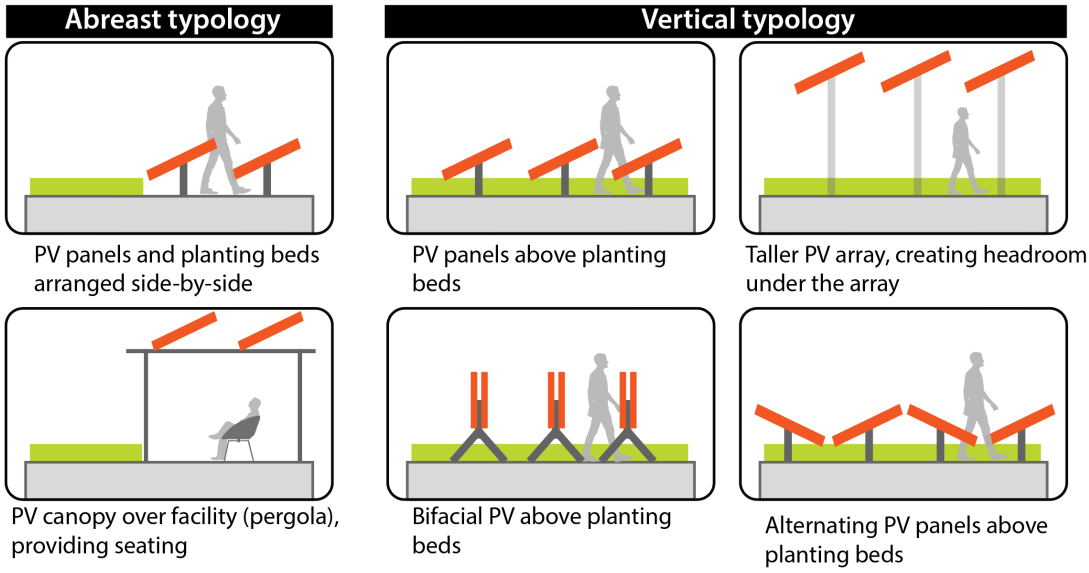


Figure 1.2 Schematic drawings for possible installation of biosolar roof, adopted from Zluwa and Pitha (2021) and modified

3.2 Multifunctional Benefits of Biosolar Roofs

3.2.1. Microclimate Cooling Benefits and PV Efficiency Improvement

Empirical studies have consistently reported that biosolar roofs have a higher PV efficiency of approximately 3–5%, compared to conventional PV roofs on black or gravel surfaces (Alshayeb & Chang, 2018; Chemisana & Lamnatou, 2014; Fleck et al., 2022; Hui & Chan, 2011; P. Irga et al., 2021; Nagengast et al., 2013). The scholars evaluate that this improvement may be primarily attributed to vegetation evapotranspiration and PV shades, which cools the microclimate (air temperature) under the panels and positively affect the temperature-dependent characteristic of PV efficiency (Alshayeb & Chang, 2018; Cook & Larsen, 2021). Beyond evapotranspiration, Zluwa and Pitha (2021) also conjectured that airflow beneath the PV array and the frequency of irrigation further enhance this cooling effect and contribute to additional efficiency gains, however their actual impact has not yet been proven.

In addition to the PV efficiency improvements, several empirical studies showed that biosolar roofs have lower ambient and surface temperatures, than either standalone PV roofs or extensive type green roofs (Bousselot et al., 2017; Hui & Chan, 2011; Köhler et al., 2002). However, Schindler et al. (2018) more specifically pointed out that the cooling benefit was largely confined to the shaded zones beneath the panels rather than the entire roof surface. Jahanfar et al. (2019) also found no significant difference in substrate temperature between Green roofs and biosolar roofs, suggesting that PV shade may not uniformly affect root-zone thermal conditions due to varying lighting condition by PV arrays. The influence of dynamic lighting regimes and specific PV configuration patterns on these localized cooling effects remains poorly understood, and no research has yet quantified the broader, city-wide impact of biosolar roofs on the urban heat island. Although the city-scale impact of biosolar roofs on urban heat island mitigation lies beyond the scope of this dissertation, future studies should model how array geometry, spacing, and orientation influence rooftop-level cooling and assess their aggregate effects across urban landscapes.

3.2.2. Stormwater Management and Longer Soil Moisture Persistence

While biosolar roofs are expected to perform similar stormwater-runoff reductions to conventional green roofs, direct experimental evidence of their hydrological performance remains limited. Early work inferred runoff retention by analogy—vegetation under PV panels should behave like a green roof—rather than measuring actual discharge (Shafique et al., 2020). However, more recent studies have begun to quantify these effects through both modeling and field experiments. Irga et al. (2021) combined hydrologic simulations with on-site measurements to show that PV-shaded substrate can both delay runoff peaks and increase total stormwater retention, compared to a green roof. Field experiment by Nagengast et al. (2013) and Bousselot et al. (2017) further reveal that PV canopies help soils retain moisture longer than unshaded green roofs—an advantage for greater plant survival during heat waves. Jahanfar et al. (2019) offer one of the most comprehensive empirical comparisons to date, analyzing 51 rainfall events

across a standalone green roof and two biosolar roof variants with PV panels elevated at 0.6 m and 1.2 m. For light storms (less than 3 mm), the green roof retained over 90% of rainfall, whereas the biosolar modules retained only 61% and 75%, respectively. In medium storms (3–10 mm), retention remained high for the green roof (93%) but dropped to 75% and 81% for the biosolar roofs. Even during heavy storms (greater than 10 mm), only the green roof achieved full (100%) retention, while both biosolar modules plateaued at around 76%. Peak-flow reduction followed a similar pattern, with the green roof outperforming biosolar systems by 9–39% depending on storm intensity. This performance gap is largely attributed to the PV canopy, which covered approximately 40% of the biosolar roof surface on their site. These PV panels block direct rainfall from reaching the underlying substrate, thereby reducing the effective infiltration area. Additionally, runoff from the tilted panels tends to concentrate along narrow strips, causing rapid local saturation and earlier onset of runoff. Despite sharing the same vegetated base, these hydrological dynamics explain why biosolar roofs reached their retention limits sooner than the standalone green roof (Jahanfar et al., 2019).

Also, strict rooftop load limits would provide designers little choice but to adopt an extensive-style planting scheme—with shallower growing media rather than an intensive green roof—thereby further constraining water-storage capacity (Jahanfar et al., 2019). Therefore, future work should consider a more controlled field experiment with process-based models, including various storm intensities, varying substrate depths and irrigation zones.

3.2.3 Urban Biodiversity Enhancement

Although biosolar roofs are widely expected to enhance biodiversity, only a few published studies empirically proved this. Theoretically, different shade levels and changes in light reflectance stimulate arthropod community growth (Schindler et al., 2018), and such abundant arthropod populations may indirectly increase plant diversity through positive arthropod–plant interactions (Schindler et al., 2018) . PV canopies also have the potential to reduce nutritional competition, except where nurse plants are

employed (Schindler et al., 2018). Also, In Denver, USA, Bousselot et al. (2017) showed that Sedum species under shaded area showed 30 % greater plant cover and 20 % higher biomass than the modules without shades. They concluded that this is attributed to reduced thermal stress under intermittent shading. In addition, Irga et al. (2021) comparatively monitored a biosolar roof with a PV roof in Sydney and found a nearly tenfold increase in insect richness (27 vs. 3 species) and a fourfold rise in avian species (4 vs. 1). They also found that rapid *Aptenia cordifolia* succession under the PV panels, coverage increased from 6 % to 85 % over eight months (P. Irga et al., 2021). Schindler et al. (2018) further demonstrated that biosolar roofs contributed to increasing arthropod abundance and Shannon diversity by roughly 25 % compared to a standalone green roof. They also found that this improvement is related to the mosaic of light and moisture where microhabitats appeared under the PV canopy (Schindler et al., 2018). However, these results may be context-dependent. That is, Biodiversity on biosolar roof may differ depending on substrate depth, irrigation regime, plant palette, and panel spacing, all mediate habitat quality and species response (Getter et al., 2009; Schindler et al., 2018). Therefore, future research should consider further experiments that can evaluate how different biosolar roof configurations influence the presence of insect and plant species, as well as associated abiotic conditions, by employing standardized biodiversity metrics such as Shannon and Simpson indices (Hölting et al., 2019).

3.2.4 Biosolar Roof as Thermal Mass and Contribution to Reducing Building Energy Use

The energy balance of biosolar roofs is crucial to understand its impact on building energy load for heating and cooling. The surface energy balance of biosolar roof is different to PV roof or Green roof in that it includes PV shading and evaporative cooling of vegetation. In general, the existence of vegetation and its substrate soilbed absorbs and dissipates heat through evapotranspiration and shades the rooftop surface, it performs as an insulating buffer, retaining heat during cooler nighttime or winter periods and impeding heat ingress during the day or summer (Castleton et al., 2010; Ogaili & Sailor, 2016; Sailor, 2008). Scherba et al., (2011) and Sailor (2008) proposed a basic understanding of rooftop surface Energy

balance of biosolar roof, Green roof, and PV roof. Scherba et al. (2011) revealed that variations in soil substrate depth (10–30 cm), plant density (LAI 0.5–5), and irrigation zone can drive annual building energy-use reductions of up to 15–25 %. They also revealed that the magnitude of energy savings may be strongly dependent on local climate (Scherba et al., 2011). At the same time, rooftop-scale experiments and models in Portland, Oregon, showed that adding PV panels to a black membrane roof reduced the total sensible heat flux into the atmosphere by 11 %, while PV-covered white or green roofs reduced sensible flux by roughly 50 %—directly translating into lower cooling loads (Scherba et al., 2011). A recent review reports that well-designed biosolar roofs can save annual cooling-load up to 20 % in a building (Iqbal & Rauf, 2025). From a field measurement, Irga et al. (2021) observed that a biosolar roof in Sydney had surface temperatures up to *20 °C* cooler than an adjacent bare roof on hot days. This cooling not only improved the solar panels' efficiency by roughly 3–4%, but also implies a substantial reduction in the building's cooling load.

Despite these clear benefits, relatively few long-term or large-scale field studies have monitored biosolar roofs' impact on parameters that affect building energy load, and there is a lack of standardized methodologies for evaluation across different projects. For example, Irga et al. (2021) point out that there are *significant discrepancies* in reported energy benefits of biosolar systems across studies, and they attributed this to differences in climate, building surface material or construction manner, and experimental design among studies. In other words, the current lack of climate-specific performance of biosolar roof may be another big missing puzzle to think of a reliable energy-saving design of biosolar roofs. Measurements or simulations demonstrating how changes in design parameters—panel angle, soil depth, or shading patterns—affect heating and cooling needs in various climate zones will help designers determine whether a given biosolar design will cut summer cooling load by 10 % or 20 % in their city.

3.3 Challenges of Biosolar Roof Implementation

3.3.1 Uncertain Net-Returning Moment and High Initial Upfront Cost

Economic uncertainty becomes a significant impediment to the investment of biosolar roofs (Shafique et al., 2020). Profitability is regarded as the primary determinant factors in investment decisions in PV projects for individuals, among various economic, environmental, and social considerations (Clark et al., 2008; Haegermark et al., 2017). Accordingly, the portfolio of PV projects used to be written in a way of how much profits the investors could obtain, with a particular focus on the estimated time of net income beginning (Kappner et al., 2019; Vargas-Salgado et al., 2022). However, the realization of this net-income timeframe is often delayed due to a myriad of factors that are not constant (Vimpari & Junnila, 2019), such as fluctuations in renewable energy certificate prices, subsidies, taxes, and tariffs changes by policies changes by political regime (Haegermark et al., 2017; Liberalesso et al., 2020; Mah et al., 2018). Accordingly, an uncertain net-return discourages stakeholders' investment in a biosolar roof.

A high initial upfront costs for biosolar roof system is another significant hurdle hindering its widespread adoption (Mah et al., 2018). Biosolar roofs require a comparatively higher amount of initial costs due to the necessity of foundations for both green roofs and PV systems, such as drainage roofing layers, vegetation and substrate soilbed, irrigation systems, and equipment of PV structures and systems. Consequently, both investors and developers may be less inclined to invest in green building initiatives (Fan & Wu, 2020).

3.3.2 Trend of Declining Benefits in Solar Electricity Costs and Duality of Subsidies and Tax

Government subsidies and regulatory frameworks play a crucial role in outlining the economic viability of solar PV projects, especially individual levels (Wee, 2016). Their non-constant factors add further complexity to the profitability equation. To be more specific, the increased PV penetration rate results in the declining trend of Solar PV electricity sales prices. This decline has not only reduced government

subsidies but also forced some small-scale producers to halt generation during peak solar hours to maintain grid stability. For example, regulators frequently adjust the cap on how much excess power can be sent back to the grid—raising it from just 0.5% to over 250% of minimum daytime demand (Coffman et al., 2016). Each tweak can abruptly reduce a small project's profit margin or make it much harder to keep operating their PV system (Coffman et al., 2016; Wee, 2016). In addition, the growing frequency of extreme weather events exacerbates these challenges, necessitating more frequent system management than initially anticipated. These constraints and situations might further complicate the economic equation of biosolar roof portfolios.

Also, the installation of PV systems could, in turn, lead to increased tax burdens by potentially increased property value. While the correlation between tax liability and biosolar roof installation has not been definitively established, several PV studies reported that the existence of PV tends to being capitalized into home or property values, and the premium is approximately 0.92-4% based on Hedonic prices models (Dastrup et al., 2012; Hoen et al., 2013, 2019), which is strongly correlated to the size of PV system but comparably less with the age of the system (Hoen et al., 2013). In addition, permanently affixed PV systems can trigger higher property-tax tariffs proportional to value increases, in California, USA;

Moreover, subsidy design itself can exacerbate equity concerns: income-tax credits only benefit homeowners with sufficient tax liability, so high-income households take most of the benefits while lower-income families and renters remain excluded (Coffman et al., 2016). Early policy ambiguity—such as vague definitions of what constitutes a "system"—allowed multiple credits to be claimed on a single rooftop until administrative rules were tightened, illustrating how incentives can be exploited (Coffman et al., 2016). Therefore, future studies should comprehensively explore how upfront costs, payback periods, and higher tax burdens affect biosolar investments to clarify the financial viability of biosolar projects.

3.2.3 Lack of Policies and Administrative Binding Force of biosolar Roof

Installation requirements play a significant role in promoting sustainable roofing measures. Many cities now include the mandates for the installation of green, PV, or cool roofs as part of their land-use ordinances and zoning codes, reflecting growing recognition of these measures' importance in coping with climate risks. While many municipalities have included green and PV roofs in policy frameworks or offer incentives due to their proven environmental benefits (Kelly et al., 2020; Manso et al., 2021; Razzaghi Asl, 2023), they have been addressed independently (Liberalesso et al., 2020).

Biosolar roofs have not yet been explicitly addressed in municipal regulations, because of their emerging status and their implementation complexities (Abdalazeem et al., 2022; Talwar et al., 2023). Although some cities require both green roofs and PV systems on newly constructed or renovated rooftops, few offer guidance on how to integrate them as a multifunctional system. For example, New York City has Local Laws 92 and 94 including "Sustainable Roofing Zones"—areas of a roof dedicated to green roofs, PV systems, or combinations thereof (Razzaghi Asl, 2023), however, there is no specific design guidelines for mixing vegetation and PV panels. Also, Portland, Oregon, mandates "eco-roofs" on new buildings over 20,000 ft^2—covering 100 percent of the roof area with at least 50 percent evergreen species (City of Portland, 2015). They simply permit replacing some of that green cover with PV panels as an alternative (City of Portland, 2015). On the other hand, California has a comparably strong Solar Mandate (effective January 1, 2020) rule, which requires all new single- and low-rise multi-family homes to include photovoltaic systems, but does not address integration with vegetation (Walmsley et al., 2015). Phoenix, Arizona, also requires cool-roof materials on all new and renovated buildings to mitigate the urban heat island effect, however, none of these regulations explicitly guide the co-design of vegetation and PV into a unified biosolar roof system (Rawat & Singh, 2022).

3.3 Design Parameters for The Biosolar Roof Design

While there is no consensus on how to define a biosolar roof's success, most studies have aimed to enhance its multiple performance metrics—solar energy yield, microclimate cooling, and stormwater management. In this context, I define a successful biosolar roof as one that delivers all of these benefits simultaneously, and I define successful biosolar roof design as the configuration that maximizes those benefits while fewest tradeoffs.

Reviewing the literature on biosolar roofs reveals three key design parameters—PV height, PV configuration, and plant species selection and planting density—because each directly influences overall system performance. Therefore, in the next section, I review these parameters in relation to performance outcomes and the definition of biosolar roof success.

3.3.1 PV Height from The Surface

The height of PV panels is a decisive parameter in biosolar roof design because it directly determines the shaded zone and under-panel airflow, which influence on both plant evapotranspiration and microclimate cooling. A recent systematic review (Talwar et al., 2023) and multiple field-scale experiments (Jahanfar et al., 2019; Toledo & Scognamiglio, 2021; Zluwa & Pitha, 2021) has regarded PV-standoff range of 0.5–1.5 m as ideal, because it can balance sufficient light penetration for photosynthesis with adequate convective exchange to lower module temperatures by 2–3 °C while boosting PV efficiency by 3–5 % (Hui & Chan, 2011; Ogaili & Sailor, 2016). In Jahanfar et al., (2019)'s rooftop experiment in Toronto, increasing the panel height from 0.6 m to 1.2 m yielded a 47 % increase in biomass under the PV array, while stormwater retention and peak flow reduction remained statistically similar between 0.6m and 1.2m PV heights, demonstrating the height-dependent vegetation benefits without compromising hydrological performance. Another study in Denver, CO showed that PV panels elevated at approximately 1.5 m created a shaded protected zone with up to 30 % higher plant biomass and more stable substrate

temperatures compared to full sun exposed modules (Bousselot et al., 2017). Conversely, Zluwa & Pitha (2021) warns that the PV standoffs below 0.3 m may trap heat and suppress evapotranspiration by blocking air ventilation. Heights above 1.5 m may be too high to expect microclimate synergy with vegetation, reducing both biological and cooling co-benefits (Ogaili & Sailor, 2016; Zluwa & Pitha, 2021). Therefore, future studies should empirically clarify how PV–vegetation distance, under-panel airflow, and planting density interact to govern microclimate cooling and overall system performance. Also, practical constraints in urban contexts—such as rooftop structural limits, safety regulations, and potential aesthetic objections to tall support structures—necessitate further context-specific study to refine biosolar-roof installation guidelines and validate optimal height-performance relationships across different climates and building types (Sánchez-Pantoja et al., 2018).

Table 1.1 Overview of biosolar roof studies with reported PV height and performance outcomes

Researchers	Finding (average)	Plant species	Location	Settings
Chemisanan and Lamnatou 2014	+1.29% +3.33% (PV improvement)	*G. rigens Gazania* *Sedum Clavatum*	Catalonia, Spain	Small study model (1*1m) (PV-green vs. PV-gravel)
Perez et al., 2012	+2.42 (PV improvement)	Varietal Sedum	New York, USA	Small study model (2*2m) (PV-green vs. PV-gravel)
Köhler et al., 2002; Köhler, Wiartalla and Feige, 2007	+6% (PV improvement)	Sedum	Berlin, Germany	Two building rooftops (400m^2) PV height (1.5m) (PV-green vs. PV roof)
Nagengast et al., 2013	+0.5% (PV improvement)	Mosses	Pittsburg, USA	Large-scale (PV-green vs. PV-black)
Alshayeb & Chang, 2018)	+1.4% (PV improvement)	Local sedum	Kansas, USA	4.23 kW PV capacity PV height (0.2m – lowest point) (PV-green vs. PV-black)
Hui & Chan, 2011	+4.30% (PV improvement)	Not-specified	Hongkong, China	(PV-green vs. PV bare roof)
Osma et al., 2016	+2.8% (PV improvement)	Sedum	Santander, Colombia	Three PV panels of 250 W PV height (0.5-75) (PV green vs. PV-black)
Sattler et al., 2020	Contribute to thermal comfort	Herbaceouns perennials Grasses Climbing plants	Vienna, Austria	PV height (2.6m; 60m$^{2)}$ (pergola attachment)

3.3.2 PV Configuration (Spacings, Array Patterns, Orientation and Angles)

PV configuration—including the arrangement pattern, density, orientation, and tilt of PV modules—determines the lighting dynamics under the PV array and thus directly influences plant health. However, no existing biosolar roof studies have examined PV configuration deeply (Talwar et al., 2023). To address this gap, I leveraged the findings from agrivoltaic (APV) research, which shares the same basic concept of colocating PV panels over vegetation, albeit at larger scales and on the ground with food crops. APV studies have explored how to optimize PV configuration to maximize both energy and crop yields (Aroca-Delgado et al., 2018; Asa'a et al., 2024; Chopdar et al., 2024), yielding several design insights that may be potentially transferable to biosolar roofs.

Regarding PV density, Dupraz et al. (2011) and Marrou, Guilioni, et al.,(Marrou et al., 2013) empirically demonstrated that a 50% PV density (i.e., half land coverage) was ideal in balancing energy and crop yields, while maintaining marketable crop quality. Their experiments underscore that neither full coverage nor overly sparse PV arrays are optimal; instead, row spacing should be tailored to local latitude, plant species' light sensitivity, and the diffuse-to-direct radiation ratio (Dupraz et al., 2011; Marrou et al., 2013). PV orientation in the Northern Hemisphere is typically toward south, with fixed module tilt set near the local latitude to maximize direct solar irradiance (Singh & Banerjee, 2015).

Regarding PV array patterns, multiple APV research teams (Cossu et al., 2018; Katsikogiannis et al., 2022) have shown that a checkerboard layout produces a more uniform light distribution across the field, enhancing photosynthesis and biomass accumulation. Particularly, Cossu et al. (2018) found that switching from straight PV rows style to a checkerboard PV pattern nearly doubled light amount in the darkest zones (from roughly 20–30 % to 40–50 % of full sun), lifting cherry tomato yields from 3.7 kg/m² to almost the 4.7 kg/m², under a greenhouse type agrivoltaic experiment.

While a checkerboard PV layout has shown promise in agrivoltaic settings by improving light uniformity and enhancing crop yields, its benefits may not universally translate to all biosolar roof applications. In rooftop contexts—especially those using low-maintenance, drought-tolerant plants such as sedum—

reduced light through denser shading may actually be more desirable to conserve water and enhance rooftop cooling. Therefore, the ideal PV layout likely depends on the intended vegetation type, climatic conditions, and functional priorities of the roof (e.g., energy yield vs. thermal performance). Future studies should explore how different PV array geometries perform across various biosolar design goals and rooftop microclimates. This study contributes to this inquiry by providing empirical evidence as well as simulation results on how different PV layouts shape microclimate and performance outcomes on biosolar roofs.

3.3.3 Plant Species Choice

Plant selection for biosolar roofs has traditionally followed extensive green-roof practice, favoring low-height, shade- and drought-tolerant succulents or hardy turfgrasses, which can withstand high winds, shallow substrates, long periods of dryness, and intense full-sun irradiation (Lamnatou & Chemisana, 2015; Sattler et al., 2020). However, only a few studies have proposed species suited to the heterogeneous conditions under PV arrays—where light levels, substrate temperatures, and airflow can vary dramatically. Although Talwar et al. (2023) reviewed plant species for biosolar roofs and organized them by their performance contributions, further research is needed to comprehensively assess plant survivability under PV canopies. Moreover, future species assessments should differentiate between irrigated and non-irrigated biosolar systems, as water availability can significantly influence plant survivability under PV-induced microclimatic stress. Thus, more trait-focused guidance on species selection is needed to ensure sustainable viability in these heterogeneous microclimates.

Some empirical evidence from earlier studies highlights the need to consider plant traits when selecting species for biosolar roofs (Table 1.1). Lamnatou and Chemisana (2015) showed that compact succulents and low-growing forbs resist combined solar and thermal stress more effectively than taller, broad-leaf species. Bousselot et al. (2017) compared cultivars under 50 % shading and found that varieties with lower light-compensation points—the minimum irradiance at which photosynthesis balances

respiration—retained over 75 % of their biomass, whereas high-compensation cultivars lost more than 30 %. This highlight the importance of carefully selecting plant species whose specific ecological and physiological characteristics—such as leaf area index, photosynthetic light-compensation points, and rooting depth—are compatible with the unique microclimatic conditions soils, and soil substrates created by PV canopies.

Additionally, Lamnatou and Chemisana (2015) proposed a useful evaluation framework—summarized in **Table 1.3**—for filtering candidate species against six overarching criteria. Each criterion captures a suite of plant traits that determine performance under the partial shading, thermal loads, and substrate constraints imposed by PV canopies. By systematically evaluating species across these dimensions, their approach may provide a robust methodological foundation for identifying vegetation capable of thriving on biosolar roofs.

While **Table 1.2** primarily highlights conventional succulents and turfgrasses, this reflects the limited scope of existing biosolar studies. With further empirical research, other plant taxa—such as native herbaceous species or shade-tolerant perennials—may also prove suitable and could be evaluated using a similar trait-based framework. Also, future research should examine the performance of both irrigated and non-irrigated vegetation systems, as water availability may vary significantly depending on the rooftop's design and regional climate.

Table 1.2 Preferred plant characteristics against PV shade

Plant species	Characteristics contributing to plant survival	Climate/Location	References
Succulent / Forbs - *Origanum vulgare*, - *Coreopsis pubescens*, - *Asteriscus maritimus*, - *Geranium molle* - *Sedum album* - *Sedum spurium*	○ Compact, low-stature species: ○ Can resist heat stress and drought ○ Can be tolerant to limited light availability	Mediterranean / Lleida, Spain	Lamnatou & Chemisana (2015)
Turfgrass cultivars	○ Low photosynthetic compensation point species: ○ Can yield net-positive photosynthesis even under shade; retains > 75 % biomass at 50 % shade	Temperate / Denver, USA	Bousselot et al. (2021)

Table 1.3 Biosolar roof plant species choice evaluation criteria (Lamnatou & Chemisana, 2015)

Scoring criteria	Sub-evaluation
1. Suitability for extensive green roofs	Shallow roots; Nutrient needs; Irrigation needs; disease/pest resistance
2. Resistance to weather conditions	Resistance to direct radiation; Resistance to drought, Resistance to frost; Resistance to wind;
3. Interaction with the PVs	Albedo (leaf color); Evapotranspiration; Height; Compactness
4. Interaction with the building	Leaf water content; Dense foliage (insulation)
5. Interaction with the external environment	Air temperature; Carbon sequestration rate; Biodiversity increase;
6. Other factors	Acoustic benefits; interests in medicine; aesthetics;

4. Discussion

This chapter comprehensively reviewed the multifunctional potential of biosolar roofs and examined how design parameters—such as PV height, configuration, and planting strategies—influence environmental performance. This review organized promising benefits across energy production, microclimate cooling, and stormwater management, and identified several key challenges, such as uncertainty in return on investment, high upfront costs, regulatory ambiguity, and a lack of practical design guidance for integrating vegetation and PV systems. Together, these findings highlight both the opportunities and constraints that shape the future of biosolar roof implementation. I synthesize these insights, exploring critical trade-offs, design considerations, and future research directions needed to advance biosolar roofs as a viable urban sustainability solution.

4.1 Place-based Biosolar Design Considering Trade-offs

An inherent trade-off in biosolar roof design centers on PV shading: greater panel coverage boosts energy yield but creates deeper shade that can disrupt plant growth and even survival. While many scholars suggest that a 50 percent PV density generally balances power generation and plant survival, I argue that each installation should be tailored to its site's specific conditions, demands, and priorities. For example, in energy-intensive buildings—factories or big-box retail stores—an energy-focused design might pair high-density PV arrays with compact, shade-tolerant species, meeting large electricity needs while still providing some ecological benefit. Conversely, in regions with extreme heat, greater PV shading may enhance both plant survival and rooftop cooling, thereby reducing building cooling loads while also improving PV efficiency. However, excessive PV coverage may limit sunlight penetration to vegetation and reduce stormwater retention by obstructing rainfall across the substrate. A more than 50% PV density may offer an optimal compromise, providing sufficient shade for thermal mitigation while preserving the hydrological function of the green roof. In contrast, in areas with frequent and intense rainfall, the design

priority may shift toward maximizing water detention and infiltration. Since PV canopies intercept rainfall and channel runoff unevenly, adopting lower-density or more spaced configurations can promote uniform water distribution across the substrate. In these settings, deep-rooted, moisture-loving species may be preferred but may require irrigation during drought periods, as long as the structural load can accommodate the saturated soil and plants with safety load margin. Because the combined environmental benefits of biosolar roofs depend critically on the interaction between panel layout and plant traits, systematic research is needed to quantify these relationships and guide optimized, context-specific designs.

4.2 Potential to Being Coupled with Urban Agriculture as Rooftop Agrivoltaics

Biosolar roofs in dense cities can be reimagined as multifunctional platforms for both urban agriculture and clean energy generation, thereby strengthening the food–energy–water nexus. By planting edible crops under photovoltaic arrays—a strategy known as rooftop agrivoltaics—it can simultaneously yield fresh vegetables and electricity for on-site consumption. This co-location may not only reduce food-miles and transport-related emissions, but also strengthen local energy resilience by alleviating energy concentration on the grid. However, large-scale urban rooftop farming brings about significant irrigation needs: Jing et al. (2022) estimated that city-wide rooftop lettuce cultivation could demand approximately millions of tons of water per year. To address this, designers should consider lightweight cultivation strategies—such as shallow-rooted species or hydroponic systems or metered drip irrigation in shallow soil—to stay within structural load limits and optimize water use.

4.3 East–West Bifacial PV: a Strategy to Flatten the *Duck Curve*

Bifacial solar PV technologies are receiving greater attention within the context of biosolar roofs. By capturing solar irradiance on both front and rear surfaces, bifacial modules can leverage reflected light.

However, the environmental performance of bifacial panels installed above vegetation remains underexplored in urban biosolar roof settings, leaving an important research gap. Additionally, when bifacial panels are erected perpendicular to the surface and are oriented toward the east and west, they can help distribute solar energy generation more evenly throughout the day—flattening the midday peak typical of south-facing systems and mitigating the *Duck Curve* effect discussed above. Therefore, integrating east–west–facing bifacial systems into biosolar roof designs could represent a promising next-generation strategy. Future research should examine how these systems perform environmentally and functionally under real-world rooftop vegetation conditions.

4.4 Enhancing Understanding at the City-wide Scale

A knowledge gap of biosolar roof discussion is the lack of city-scale site-selection process and guidelines. Without structured guidelines, policymakers cannot map which buildings or neighborhoods are best suited, nor can they quantify the cumulative energy, cooling, and stormwater benefits of widespread deployment. Therefore, developing such guidelines is crucial not only to envision planning scenarios that incentivize optimal locations but also to produce the robust quantitative evidence needed to guide urban policy and design.

Biosolar roof placement suitability analysis should integrate multiple metrics, such as building characteristics (structural load capacity, membrane type, roof slope, rooftop footprint), urban-form indicators (e.g., Floor Area Ratio, density/compactness, and building heights variation that can affect shade by neighboring structures), and building use and typology (residential, commercial and industrial). For instance, at a FAR, low-rise buildings with large rooftops can accommodate more PV panels and vegetation than taller and small rooftop buildings, so that they may have greater economies of scale for potential of biosolar roof benefits by deploying larger scale systems. Likewise, big-box retail, warehouses, and industrial facilities—already known as prime candidates for either PV or green roofs—

logically emerge as top contenders for commercial scale integrated biosolar systems given their significant amount of energy demand and stormwater discharge. Embedding these parameters in a GIS-based model could enable planners to pinpoint suitable locations and quantify city-wide benefits efficiently.

4.5 Criteria for Biosolar roof Placement

The placement criteria for biosolar roofs may encompass both sets of requirements of PV and green roof. PV arrays need unobstructed solar access, robust structural stability, proper surface orientation, and flat or gentle roof slope (Kucuksari et al., 2014; Santos et al., 2014). Green roofs require sufficient load-bearing capacity to support saturated substrate and plants, adequate drainage, and sufficient soil substrate depth (W. Hong et al., 2019; Slootweg et al., 2023; Thebault et al., 2020). Therefore, meeting both sets of requirements could support successful biosolar roof placement.

One systematic approach from rooftop PV analysis categorizes site suitability into three hierarchical potentials—geographic, physical, and technical potentials—originally proposed to estimate urban PV feasibility (T. Hong et al., 2017). I adapted this framework to organize parameters that may be closely related to the biosolar roofs placement.

Physical potential (solar and climate resource):

- Solar Irradiance and Shading: Roof areas with high year-round solar irradiance and minimal shading from adjacent structures or buildings are preferred. For example, Santos et al. (2014) evaluated rooftops receiving less than about 800 kWh/m² per year of sunlight as improper.
- Climate & Microclimate Conditions: Regions with abundant sunlight, moderate temperatures, and sufficient rainfall likely best support both PV output and plant health; future comparative studies should pinpoint which climate zones most effectively maximize biosolar roof performance.

Geographic potential (spatial and morphological rooftop characteristics):

- Roof Slope and Orientation: Flat or gentle slope rooftops (up to 8°) are generally suitable (Slootweg et al., 2023). Orientation influences solar gain: south-facing (in the northern hemisphere) is preferred, though panels on flat roofs can be oriented as needed.
- Roof Size and Layout: Sufficient continuous area is needed to install PV arrays and a green roof without obstruction. Large, unobstructed roof sections are preferable to maximize solar coverage and allow a significant vegetated area. Small or highly congested rooftops by HVAC units, venting chimneys, and ventilation system may limit the feasible biosolar installation or make maintenance difficult.
- Drainage and Water Management: Proper roof drainage is essential to prevent standing water from damaging both the building and the PV system. A suitable site must allow the installation of drainage membranes, drainage pipe systems, and substrate layers required for the green roof, and provide easy access to water for irrigation.

Technical potential (installability, structural, and regulatory feasibility):

- Structural Load Capacity: The roof must support the combined weight of PV modules and vegetation, and green roof substrates, including an adequate safety margin.
- Access for Maintenance: The roof should be safely accessible for installation and ongoing maintenance of both the solar panels and the green roof. This includes having adequate access points (hatches, ladders), walking paths between beds, and perimeter safety (railings or parapets). The roof should be safely accessible for maintenance such ass cleaning PV panels, servicing electrical components, and caring for plants (irrigation, weeding, replacing species as needed).

- Regulatory and Zoning Considerations: Permitting requirements—setback rules, fire-lane clearances, waterproofing standards, historic-district restrictions, stormwater management, and available incentives—could be considered in biosolar roof placement.

5. Conclusion

This chapter has comprehensively reviewed biosolar roofs' environmental benefits, implementation challenges, and the critical design parameters that shape their performance. Empirical studies have consistently shown that biosolar can enhance PV efficiency, cool the microclimate, retain stormwater, enhance biodiversity, and decrease building energy load. On the contrary, economic uncertainties—fluctuating subsidies, high upfront costs, and complex regulations—hinder investment and adoption and construction of biosolar roof. Above all, the lack of clear and standardized guidelines for biosolar design and integration into urban planning further complicates implementation.

To overcome this, future work should:

- Identify optimal design configurations (e.g., panel height, density, plant choice) to maximize combined energy and ecological returns.
- Develop a city-scale suitability guidelines for site selection based on structural, climatic, and regulatory criteria.
- Explore the trade-offs inherent in balancing energy yield against ecosystem services when tuning panel layouts and vegetation strategies.
- Investigate the synergy between biosolar systems, irrigation systems, and rooftop agriculture to bolster local food–energy–water resilience.
- Assess the environmental and energy performance of bifacial PV modules integrated within biosolar roof settings, particularly under different climate conditions.

Ultimately, scaling up biosolar roofs will demand interdisciplinary approaches—including rigorous empirical testing, standardized performance metrics, supportive policy frameworks, and inventive design solutions—to unlock their full potential as multifunctional urban infrastructure.

References

Abdalazeem, M. E., Hassan, H., Asawa, T., & Mahmoud, H. (2022). Review on integrated photovoltaic-green roof solutions on urban and energy-efficient buildings in hot climate. *Sustainable Cities and Society*, *82*(April), 103919. https://doi.org/10.1016/j.scs.2022.103919

Alshayeb, M. J., & Chang, J. D. (2018). Variations of PV panel performance installed over a vegetated roof and a conventional black roof. *Energies*, *11*(5). https://doi.org/10.3390/en11051110

Aroca-Delgado, R., Pérez-Alonso, J., Callejón-Ferre, Á. J., & Velázquez-Martí, B. (2018). Compatibility between crops and solar panels: An overview from shading systems. *Sustainability (Switzerland)*, *10*(3). https://doi.org/10.3390/su10030743

Asa'a, S., Reher, T., Rongé, J., Diels, J., Poortmans, J., Radhakrishnan, H. S., van der Heide, A., Van de Poel, B., & Daenen, M. (2024). A multidisciplinary view on agrivoltaics: Future of energy and agriculture. *Renewable and Sustainable Energy Reviews*, *200*(August 2023). https://doi.org/10.1016/j.rser.2024.114515

Bousselot, J., Slabe, T., Klett, J., & Koski, R. (2017). Photovoltaic Array Influences the Growth of Green Roof Plants. *Journal of Living Architecture*, *4*(3), 9–18. https://doi.org/10.46534/jliv.2017.04.03.009

Castleton, H. F., Stovin, V., Beck, S. B. M., & Davison, J. B. (2010). Green roofs; Building energy savings and the potential for retrofit. *Energy and Buildings*, *42*(10), 1582–1591. https://doi.org/10.1016/j.enbuild.2010.05.004

Chemisana, D., & Lamnatou, C. (2014). Photovoltaic-green roofs: An experimental evaluation of system performance. *Applied Energy*, *119*, 246–256. https://doi.org/10.1016/j.apenergy.2013.12.027

Chopdar, R. K., Sengar, N., Giri, N. C., & Halliday, D. (2024). Comprehensive review on agrivoltaics with technical, environmental and societal insights. *Renewable and Sustainable Energy Reviews*, *197*(October 2023), 114416. https://doi.org/10.1016/j.rser.2024.114416

Ciriminna, R., Meneguzzo, F., Pecoraino, M., & Pagliaro, M. (2019). Solar Green Roofs: A Unified Outlook 20 Years On. *Energy Technology*, *7*(6), 1–7. https://doi.org/10.1002/ente.201900128

Clark, C., Adriaens, P., & Talbot, F. B. (2008). Green roof valuation: A probabilistic economic analysis of environmental benefits. *Environmental Science and Technology*, *42*(6), 2155–2161. https://doi.org/10.1021/es0706652

Coffman, M., Wee, S., Bonham, C., & Salim, G. (2016). A policy analysis of Hawaii's solar tax credit. *Renewable Energy*, *85*, 1036–1043. https://doi.org/10.1016/j.renene.2015.07.061

Cook, L. M., & Larsen, T. A. (2021). Towards a performance-based approach for multifunctional green roofs: An interdisciplinary review. *Building and Environment*, *188*(September 2020), 107489. https://doi.org/10.1016/j.buildenv.2020.107489

Cossu, M., Cossu, A., Deligios, P. A., Ledda, L., Li, Z., Fatnassi, H., Poncet, C., & Yano, A. (2018). Assessment and comparison of the solar radiation distribution inside the main commercial photovoltaic greenhouse types in Europe. *Renewable and Sustainable Energy Reviews*, *94*(March), 822–834. https://doi.org/10.1016/j.rser.2018.06.001

Dastrup, S. R., Graff Zivin, J., Costa, D. L., & Kahn, M. E. (2012). Understanding the Solar Home price premium: Electricity generation and "Green" social status. *European Economic Review*, *56*(5), 961–973. https://doi.org/10.1016/j.euroecorev.2012.02.006

Dupraz, C., Marrou, H., Talbot, G., Dufour, L., Nogier, A., & Ferard, Y. (2011). Combining solar photovoltaic panels and food crops for optimising land use: Towards new agrivoltaic schemes. *Renewable Energy*, *36*(10), 2725–2732. https://doi.org/10.1016/j.renene.2011.03.005

Fan, K., & Wu, Z. (2020). Incentive mechanism design for promoting high-level green buildings. *Building and Environment*, *184*(May), 107230. https://doi.org/10.1016/j.buildenv.2020.107230

Fleck, R., Gill, R., Pettit, T. J., Torpy, F. R., & Irga, P. J. (2022). Bio-solar green roofs increase solar energy output:

The sunny side of integrating sustainable technologies. *Building and Environment*, *226*(August), 109703. https://doi.org/10.1016/j.buildenv.2022.109703

Getter, K. L., Bradley Rowe, D., & Cregg, B. M. (2009). Solar radiation intensity influences extensive green roof plant communities. *Urban Forestry and Urban Greening*, *8*(4), 269–281. https://doi.org/10.1016/j.ufug.2009.06.005

Haegermark, M., Kovacs, P., & Dalenbäck, J. O. (2017). Economic feasibility of solar photovoltaic rooftop systems in a complex setting: A Swedish case study. *Energy*, *127*, 18–29. https://doi.org/10.1016/J.ENERGY.2016.12.121

Hoen, B., Rand, J., & Elmallah, S. (2019). *Commercial PV Property Characterization: An Analysis of Solar Deployment Trends in Commercial Real Estate*. *2019*(September). https://escholarship.org/uc/item/4wt0p3nk

Hoen, B., Wiser, R., Thayer, M., & Cappers, P. (2013). Residential photovoltaic energy systems in California: The effect on home sales prices. *Contemporary Economic Policy*, *31*(4), 708–718. https://doi.org/10.1111/j.1465-7287.2012.00340.x

Hölting, L., Beckmann, M., Volk, M., & Cord, A. F. (2019). Multifunctionality assessments – More than assessing multiple ecosystem functions and services? A quantitative literature review. *Ecological Indicators*, *103*(April), 226–235. https://doi.org/10.1016/j.ecolind.2019.04.009

Hong, T., Lee, M., Koo, C., Jeong, K., & Kim, J. (2017). Development of a method for estimating the rooftop solar photovoltaic (PV) potential by analyzing the available rooftop area using Hillshade analysis. *Applied Energy*, *194*, 320–332. https://doi.org/10.1016/J.APENERGY.2016.07.001

Hong, W., Guo, R., & Tang, H. (2019). Potential assessment and implementation strategy for roof greening in highly urbanized areas: A case study in Shenzhen, China. *Cities*, *95*(October 2018), 102468. https://doi.org/10.1016/j.cities.2019.102468

Hui, S. C. M., & Chan, S.-C. (2011). Integration of green roof and solar photovoltaic systems. *Joint Symposium*, 1–12.

Iqbal, A., & Rauf, S. (2025). Bridging Nature And Building Energy Demands Through Bio-Solar Green Roofs: A Review. *Spectrum of Engineering Sciences*, *3*(2), 249–271.

Irga, P., Fleck, R., Wooster, E., Torpy, F., Pettit, T., Gill, R., & Ball, J. (2021). *Green Roof & Solar Array Comparative Research Project Final Report July 2021*. City of Sydney Council.

Irga, P. J., Fleck, R., Arsenteva, E., & Torpy, F. R. (2022). Biosolar green roofs and ambient air pollution in city centres: Mixed results. *Building and Environment*, *226*(October), 109712. https://doi.org/10.1016/j.buildenv.2022.109712

Jahanfar, A., Drake, J., Sleep, B., & Margolis, L. (2019). Evaluating the shading effect of photovoltaic panels on green roof discharge reduction and plant growth. *Journal of Hydrology*, *568*(October 2018), 919–928. https://doi.org/10.1016/j.jhydrol.2018.11.019

Jing, R., Liu, J., Zhang, H., Zhong, F., Liu, Y., & Lin, J. (2022). Unlock the hidden potential of urban rooftop agrivoltaics energy-food-nexus. *Energy*, *256*, 124626. https://doi.org/10.1016/j.energy.2022.124626

Kappner, K., Letmathe, P., & Weidinger, P. (2019). Optimisation of photovoltaic and battery systems from the prosumer-oriented total cost of ownership perspective. *Energy, Sustainability and Society*, *9*(1). https://doi.org/10.1186/s13705-019-0231-2

Katsikogiannis, O. A., Ziar, H., & Isabella, O. (2022). Integration of bifacial photovoltaics in agrivoltaic systems: A synergistic design approach. *Applied Energy*, *309*(January), 118475. https://doi.org/10.1016/j.apenergy.2021.118475

Kelly, C., Sen, B., & Tatari, O. (2020). A system dynamics analysis of the alternative roofing market and its potential impacts on urban environmental problems: A case study in Orlando, Florida. *Resources, Conservation and Recycling*, *153*. https://doi.org/10.1016/J.RESCONREC.2019.104556

Köhler, M., Schmidt, M., Laar, M., Wachsmann, U., & Krauter, S. (2002). Photovoltaic-panels on greened roofs: positive interaction between two elements of sustainable architecture. *RIO 02 - World Climate & Energy Event*, *1*, 151–158. http://commons.bcit.ca/greenroof/files/2012/01/photovoltaic_kohler.pdf

Kucuksari, S., Khaleghi, A. M., Hamidi, M., Zhang, Y., Szidarovszky, F., Bayraksan, G., & Son, Y. J. (2014). An Integrated GIS, optimization and simulation framework for optimal PV size and location in campus area environments. *Applied Energy*, *113*, 1601–1613. https://doi.org/10.1016/j.apenergy.2013.09.002

Lamnatou, C., & Chemisana, D. (2015). A critical analysis of factors affecting photovoltaic-green roof performance. *Renewable and Sustainable Energy Reviews*, *43*, 264–280. https://doi.org/10.1016/j.rser.2014.11.048

Liberalesso, T., Oliveira Cruz, C., Matos Silva, C., & Manso, M. (2020). Green infrastructure and public policies: An international review of green roofs and green walls incentives. *Land Use Policy*, *96*(April), 104693. https://doi.org/10.1016/j.landusepol.2020.104693

Mah, D. N. yin, Wang, G., Lo, K., Leung, M. K. H., Hills, P., & Lo, A. Y. (2018). Barriers and policy enablers for solar photovoltaics (PV) in cities: Perspectives of potential adopters in Hong Kong. *Renewable and Sustainable Energy Reviews*, *92*(May), 921–936. https://doi.org/10.1016/j.rser.2018.04.041

Manso, M., Teotónio, I., Silva, C. M., & Cruz, C. O. (2021). Green roof and green wall benefits and costs: A review of the quantitative evidence. *Renewable and Sustainable Energy Reviews*, *135*(November 2019). https://doi.org/10.1016/j.rser.2020.110111

Marrou, H., Guilioni, L., Dufour, L., Dupraz, C., & Wery, J. (2013). Microclimate under agrivoltaic systems: Is crop growth rate affected in the partial shade of solar panels? *Agricultural and Forest Meteorology*, *177*(August), 117–132. https://doi.org/10.1016/j.agrformet.2013.04.012

Nagengast, A., Hendrickson, C., & Scott Matthews, H. (2013). Variations in photovoltaic performance due to climate and low-slope roof choice. *Energy and Buildings*, *64*, 493–502. https://doi.org/10.1016/j.enbuild.2013.05.009

Ogaili, H., & Sailor, D. J. (2016). Measuring the Effect of Vegetated Roofs on the Performance of Photovoltaic Panels in a Combined System. *Journal of Solar Energy Engineering, Transactions of the ASME*, *138*(6). https://doi.org/10.1115/1.4034743

Pan, Z., Wang, C., Yu, B., Chen, Z., Yuan, Y., Li, G., Zhang, J., & Xiao, T. (2024). Assessing multifunctional retrofit potential of urban roof areas and evaluating the power and carbon benefits under efficient retrofit scenarios. *Journal of Cleaner Production*, *444*(October 2023), 141270. https://doi.org/10.1016/j.jclepro.2024.141270

Rawat, M., & Singh, R. N. (2022). A study on the comparative review of cool roof thermal performance in various regions. *Energy and Built Environment*, *3*(3), 327–347. https://doi.org/10.1016/j.enbenv.2021.03.001

Razzaghi Asl, S. (2023). Rooftops for Whom? Some Environmental Justice Issues in Urban Green Roof Policies of Three North American Cities. *Environmental Policy and Law*, *53*(1), 49–60. https://doi.org/10.3233/EPL-220015

Sailor, D. J. (2008). A green roof model for building energy simulation programs. *Energy and Buildings*, *40*(8), 1466–1478. https://doi.org/10.1016/j.enbuild.2008.02.001

Sánchez-Pantoja, N., Vidal, R., & Pastor, M. C. (2018). Aesthetic impact of solar energy systems. *Renewable and Sustainable Energy Reviews*, *98*(August), 227–238. https://doi.org/10.1016/j.rser.2018.09.021

Santos, T., Gomes, N., Freire, S., Brito, M. C., Santos, L., & Tenedório, J. A. (2014). Applications of solar mapping in the urban environment. *Applied Geography*, *51*, 48–57. https://doi.org/10.1016/j.apgeog.2014.03.008

Sattler, S., Zluwa, I., & Österreicher, D. (2020). The “PV rooftop garden”: providing recreational green roofs and renewable energy as a multifunctional system within one surface area. *Applied Sciences*, *10*(5), 1791.

Scherba, A., Sailor, D. J., Rosenstiel, T. N., & Wamser, C. C. (2011). Modeling impacts of roof reflectivity, integrated photovoltaic panels and green roof systems on sensible heat flux into the urban environment.

Building and Environment, *46*(12), 2542–2551. https://doi.org/10.1016/j.buildenv.2011.06.012

Schindler, B. Y., Blaustein, L., Lotan, R., Shalom, H., Kadas, G. J., & Seifan, M. (2018). Green roof and photovoltaic panel integration: Effects on plant and arthropod diversity and electricity production. *Journal of Environmental Management*, *225*(August), 288–299. https://doi.org/10.1016/j.jenvman.2018.08.017

Shafique, M., Luo, X., & Zuo, J. (2020). Photovoltaic-green roofs: A review of benefits, limitations, and trends. *Solar Energy*, *202*(February), 485–497. https://doi.org/10.1016/j.solener.2020.02.101

Singh, R., & Banerjee, R. (2015). Estimation of rooftop solar photovoltaic potential of a city. *Solar Energy*, *115*, 589–602. https://doi.org/10.1016/J.SOLENER.2015.03.016

Slootweg, M., Hu, M., Vega, S. H., 't Zelfde, M. van, Leeuwen, E. van, & Tukker, A. (2023). Identifying the geographical potential of rooftop systems: Space competition and synergy. *Urban Forestry and Urban Greening*, *79*, 127816. https://doi.org/10.1016/j.ufug.2022.127816

Talwar, P., Verma, N., Khatri, H., Ahire, P. D., Chaudhary, G., Lindenberger, C., & Vivekanand, V. (2023). A systematic review of photovoltaic-green roof systems in different climatic conditions focusing on sustainable cities and societies. *Sustainable Cities and Society*, *98*(July), 104813. https://doi.org/10.1016/j.scs.2023.104813

Thebault, M., Clivillé, V., Berrah, L., & Desthieux, G. (2020). Multicriteria roof sorting for the integration of photovoltaic systems in urban environments. *Sustainable Cities and Society*, *60*(May), 102259. https://doi.org/10.1016/j.scs.2020.102259

Toledo, C., & Scognamiglio, A. (2021). Agrivoltaic systems design and assessment: A critical review, and a descriptive model towards a sustainable landscape vision (three-dimensional agrivoltaic patterns). *Sustainability (Switzerland)*, *13*(12). https://doi.org/10.3390/su13126871

Vargas-Salgado, C., Aparisi-Cerdá, I., Alfonso-Solar, D., & Gómez-Navarro, T. (2022). Can photovoltaic systems be profitable in urban areas? Analysis of regulation scenarios for four cases in Valencia city (Spain). *Solar Energy*, *233*(February), 461–477. https://doi.org/10.1016/j.solener.2022.01.057

Vimpari, J., & Junnila, S. (2019). Estimating the diffusion of rooftop PVs: A real estate economics perspective. *Energy*, *172*, 1087–1097. https://doi.org/10.1016/J.ENERGY.2019.02.049

Walmsley, M. R. W., Walmsley, T. G., & Atkins, M. J. (2015). Achieving 33% renewable electricity generation by 2020 in California. *Energy*, *92*(2015), 260–269. https://doi.org/10.1016/j.energy.2015.05.087

Wee, S. (2016). The effect of residential solar photovoltaic systems on home value: A case study of Hawai'i. *Renewable Energy*, *91*, 282–292. https://doi.org/10.1016/j.renene.2016.01.059

Zluwa, I., & Pitha, U. (2021). The combination of building greenery and photovoltaic energy production—a discussion of challenges and opportunities in design. *Sustainability (Switzerland)*, *13*(3), 1–29. https://doi.org/10.3390/su13031537

CHAPTER 2

EXPLORING IDEAL DESIGN PARAMETERS TO ENHANCE COOLING PERFORMANCE OF BIOSOLAR ROOF

1. Introduction

1.1 Background and Purpose

Biosolar roof systems are emerging as a promising multifunctional roofing solution as they can provide dual benefits of green and PV roof in dense urban environments. In addition to regulatory services by vegetation and clean energy opportunity, a vertical stacked structure of biosolar roof can create additional synergies, such as a longer soil moisture persistence and PV efficiency improvement (Abdalazeem et al., 2022; Talwar et al., 2023). It is regarded as a promising urban roofing solution that can promote climate change mitigation and adaptation simultaneously (Abdalazeem et al., 2022; Talwar et al., 2023).

Many cities have adopted green, solar Photovoltaic (PV), or cool roof mandates in their zoning and building codes—California's 2020 residential solar requirement, Portland's eco-roof ordinance, Phoenix's reflective-roof rules, and New York City's Sustainable Roofing Zones, to name a few (City of Portland, 2015; Razzaghi Asl, 2023; Walmsley et al., 2015). However, each was crafted for a single purpose, and few frameworks support truly integrated, multifunctional roofing. Consequently, biosolar roofs remain without clear, performance-based standards in urban policy, even as their multiple benefits continue to gain recognition (Rawat & Singh, 2022).

To date, biosolar roof studies have mainly focused on how PV elevation above vegetation affects PV yields—while a few studies paying attention to its ecological performance (Abdalazeem et al., 2022; Fleck et al., 2022; Jahanfar et al., 2019; Lamnatou & Chemisana, 2015; Talwar et al., 2023). Empirical studies consistently report that a PV height of roughly 0.5–1.5 m is ideal to balance sufficient airflow for evaporative cooling while still allowing enough light for photosynthesis (Abdalazeem et al., 2022; Talwar

et al., 2023). By contrast, PV density and PV configuration layout remain underexplored in the urban rooftop context. Agrivoltaic studies have suggested that roughly 50% of PV coverage and a checkerboard PV pattern can optimize both energy and crop yields by maximizing light uniformity and airflow (Cossu et al., 2018; Dupraz et al., 2011; Marrou et al., 2013), but these findings have yet to be validated on actual urban rooftops. Also, earlier biosolar studies recommended using drought-tolerant, low-growing species such as Sedum for plants viability and survival (Abdalazeem et al., 2022; Talwar et al., 2023). However, several scholars emphasize that species selection should be site-specific, as plants vary widely in evapotranspiration rates, shade tolerance, and cooling contributions, and these traits critically effect both vegetation health and rooftop microclimate (Bousselot et al., 2017; Lamnatou & Chemisana, 2015).

The combination of four key design parameters of biosolar roofs—PV panel height, PV density, array configuration, and plant species/spacing— effect determining the net-performance of biosolar roof. A critical unresolved question is how PV panel-induced shading, plant's evapotranspiration, and airflow between PV and vegetation layers combine to drive that performance (Zluwa & Pitha, 2021). A few earlier studies presumed that low height panel (< 0.5m) may block airflow so it would rather degrade cooling effect and PV efficiency, although clarifying this uncertain mechanism is crucial to propose a performance-based design guideline for biosolar roof.

Addressing the thermal performance of biosolar roofs is critical not only for balancing energy and ecological trade-offs at the module scale but also for mitigating urban heat islands at the city scale. Although evaporative cooling by vegetation and convective shading from PV panels clearly lowers rooftop and ambient temperatures, the coupled interactions of airflow, heat transfer, and moisture flux under a biosolar's PV canopy remain barely quantified. Panel height, spacing, and plant density jointly shape wind pathways and thermal stratification, yet their combined effect on both roof and under-panel surface temperatures is still unclear. Without this understanding, designers cannot reliably predict how a given configuration will perform in cooling buildings or alleviating neighborhood-scale heat stress, leaving a key avenue for urban climate adaptation unexplored.

In urban areas, rooftop surface temperatures are directly linked to the intensity of the Surface Urban Heat Island (SUHI) effect, making them essential indicators for evaluating rooftop-based cooling interventions. Rooftops typically occupy substantial portions of urban surfaces and frequently experience direct solar radiation, accumulating heat during the day and releasing it slowly at night (Santamouris, 2014). Consequently, measuring rooftop surface temperatures effectively captures the localized cooling potentials of different rooftop design interventions. For instance, vegetation layers on green roofs mitigate heat buildup through evapotranspiration and shading effects, significantly reducing daytime surface temperatures compared to conventional bare or gravel-covered roofs (Li et al., 2014; Santamouris, 2014). When combined with photovoltaic (PV) panels, additional shading further modifies the rooftop energy balance. The vegetation beneath PV arrays cools both the substrate and the PV panel surfaces by reducing convective and radiative heat fluxes, thus enhancing panel efficiency and thermal performance (Sailor, 2008; Scherba et al., 2011; Stewart et al., 2021). Therefore, analyzing vegetation and PV panel surface temperatures—both empirically via field experiments and computationally through simulations—provides precise insights into how biosolar roofs can alleviate rooftop heat accumulation and, ultimately, contribute to mitigating the SUHI effect at the urban scale. However, surface-temperature measurements alone can't reveal the underlying flow and heat-exchange mechanisms that drive SUHI under PV.

To investigate this coupled airflow–thermal–vegetation processes in urban canopies, scholars have adopted computational fluid dynamics (CFD) approaches. Among the tools, ENVI-met software has been widely selected because it can couple leaf- and surface-energy balances, radiative exchanges with the atmosphere, and fully three-dimensional airflow at sub-meter resolution (0.5m) at a fine scale. Researchers have used ENVI-met at neighborhood or a building scales to quantify Urban Heat Island Effect mitigation by different design scenarios of green roofs, high-albedo surfaces, or shading interventions (Crank et al., 2018; McRae et al., 2020; Nazarian & Kleissl, 2015). The studies have shown that ENVI-met can predict reliable temperature and humidity patterns by the comparison to field measurements, though some found a tendency of overprediction of temperature under high wind speed or

complex geometry conditions (Ouyang et al., 2022).

1.2 Research Frameworks

Chapter 2 aims to address the research question: *What is the optimal combination of design parameters—PV height, PV configuration, PV density, and planting density—for enhancing a biosolar roof's cooling performance?*

To answer this question, I employed a four-stage methodological approach (**Figure 2.1**). First, I developed 28 different biosolar roof scenarios by varying the combinations of four design parameters: PV height, PV configuration, PV density, and planting density. Using these scenarios, I conducted ENVI-met simulations under Eugene, Oregon, USA's climate conditions for a single diurnal cycle (9 am to 6 pm) to evaluate the cooling performance both at vegetation surfaces and around PV panel surfaces. In the next stage, to validate the simulation results, I constructed reduced-scale experimental modules and installed air temperature sensors to collect empirical data. Then, I built an additional ENVI-met 3D model mimicking these experimental modules and ran another simulation, incorporating meteorological data obtained from the University of Oregon Solar Monitoring Lab, located on the same rooftop as my experimental site. Finally, I compared the results from this second ENVI-met simulation against the field measurements to verify the accuracy and reliability of my simulation approach.

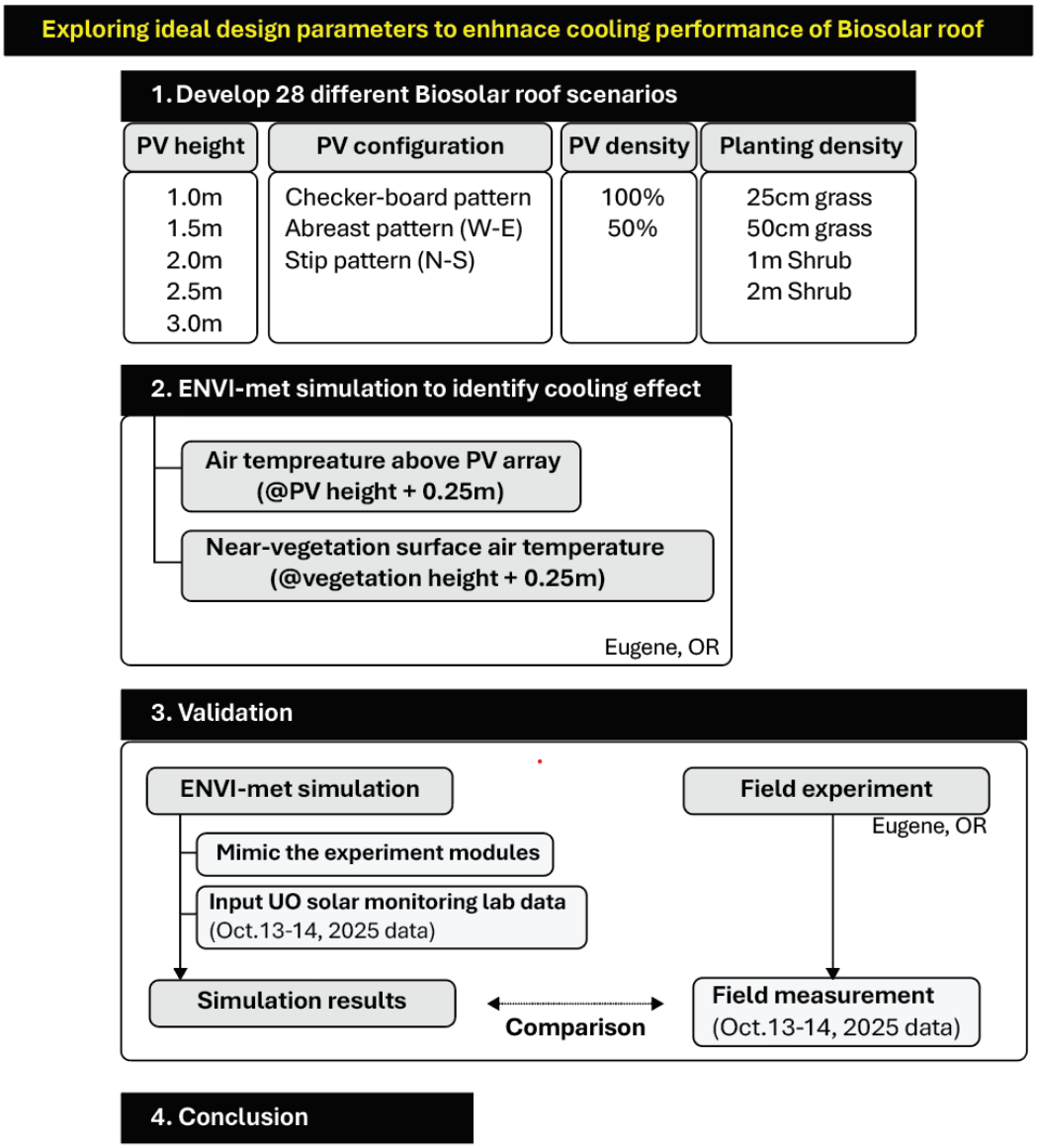


Figure 2.1 Chapter 2 research framework

2. Methods

2.1. Biosolar Roof Modeling and Composing 28 Different Design Scenarios

I used ENVI-met CFD simulation software to evaluate biosolar roof's cooling performance on microclimate. I created 3D domains of 28 different biosolar roof models with the Space tool. I set the foundational voxel grid resolution of grid to 0.5 × 0.5 × 0.5 m. Each domain measures 25 × 25 × 6 m (50 × 50 × 12 grid cells) and is geolocated at 44.05° N, 123.09° W (Eugene, Oregon) under Pacific Standard Time.

Based on Chapter 1, I selected four key biosolar-roof design parameters—PV height, PV density, array configuration, and planting density—and developed 28 distinct design scenarios as Table 2.1. Drawing on prior biosolar-roof studies, I defined five PV heights at 0.5 m intervals and two coverage levels (100 % and 50 %). For the half-density layouts, I tested three array configurations: a checkerboard pattern, an Abreast pattern (East–West row layout), and a Strip pattern (North–South column layout). To streamline the analysis, I standardized the vegetation to a perennial ryegrass with, reflecting both the extensive green roof modules used in my field experiment and the low-height sedums or grasses commonly employed on most biosolar roofs studies (Talwar et al., 2023). As ENVI-met does not directly simulate irrigation, the model assumed optimal soil moisture conditions to reflect a well-maintained green roof.

Table 2.1 28 Different biosolar roof design scenarios

Typology	PV height (m)	PV density (%)	PV configuration	Plant* density (Envi-met)
Biosolar 1	1.0m	100%	N/A	25cm Grass
Biosolar 2	1.5m			25cm Grass
Biosolar 3	2.0m			25cm Grass
Biosolar 4	2.5m			25cm Grass
Biosolar 5	3.0m			25cm Grass
Biosolar 6	1.0m	100%	N/A	50cm Grass
Biosolar 7A	1.5m	100%	N/A	50cm Grass
Biosolar 7B				1m Dense Hedge
Biosolar 8A	2.0m	100%	N/A	50cm Grass
Biosolar 8B				1m Dense Hedge
Biosolar 9A	2.5m	100%	N/A	50cm grass
Biosolar 9B				1m Dense Hedge
Biosolar 9C				2m Dense Hedge
Biosolar 10A	3.0m	100%	N/A	50cm grass
Biosolar 10B				1m Dense Hedge

Biosolar 10C				2m Dense Hedge
Biosolar 11	1.0m	50%	Checker-board Pattern	25cm Grass
Biosolar 12			Abreast pattern (W-E)	
Biosolar 13			Strip pattern (N-S)	
Biosolar 14	2.0m	50%	Checker-board pattern	25cm Grass
Biosolar 15			Abreast pattern (W-E)	
Biosolar 16			Mass pattern (N-S)	
Biosolar 17	3.0m	50%	Checker-board pattern	25cm Grass
Biosolar 18			Abreast pattern (W-E)	
Biosolar 19			Mass pattern (N-S)	
Biosolar 20	1.0m	50%	Checker-board pattern	50cm Grass
Biosolar 21			Abreast pattern (W-E)	
Biosolar 22			Mass pattern (N-S)	
Biosolar 23	2.0m	50%	Checker-board pattern	1m Dense Hedge
Biosolar 24			Abreast pattern (W-E)	
Biosolar 25			Mass pattern (N-S)	
Biosolar 26	3.0m	50%	Checker-board pattern	2m Dense Hedge
Biosolar 27			Abreast pattern (W-E)	
Biosolar 28			Mass pattern (N-S)	

2.2 ENVI-met Simulation

Simulations were conducted on August 8, 2018, from 09:00 to 18:00 local time, a nine-hour corresponding to one of the hottest recorded days in Eugene. I also employed the full-forcing method, inputting the model with the Eugene, OR EPW weather dataset. The full-forcing method applies key meteorological variables—such as air temperature, humidity, wind speed, and radiation—throughout the simulation period to closely replicate real-world conditions.

ENVI-met's simulation algorithm is organized around three coupled sub-models: the atmospheric module, the soil–vegetation module, and the radiation–surface–numerical-scheme module. During pre-processing, ENVI-met allows users to select which turbulence model, soil parameters, and radiation schemes to apply. In my simulation, I employed the Mellor–Yamada (1982) turbulence closure with a 1.5-order E–ε scheme—a widely used approach for predicting turbulent kinetic energy and its dissipation rate (McRae et al., 2020). For the soil–vegetation model, I specified a topsoil moisture content of 50% and an intermediate soil layer moisture content of 60%, reflecting an extensive green roof irrigated substrate beneath the PV array. In the radiation–surface–numerical-scheme sub-model, I set the Indexed View

Sphere resolution to Very High (5′), ensuring that reflected shortwave and longwave fluxes fully account for multiple interactions among vegetation, surfaces, and PV modules. This level of parameter specifications is critical for my study, which aims to accurately quantify net radiation beneath the PV canopy—integrating sensible and latent heat fluxes with conductive heat transfer through the soil substrate.

2.3 Simulation Data Processing and Visualization

ENVI-MET outputs a 3-D stack of two-dimensional raster images, each corresponding to a fixed height level in the model domain. These "z-profiles" are spaced according to the voxel resolution (0.5 m^3 in this case), so that scrolling through the stack in Leonardo reveals the full microclimate structure—from vegetation layer up through the PV canopy and onto the overlying air. Each raster cell, indexed by its (x, y) coordinates, contains the complete suite of prognostic variables (air temperature, relative humidity, wind-vector components, etc.), allowing both spatial mapping and point-wise time series extraction. I extracted near-surface air temperatures at two specific heights—0.25 m above the vegetation layer and 0.25 m above the PV array—for each of the 28 biosolar design scenarios.

2.4 Validating the Simulation Results with Field Measurements

To validate the ENVI-met simulations (**Figure 2.2**), I installed a small-scale biosolar-roof testbed on the rooftop of Pacific Hall at the University of Oregon. The field installation comprised a 6 ft × 6 ft array of PV modules mounted over a complete green roof substrate. Over two days (October 13–14, 2024), I deployed paired air-temperature sensors (HOBO Pro v2) at two locations within the testbed—directly under the PV canopy and in an adjacent, unshaded area—both positioned 0.25 m above the soil surface. Sensors logged data every 30-seconds and aggregated to 1-minute intervals to capture both the convective shading by the PV array and the evaporative cooling from the grass layer. This field experiment will be

articulated in Chapter 4 with more details.

Each day's field measurements were directly compared with ENVI-met outputs driven by the same weather data collected by the UO Solar Monitoring Lab—fully forcing the model's boundary conditions (temperature, humidity, wind speed and direction, and global radiation). I also created an additional ENVI-met Model that exactly replicates the testbed's geometry at actual scale. Then, I extracted simulated air-temperature time series at the exact sensor heights and locations. Finally, I compared simulation results and observed temperatures from 09:00 to 18:00 LST on October 13 and 14 for the validation and evaluated their statistical significance of any differences between the simulations and measurements.

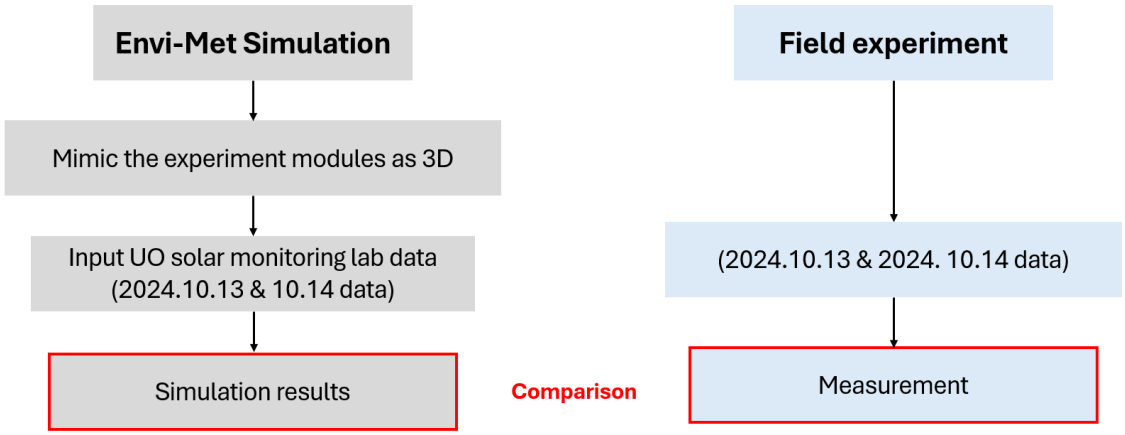


Figure 2.2 Validation process

3. Results

3.1 Air Temperature Simulation Results at Near-Vegetation Under PV Array

Sections 3.1 and 3.2 present findings derived solely from ENVI-met simulations. Empirical field data are used in Section 3.3 for simulation validation.

3.1.1 Effect of PV Height On Near-Vegetation Surface Air Temperature

A very subtle cooling effect appeared as PV canopy height increased. When we varied only the PV heights (Types 1–5), mean near-vegetation air temperatures fell by barely 0.1 °C. Similarly, varied PV height scenarios at half PV density (Types 11–19) showed very minimal air temperature differences of less than 0.1 °C—as represented in **Figure 2.3**. Given ENVI-met's limited spatial resolution (0.5m) and the inability to adjust PV tilt, this temperature change is too small to support any firm conclusion that taller PV arrays improve cooling performance. Even if this slight trend might tentatively suggest that increased overhead space under PV arrays can modestly enhance microclimate cooling, confirming this hypothesis will require more robust investigations or direct measurements.

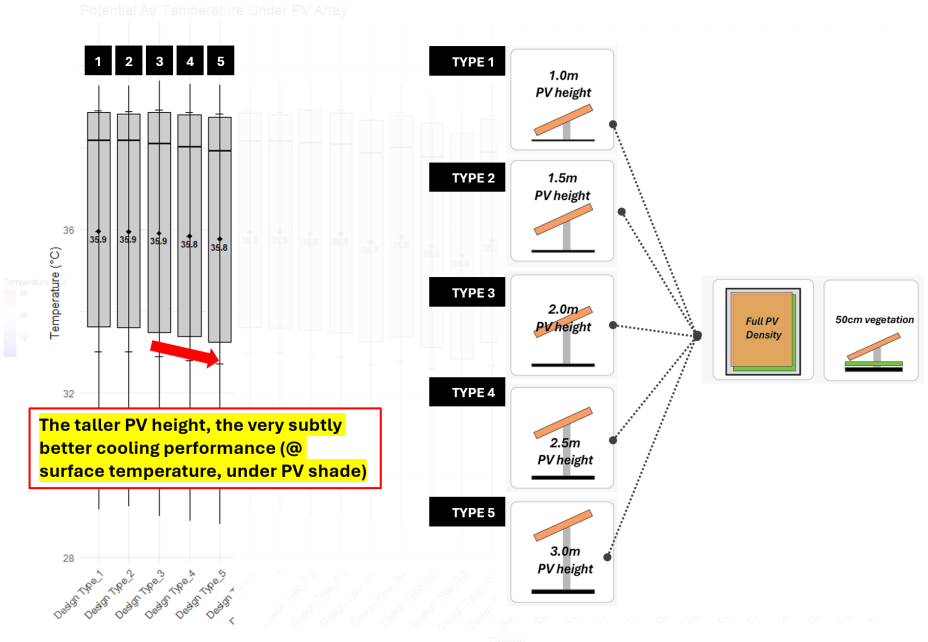


Figure 2.3 Boxplot comparison of near-vegetation air temperature under different PV heights (1.0 m–3.0 m)

3.1.2 Effect of PV Density on Near-Vegetation Surface Air Temperature

Scenarios configured with full PV density arrays (Types 1–8C) showed that mean near-vegetation air temperatures were 0.7 °C lower than those recorded for half PV density arrays (Types 12–28) —as represented in **Figure 2.4**. In a full-density canopy, a larger fraction of incoming solar radiation is blocked, creating more shaded areas over the vegetation layer. This increased shaded area drives the overall drop in mean near-vegetation air temperature, compared to half PV density cases. This finding is consistent with earlier studies linking greater shade coverage to enhanced rooftop heat mitigation (Irga et al., 2021; Teng et al., 2022).

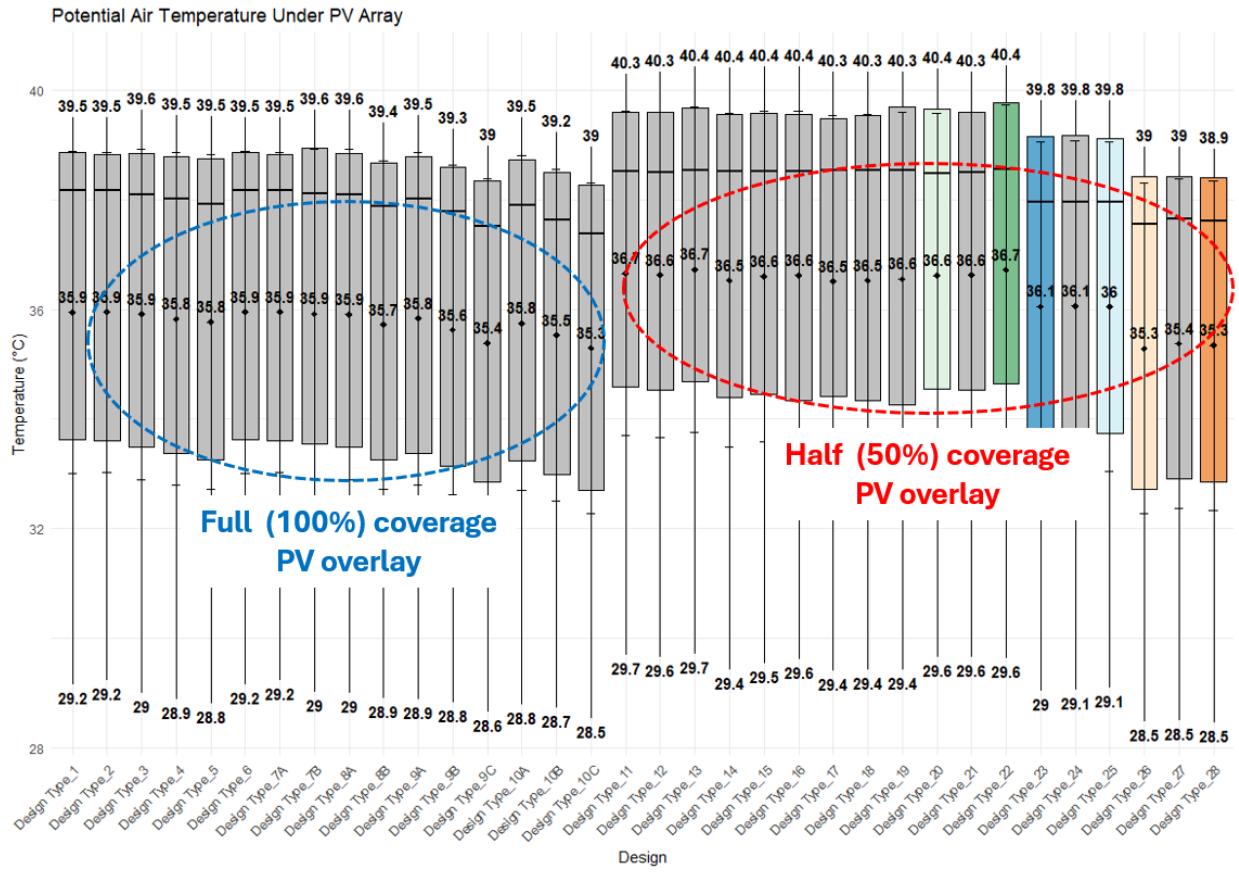


Figure 2.4 Boxplot comparison of near-vegetation air temperature under full (100%) versus half (50%) PV coverage conditions

3.1.3 Effect of Planting Density on Near-Surface Air Temperature

Higher vegetation density resulted in better cooling performance. Scenarios featuring dense planting—specifically Types 23–25, 26–28, 9A–9C, and 10A–10C—consistently showed a decreasing trend in near-vegetation air temperature as plant density increased, with average reductions of 0.3 °C under full PV density and 0.6 °C under half PV density. This outcome aligns with the general findings that plants' evapotranspiration contributes to enhance cooling effect more than shade density (Talwar et al., 2023).

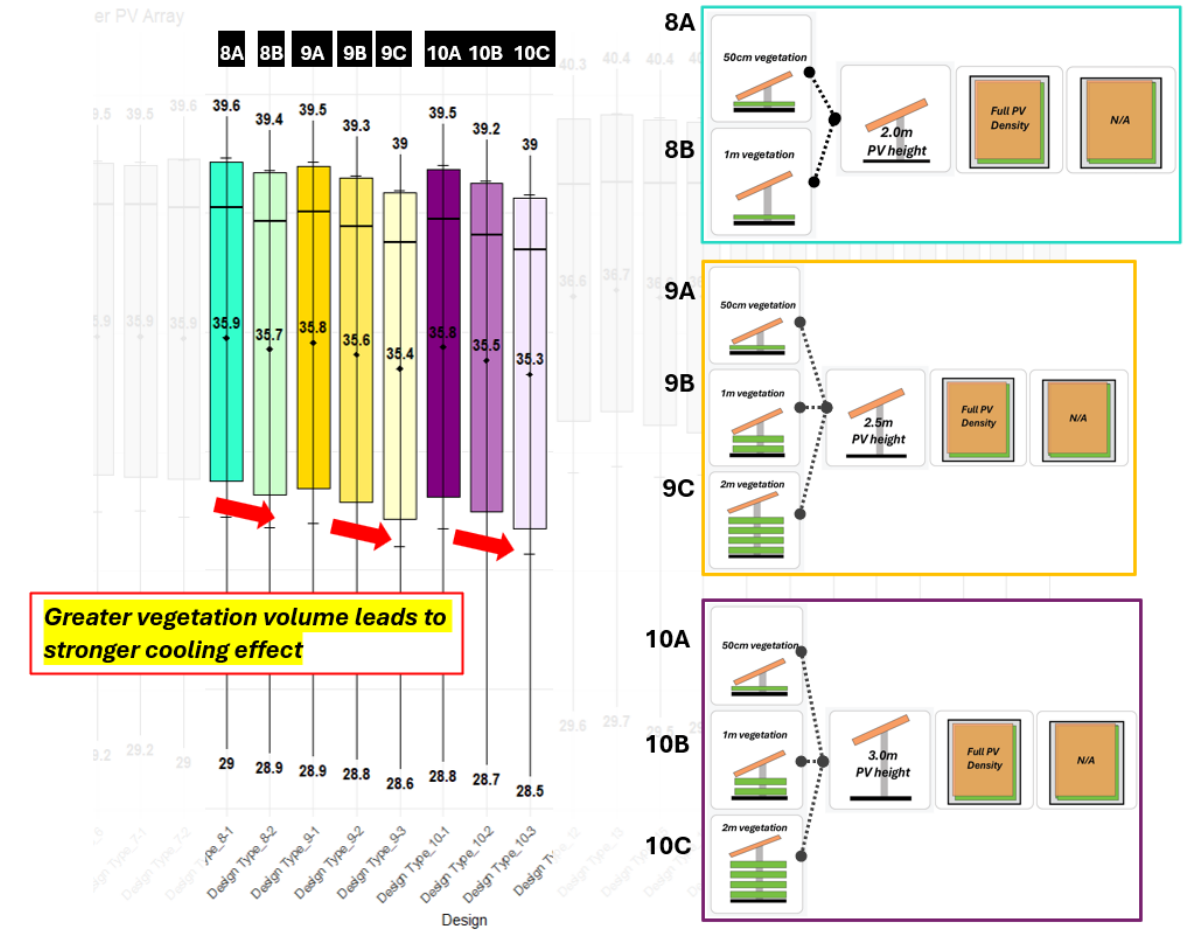


Figure 2.5 Boxplot comparison of biosolar roof designs (Designs 8A–10C) with varying vegetation heights under consistent PV settings (full PV density and fixed configuration)

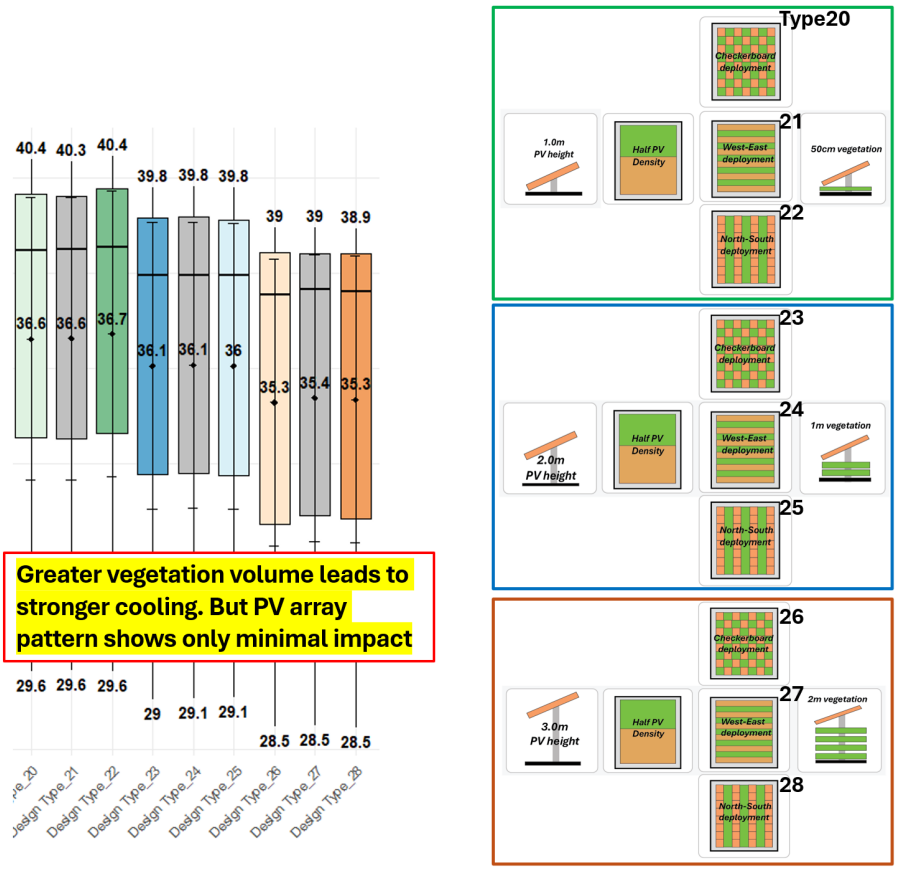


Figure 2.6 Comparison of additional design variations (Designs 20–28) that combine changes in vegetation height with different PV array configurations (row spacing and East–West orientation) under half PV density

3.1.4 Effect of PV Configuration on Near-Surface Air Temperature

PV panel configuration had only a marginal effect on near-vegetation air temperatures: we observed no meaningful cooling differences among the three layouts—checkerboard, abreast (east–west), and strip (north–south). From a geometric standpoint in the real world, the strip (north–south orientation) pattern might carry a higher risk of self-shading, as solar radiation moves southward across the sky in the Northern Hemisphere, in the strip pattern, each row of panels can cast a shadow onto its neighbor, not only reducing the panels' energy yield but also creating uneven light conditions for the plants below. Also, avoiding this self-shading would require increased row spacing, which in turn reduces the total number of panels that can be installed compared to the checkerboard or abreast (east–west) configurations.

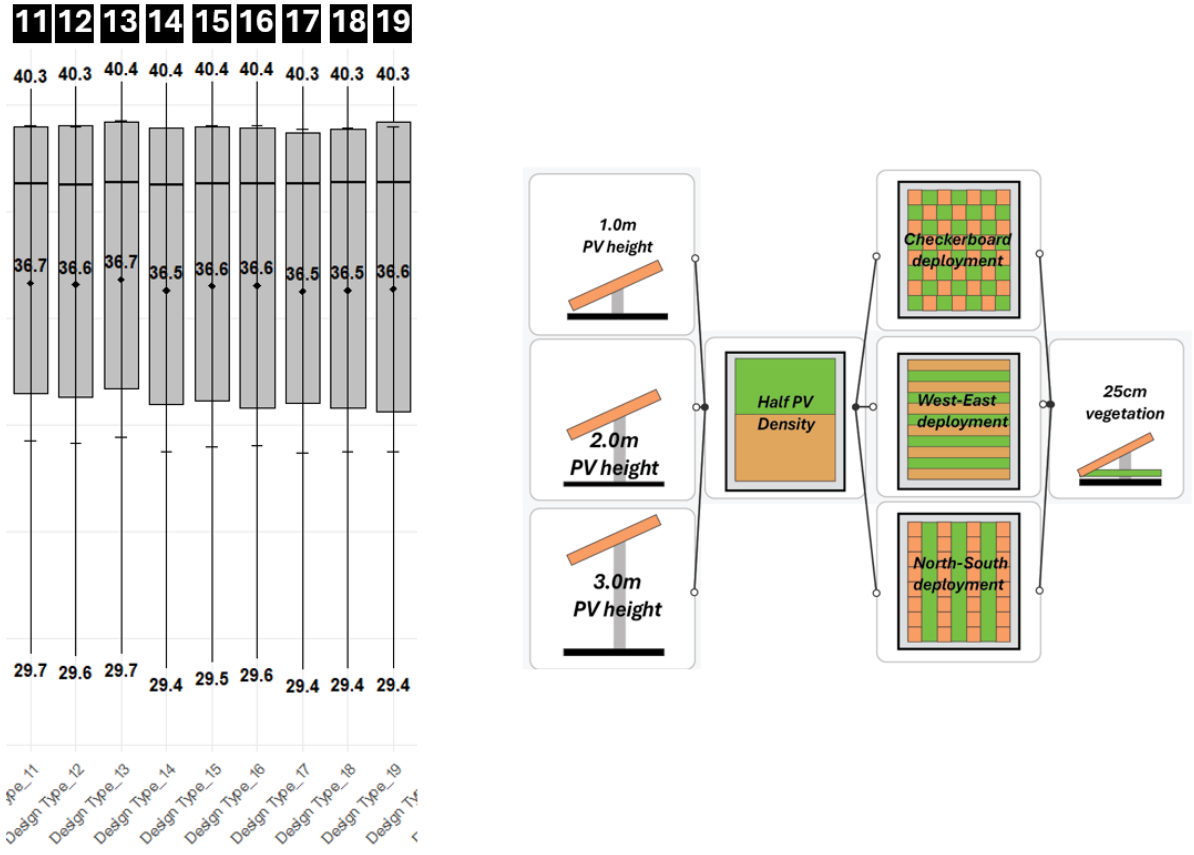


Figure 2.7 Boxplot comparison of near-vegetation air temperature under various PV configuration patterns

3.2 Air Temperature Simulation Results Above PV Panel

In the 28 biosolar roof simulations (**Figure 2.8**), near-PV panel air temperatures[1] were consistent at about 36.0 °C—except in six outlier scenarios (Types 11, 12, 13, 20, 21, and 22), where peaks reached 36.3 °C. All six outliers shared a 1 m PV height, 50% PV density, and sparse planting (25 cm or 50 cm spacing). Reduced shading and proximity to the rooftop surface increased heat radiation from the roof, warming the air above the panels compared to the full PV density scenarios. Also, this pattern might suggest a threshold effect: planting densities taller than roughly 50 cm may supply enough leaf area and evapotranspiration opportunity, which begin offsetting the microclimate warming but such planting biomass levels will often require irrigation through dry seasons. Given that this magnitude is very subtle, a further in-depth analysis may be required by including airflow pathways, convective heat exchange, or canopy–air coupling which probably may underlie these differences, in finer spatial resolution (less than 0.5 m) and longer simulation durations.

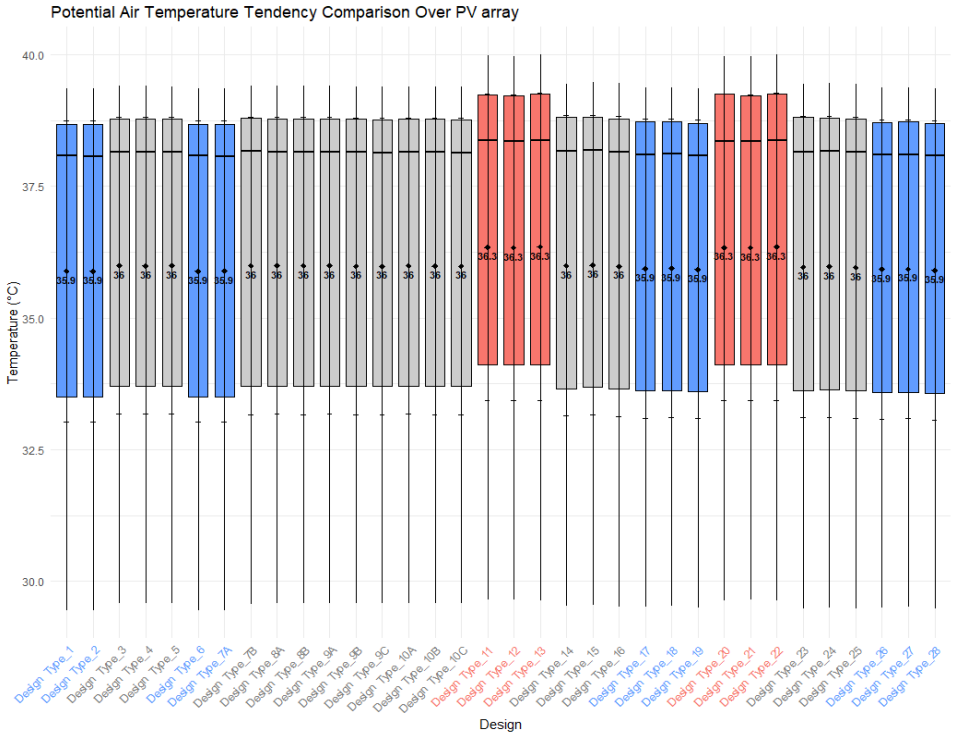


Figure 2.8 Potential air temperature tendency comparison over PV array

[1] The air temperature at above PV panels (Each PV height + 0.25m)

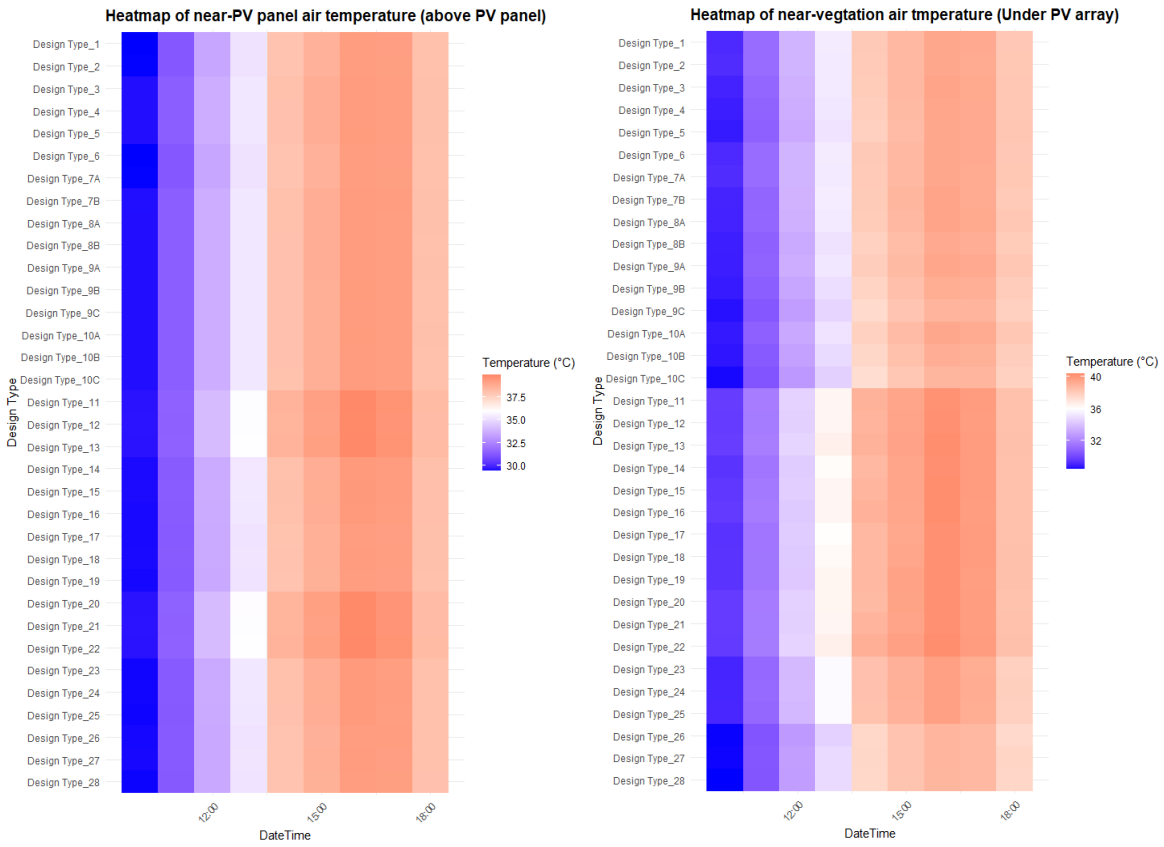


Figure 2.9 Heatmaps in both under and above PV array

3.3 Simulation Validation

This section shifts from simulation-based findings to empirical field measurements to assess how well the simulation model represents real-world biosolar roof conditions. Additional details of the field experiment will be provided in Chapter 4.

Figure 2.10 shows the comparison between the measurement and ENVI-met–predicted air temperatures for three roof typologies—concrete, biosolar (non-shaded area), and biosolar (under shaded area)—monitored on 13–14 October between 10:00 and 18:00. The concrete roof recorded the highest daytime temperatures—peaking at 29.4 °C on 13 October and 28.9 °C on 14 October—and its measured near-surface air temperatures consistently exceeded the ENVI-met model's predictions during peak solar hours.

By contrast, in all biosolar scenarios, the ENVI-met model consistently over-predicted near-vegetation air temperatures compared to field measurements. This contrasts with prior ENVI-met studies, which often report that the model overestimates the cooling effect of vegetation—particularly under intense radiation and wind-still conditions (Liu et al., 2024; Tsoka et al., 2018). However, those earlier studies focused on simple greenery (grasses and shrubs) without the additional influence of PV shading (Liu et al., 2024; Tsoka et al., 2018). The presence of a PV canopy introduces a distinct thermal dynamic that complicates energy balance modeling beneath. In our case, we not only modeled the PV structure but also input on-site wind data, which may have complicated the energy balance calculations under shaded vegetation. It's possible that ENVI-met underestimated the cooling contribution of evapotranspiration under this ventilation and shading conditions, resulting in warmer simulated near vegetation air temperatures than those observed. As a result, the model–measurement discrepancy was most pronounced in the shaded zones. While modeled and measured peaks were closely aligned in the unshaded portion (27.6 °C vs. 27.1 °C), the shaded portion exhibited a notable gap of 3–4 °C as shown in Figure 2.6—specifically in the graphs for the shaded area of the biosolar roof.

Statistical correlation between simulation versus experiment also supports these patterns. For the concrete roof, the simulated results showed a moderate level of agreement with its field measurement ($r = 0.78$, slope = 0.87, RMSE = 3.11 °C), reflecting substantial heat retention near the surface. The non-shaded biosolar roof showed a slightly stronger correlation ($r = 0.81$) but a lower slope (0.71) and reduced RMSE (1.50 °C), indicating effective thermal mitigation. The shaded biosolar area showed the lowest slope (0.70) and an RMSE of 2.78 °C; despite the larger error, its absolute temperatures were the lowest of all cases, which may mean that the additional cooling effect resulted from PV shade and vegetation.

Overall, these field measurements validate the simulation trend regarding biosolar roofing. These findings support the promotion and adoption of multifunctional green infrastructure solutions within urban environments to mitigate urban heat island effects and enhance urban resilience. Rather than pointing to a limitation of the simulation, the results emphasize the real-world potential of biosolar roofs to provide substantial thermal benefits when carefully designed. They also reinforce the importance of refining key design parameters—such as PV height, spacing, and planting density—to fully harness the synergistic cooling effects of vegetation and shading in practical applications.

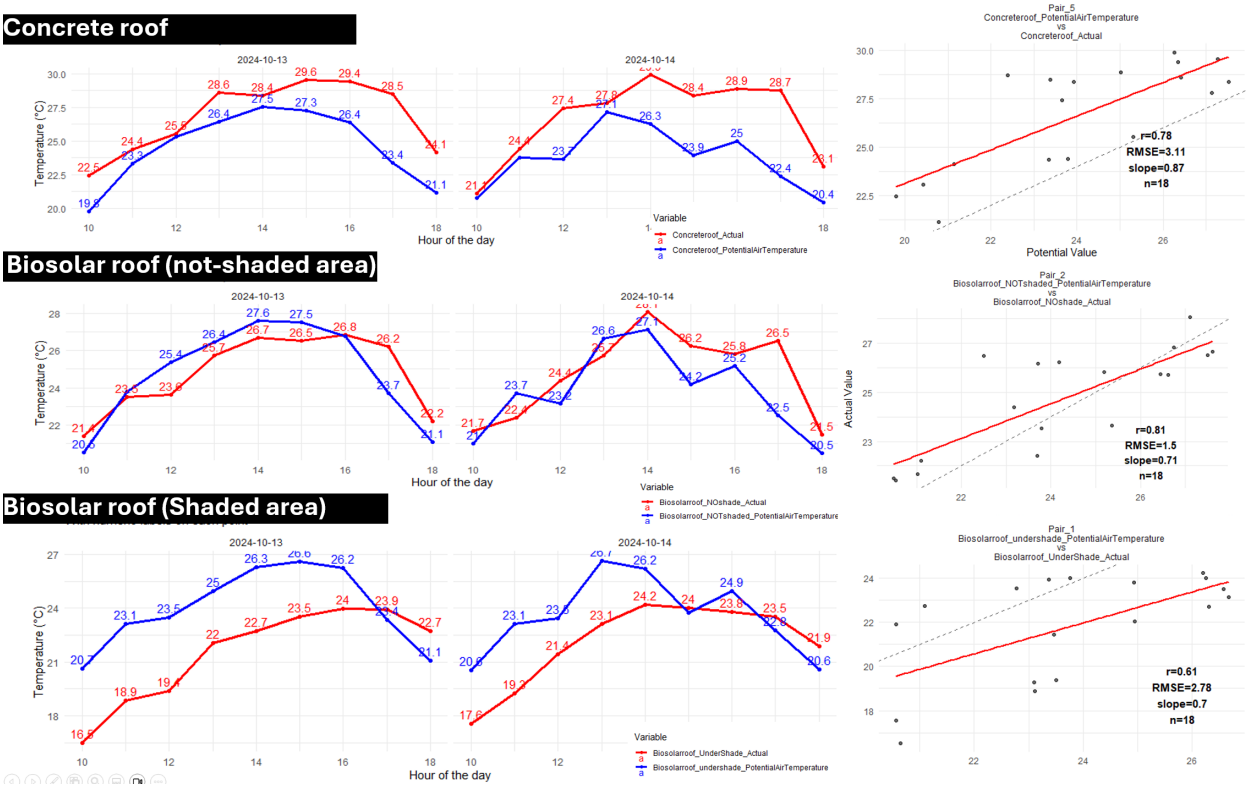


Figure 2.10 Comparison between field measurement and ENVI-met simulation and their statistical significance. Red lines mean field measured temperature, blue line means the predicted temperature

4. Discussion

The simulation and field results together suggest clear design directions for enhancing the cooling performance of biosolar roofs. Rather than one dominant factor, the interaction among PV height, PV density, PV configuration, and planting density emerged as central to shaping the microclimate of biosolar roof. Specifically, full PV density consistently led to greater reductions in near-vegetation air temperature by providing broader shading coverage. Densely planted vegetation provides increased cooling effect by plants' evapotranspiration. However, not all parameters contributed equally to cooling. The effects of PV height and configuration were relatively minor within the resolution of the simulation.

Nevertheless, these elements may still play a meaningful role in broader system performance when considered alongside other practical design goals such as plant viability, rooftop usability, and long-term maintenance. For example, while high PV density enhances shading and cooling, it also introduces the risk of excessive shading that may compromise vegetation viability. In this context, a checkerboard PV layout can offer a useful compromise—maintaining sufficient solar access for the vegetation while distributing shading more evenly across the roof. Since this research found that there was no significant temperature difference among three PV patterns, designers may instead choose configurations based on their primary objectives. For example, a dense PV array might be preferred to maximize solar energy production as well as to protect plants from intense radiation in hot and dry climates, whereas more opened PV layouts with checkerboard patterns could be preferred in mild climate conditions to support better plant growth and balanced PV yields. This flexibility reinforces the value of adapting biosolar roof designs to site-specific goals—balancing energy yield, plant health, and climate resilience. These trade-offs, particularly in relation to different climatic contexts, will be further examined in the next chapter.

Despite the growing body of research on biosolar (PV-green) roofs, plant species selection remains an underexplored variable (Abdalazeem et al., 2022; Talwar et al., 2023). Existing studies tend to recommend broadly defined shade- and drought-tolerant plant species such as Sedum or other low-

growing succulents—due to their ability to survive in shallow substrates, with limited irrigation, and under the hot, dry microclimatic conditions often found on rooftops (Lamnatou & Chemisana, 2015; Talwar et al., 2023). However, such guidance is often overly generic and fails to address region-specific climate conditions, biodiversity considerations, or the additional complexity introduced by partial shading from PV arrays. Emerging empirical evidence suggests that PV shading may enhance above-ground biomass in certain turf and forage grasses by moderating leaf temperatures and reducing evapotranspiration stress (Bousselot et al., 2017). This promising interaction should be further investigated across diverse climate zones and shade areas. Additionally, the use of indigenous plant species may offer multiple benefits, including improved survivability, reduced irrigation demand, resilience against local pests, and support for urban biodiversity (Schindler et al., 2018)—all of which may contribute to long-term ecological performance and reduced maintenance costs. Therefore, future research should move beyond generalized recommendations and focus on developing evidence-based planting palettes tailored to local climate conditions, substrate depth, and PV-shade geometry. Long-term monitoring of variables such as biomass production, survivability, and ecosystem service delivery under different planting strategies will be essential for refining biosolar roof design guidelines and realizing their full multifunctional potential in dense urban environments.

A technical limitation of this chapter lies in its heavy reliance on ENVI-met CFD simulation software. While ENVI-met is widely recognized among landscape scholars as a robust tool for assessing microclimatic thermal performance in the way of CFD (Berardi & Graham, 2020; Makido et al., 2019; McRae et al., 2020; Tsoka et al., 2018), it only provides limited settings of PV panel tilts—perpendicular or parallel to the ground surface—not allowing varying its tilted angles. Also, the 0.5 m grid resolution—though often considered sufficiently detailed in neighborhood scale urban microclimate applications (McRae et al., 2020)—may still be seen as relatively coarse given that at rooftop scales each module of the actual experiment has the scale of 2 m in width or length. This grid size may restrict elaborate analysis on a finer scale, limiting the model's ability to capture finer-scale processes that may occur within smaller

portions of the rooftop system.

While the modeling limitations may limit the precision of ENVI-met predictions at small scales, they would not diminish the overall significance of simulation in guiding biosolar roof design. In fact, the comparison between simulated and measured temperatures provided in this chapter reveals meaningful insights into real-world biosolar roof performance. While previous studies noted ENVI-met's tendency to overestimate vegetation cooling, especially under wind-still or high-radiation conditions, this study found the opposite: the model underestimated cooling under the shaded biosolar zone, where measured air temperatures were 3–4 °C lower than predicted. This may ironically highlight the importance of field-based calibration and site-specific refinement, especially when modeling complex canopy-vegetation interactions.

This discrepancy also suggests that current modeling tools may systematically underestimate the compound cooling effects generated by vegetation and PV shading, especially under dynamic lighting conditions and convective airflow by PV canopy. Although wind data and PV structures were reflected in the simulation inputs, the model may still oversimplify how evapotranspiration interactions with shade-induced temperature gradients. For example, fixed PV tilt settings and uniform soil parameters in ENVI-met likely limited its ability to replicate microclimatic feedbacks—such as increased soil moisture persistence or intensified convective cooling under the PV canopy. On the other hand, the discrepancy demonstrates how real-world biosolar configurations may outperform modeled expectations under certain conditions. This highlights the importance of considering subtle design parameters adjustment—like PV height and configuration—not just as fixed inputs for modeling, but as flexible variables in the design process.

Ultimately, this finding suggests that simulation tools should be interpreted as generative approximations rather than precise predictors. Their true strength lies in guiding early-stage exploration without demanding significant upfront time or cost, becoming even more powerful when refined through empirical feedback from site-specific data. Together, simulations paired with validation create an iterative

framework that can identify climate-responsive biosolar roof systems. However, recognizing that real-world projects often have limited resources for extensive experimentation, simulation tools themselves must evolve to provide more reliable initial guidance. Thus, enhancing model accuracy and context-sensitive calibration will be critical to expanding the practical utility and reliability of simulation in biosolar roof design practice.

5. Conclusion

Chapter 2 provides a comprehensive evaluation of the cooling performance of biosolar roofs by systematically varying PV and planting design parameters. The results underscore that no single factor drives microclimate cooling. Instead, the interaction among PV density, planting density, height, and configuration collectively shapes thermal outcomes. Among these, full PV density and dense vegetation were the most influential in reducing near vegetation air temperatures—primarily through enhanced shading and evapotranspiration. Meanwhile, PV height and layout had only marginal effects within the simulation's spatial resolution. Validation with field data further confirmed the model's ability to reflect general cooling trends, while also revealing its limitations in modeling shaded conditions.

Future studies should refine planting strategies under PV shade and develop region-specific palettes that align with climate. Further modeling improvements—including finer spatial resolution and enhanced PV geometry settings—will also be critical in advancing evidence-based design guidance for biosolar roofs as resilient urban infrastructure.

References

Abdalazeem, M. E., Hassan, H., Asawa, T., & Mahmoud, H. (2022). Review on integrated photovoltaic-green roof solutions on urban and energy-efficient buildings in hot climate. *Sustainable Cities and Society*, *82*(April), 103919. https://doi.org/10.1016/j.scs.2022.103919

Berardi, U., & Graham, J. (2020). Investigation of the impacts of microclimate on PV energy efficiency and outdoor thermal comfort. *Sustainable Cities and Society*, *62*. https://doi.org/10.1016/J.SCS.2020.102402

Bousselot, J., Slabe, T., Klett, J., & Koski, R. (2017). Photovoltaic Array Influences the Growth of Green Roof Plants. *Journal of Living Architecture*, *4*(3), 9–18. https://doi.org/10.46534/jliv.2017.04.03.009

City of Portland. (2015). *33.510 Central City Plan District*. 510-1-510–168. http://www.portlandonline.com/shared/cfm/image.cfm?id=53363

Cossu, M., Cossu, A., Deligios, P. A., Ledda, L., Li, Z., Fatnassi, H., Poncet, C., & Yano, A. (2018). Assessment and comparison of the solar radiation distribution inside the main commercial photovoltaic greenhouse types in Europe. *Renewable and Sustainable Energy Reviews*, *94*(March), 822–834. https://doi.org/10.1016/j.rser.2018.06.001

Crank, P. J., Sailor, D. J., Ban-Weiss, G., & Taleghani, M. (2018). Evaluating the ENVI-met microscale model for suitability in analysis of targeted urban heat mitigation strategies. *Urban Climate*, *26*(July), 188–197. https://doi.org/10.1016/j.uclim.2018.09.002

Dupraz, C., Marrou, H., Talbot, G., Dufour, L., Nogier, A., & Ferard, Y. (2011). Combining solar photovoltaic panels and food crops for optimising land use: Towards new agrivoltaic schemes. *Renewable Energy*, *36*(10), 2725–2732. https://doi.org/10.1016/j.renene.2011.03.005

Fleck, R., Gill, R., Pettit, T. J., Torpy, F. R., & Irga, P. J. (2022). Bio-solar green roofs increase solar energy output: The sunny side of integrating sustainable technologies. *Building and Environment*, *226*(August), 109703. https://doi.org/10.1016/j.buildenv.2022.109703

Irga, P., Fleck, R., Wooster, E., Torpy, F., Pettit, T., Gill, R., & Ball, J. (2021). *Green Roof & Solar Array Comparative Research Project Final Report July 2021*. City of Sydney Council.

Jahanfar, A., Drake, J., Sleep, B., & Margolis, L. (2019). Evaluating the shading effect of photovoltaic panels on green roof discharge reduction and plant growth. *Journal of Hydrology*, *568*(October 2018), 919–928. https://doi.org/10.1016/j.jhydrol.2018.11.019

Lamnatou, C., & Chemisana, D. (2015). A critical analysis of factors affecting photovoltaic-green roof performance. *Renewable and Sustainable Energy Reviews*, *43*, 264–280. https://doi.org/10.1016/j.rser.2014.11.048

Li, D., Bou-Zeid, E., & Oppenheimer, M. (2014). The effectiveness of cool and green roofs as urban heat island mitigation strategies. *Environmental Research Letters*, *9*(5). https://doi.org/10.1088/1748-9326/9/5/055002

Liu, S., Middel, A., Fang, X., & Wu, R. (2024). ENVI-met model performance evaluation for courtyard simulations in hot-humid climates. *Urban Climate*, *55*(April 2023), 101909. https://doi.org/10.1016/j.uclim.2024.101909

Makido, Y., Hellman, D., & Shandas, V. (2019). Nature-based designs to mitigate urban heat: The efficacy of green infrastructure treatments in Portland, Oregon. *Atmosphere*, *10*(5). https://doi.org/10.3390/atmos10050282

Marrou, H., Guilioni, L., Dufour, L., Dupraz, C., & Wery, J. (2013). Microclimate under agrivoltaic systems: Is crop growth rate affected in the partial shade of solar panels? *Agricultural and Forest Meteorology*, *177*(August), 117–132. https://doi.org/10.1016/j.agrformet.2013.04.012

McRae, I., Freedman, F., Rivera, A., Li, X., Dou, J., Cruz, I., Ren, C., Dronova, I., Fraker, H., & Bornstein, R. (2020). Integration of the WUDAPT, WRF, and ENVI-met models to simulate extreme daytime temperature mitigation strategies in San Jose, California. *Building and Environment*, *184*(August), 107180. https://doi.org/10.1016/j.buildenv.2020.107180

Mellor, G. L., & Yamada, T. (1982). Development of a turbulence closure model for geophysical fluid problems.

Reviews of Geophysics, *20*(4), 851–875.

Nazarian, N., & Kleissl, J. (2015). CFD simulation of an idealized urban environment: Thermal effects of geometrical characteristics and surface materials. *Urban Climate*, *12*, 141–159. https://doi.org/10.1016/j.uclim.2015.03.002

Ouyang, W., Sinsel, T., Simon, H., Morakinyo, T. E., Liu, H., & Ng, E. (2022). Evaluating the thermal-radiative performance of ENVI-met model for green infrastructure typologies: Experience from a subtropical climate. *Building and Environment*, *207*(PB), 108427. https://doi.org/10.1016/j.buildenv.2021.108427

Rawat, M., & Singh, R. N. (2022). A study on the comparative review of cool roof thermal performance in various regions. *Energy and Built Environment*, *3*(3), 327–347. https://doi.org/10.1016/j.enbenv.2021.03.001

Razzaghi Asl, S. (2023). Rooftops for Whom? Some Environmental Justice Issues in Urban Green Roof Policies of Three North American Cities. *Environmental Policy and Law*, *53*(1), 49–60. https://doi.org/10.3233/EPL-220015

Sailor, D. J. (2008). A green roof model for building energy simulation programs. *Energy and Buildings*, *40*(8), 1466–1478. https://doi.org/10.1016/j.enbuild.2008.02.001

Santamouris, M. (2014). Cooling the cities - A review of reflective and green roof mitigation technologies to fight heat island and improve comfort in urban environments. *Solar Energy*, *103*, 682–703. https://doi.org/10.1016/j.solener.2012.07.003

Scherba, A., Sailor, D. J., Rosenstiel, T. N., & Wamser, C. C. (2011). Modeling impacts of roof reflectivity, integrated photovoltaic panels and green roof systems on sensible heat flux into the urban environment. *Building and Environment*, *46*(12), 2542–2551. https://doi.org/10.1016/j.buildenv.2011.06.012

Schindler, B. Y., Blaustein, L., Lotan, R., Shalom, H., Kadas, G. J., & Seifan, M. (2018). Green roof and photovoltaic panel integration: Effects on plant and arthropod diversity and electricity production. *Journal of Environmental Management*, *225*(August), 288–299. https://doi.org/10.1016/j.jenvman.2018.08.017

Stewart, I. D., Krayenhoff, E. S., Voogt, J. A., Lachapelle, J. A., Allen, M. A., & Broadbent, A. M. (2021). Time Evolution of the Surface Urban Heat Island. *Earth's Future*, *9*(10). https://doi.org/10.1029/2021EF002178

Talwar, P., Verma, N., Khatri, H., Ahire, P. D., Chaudhary, G., Lindenberger, C., & Vivekanand, V. (2023). A systematic review of photovoltaic-green roof systems in different climatic conditions focusing on sustainable cities and societies. *Sustainable Cities and Society*, *98*(July), 104813. https://doi.org/10.1016/j.scs.2023.104813

Teng, J. W. C., Soh, C. B., Devihosur, S. C., Tay, R. H. S., & Jusuf, S. K. (2022). Effects of Agrivoltaic Systems on the Surrounding Rooftop Microclimate. *Sustainability (Switzerland)*, *14*(12), 1–13. https://doi.org/10.3390/su14127089

Tsoka, S., Tsikaloudaki, A., & Theodosiou, T. (2018). Analyzing the ENVI-met microclimate model's performance and assessing cool materials and urban vegetation applications–A review. *Sustainable Cities and Society*, *43*(April), 55–76. https://doi.org/10.1016/j.scs.2018.08.009

Walmsley, M. R. W., Walmsley, T. G., & Atkins, M. J. (2015). Achieving 33% renewable electricity generation by 2020 in California. *Energy*, *92*(2015), 260–269. https://doi.org/10.1016/j.energy.2015.05.087

Zluwa, I., & Pitha, U. (2021). The combination of building greenery and photovoltaic energy production—a discussion of challenges and opportunities in design. *Sustainability (Switzerland)*, *13*(3), 1–29. https://doi.org/10.3390/su13031537

CHAPTER 3

COMPARATIVE ENVIRONMENTAL PERFORMANCE OF BIOSOLAR ROOF ACROSS THREE CLIMATE ZONES

1.Introduction

1.1. Background

Biosolar roofs have gained attention as a multifunctional strategy for sustainable urban design. However, current research remains fragmented and largely limited in scope (Pan et al., 2024). A notable gap in the literature is the lack of comparative studies that systematically evaluate biosolar roofs alongside alternative rooftop strategies, such as green roofs, PV roofs, and conventional concrete roofs (Abdalazeem et al., 2022; Shafique et al., 2020; Talwar et al., 2023). While it is commonly assumed that integrating vegetation and photovoltaic (PV) arrays can yield various synergistic benefits, only a few studies have empirically verified this (Fleck et al., 2022; Irga et al., 2021; Jahanfar et al., 2019; Lamnatou & Chemisana, 2015). Consequently, the magnitude of these integrated benefits—particularly rooftop cooling, stormwater management, solar energy potential, and impact on building energy load—remain poorly understood. Without systematic, comparative benchmarks, it becomes difficult to determine under what conditions biosolar roofs can outperform other roofing alternatives such as standalone PV, green, or typical concrete roof (Shafique et al., 2020). This lack of clear evidence makes it harder for designers and decision-makers to compare options and choose the most effective roof system (Kelly et al., 2020).

Moreover, most existing studies on biosolar roofs have focused on single performance metrics, such as surface cooling or PV output, without capturing the biosolar roof's full range of environmental performance (Chemisana & Lamnatou, 2014; Sattler et al., 2020; Talwar et al., 2023). Few investigations have holistically assessed multiple key factors at the same time, such as microclimate regulation,

stormwater performance, building energy demand, and solar energy generation within the same rooftop footprint (Irga et al., 2021; Jahanfar et al., 2018). A more comprehensive approach is imperative to draw conclusions about how biosolar systems perform as a unified strategy in real-world conditions. In particular, little is known about how the performances of biosolar roofs varies across different climate zones, and it remains unclear which climatic contexts are most suitable for their implementation (Abdalazeem et al., 2022; Talwar et al., 2023). A comparative assessment across climate zones will enable development of climate-specific design strategies or prioritize regions where biosolar systems would be most beneficial.

Understanding the rooftop surface energy balance is essential to interpret biosolar roof performance in a comparative context (Ogaili & Sailor, 2016; Sailor, 2008; Scherba et al., 2011). As **Figure 3.1** describes, on a conventional concrete roof, most incoming solar radiation is absorbed as sensible heat, which is then conducted downward into the building or released back to the atmosphere at night—contributing to both indoor overheating and urban heat island effects. In contrast, PV panels intercept this energy, converting a portion into electricity and reducing direct heat gain. When vegetation is introduced under PV arrays, as biosolar roofs, the surface energy dynamics shift even further. Plants dissipate radiation through evapotranspiration, converting sensible heat into latent heat flux and thereby disrupting the conduction pathway into the building interior (Ogaili & Sailor, 2016; Sailor, 2008; Scherba et al., 2011). This dual process—radiation interception and latent cooling—not only moderates rooftop and indoor temperatures but also can reduce total HVAC energy demand throughout the day and night. Thus, biosolar roofs can become a thermodynamically strategic intervention, with the potential to maximize energy efficiency through surface energy redistribution.

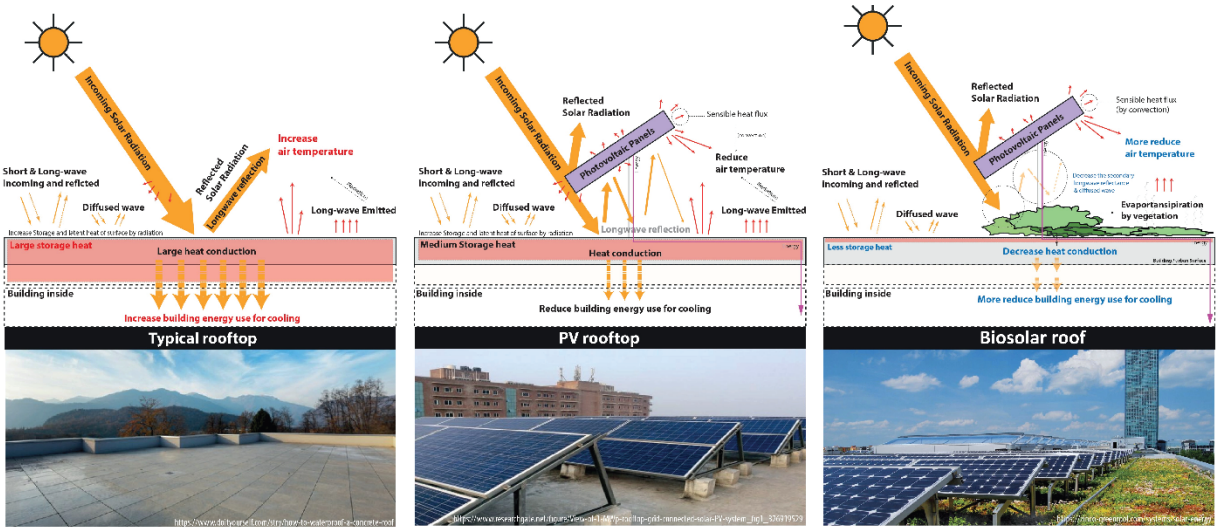


Figure 3.1 Rooftop energy balance comparison between plain rooftop, PV rooftop, and biosolar roof (adopted from Ogali & Sailor (2016) and improved)

This chapter aims to conduct a comprehensive performance evaluation of biosolar roofs by comparing them with three conventional rooftop typologies—green roofs, PV roofs, and concrete roofs—across three distinct climate zones in the United States: Eugene (marine), Tucson (hot-dry), and Buffalo (cold-humid). The study investigates how each roof type performs in terms of four key environmental metrics: microclimate cooling, stormwater runoff reduction, building energy load, and solar energy generation. By examining how these outcomes vary across climates, this research seeks to clarify which roof strategy is most effective, and under what climatic conditions biosolar roofs deliver the greatest benefits.

1.2 Research Framework

Chapter 3 aims to answer the research question: "In which climate conditions do biosolar roofs show the most significant environmental performance compared to typical concrete roofs, green roofs, and PV roofs?"

To address this question, the chapter follows a four-stage approach (**Figure 3.2**). In the first stage, I construct hypothetical 3D models of the four roof types at a rooftop scale, with each module represented

by a separate 3D model tailored to its respective analysis tools. In the second stage, I evaluate the environmental performance of each typology through multiple simulations: thermal environment analysis using ENVI-met, stormwater runoff reduction via the SWMM model, solar energy yield estimation using Rhino-Grasshopper, and building energy impact assessment with OpenStudio–EnergyPlus. Each simulation incorporates meteorological data from three cities—Eugene, OR; Tucson, AZ; and Buffalo, NY—to compare roof performance across diverse climate conditions.

To validate the simulation results and capture actual performance, the third stage involves a field experiment on the Pacific Hall rooftop on the University of Oregon campus, where scaled-down versions of each roof type were constructed. The environmental data collected from this experiment is then compared against the simulation outputs to assess their reliability and accuracy. Finally, in the fourth stage, I synthesize findings across all analyses to draw conclusions and address the central research question.

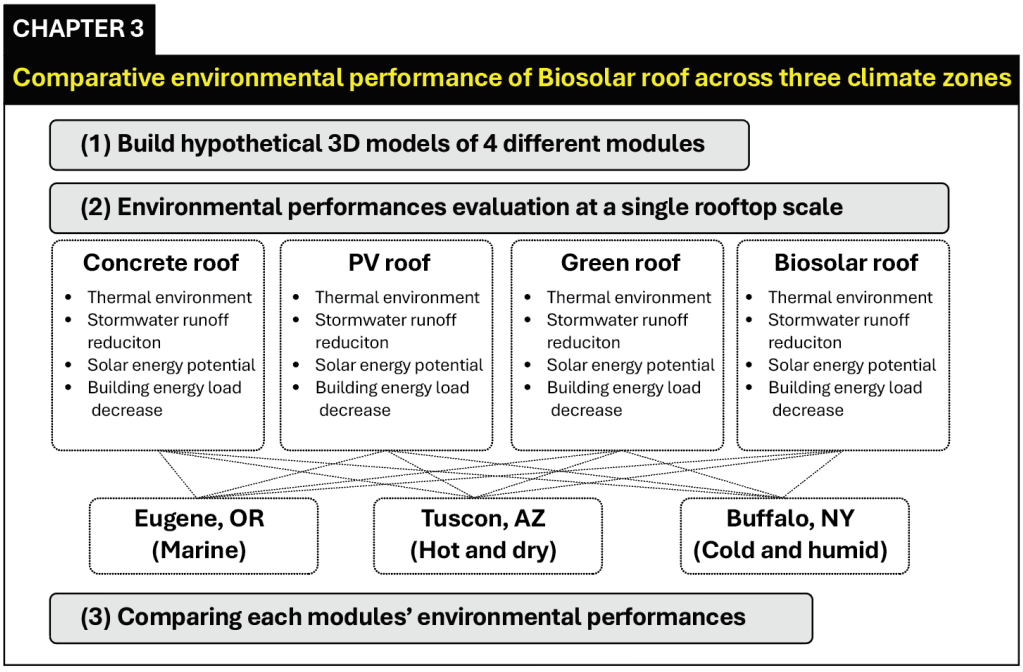


Figure 3.2 Chapter 3 research framework

2. Methodology

This study employed a combination of specialized simulation tools, each selected to evaluate the environmental performances of each rooftop typology. ENVI-met was used to assess microclimate cooling performance under different rooftop configurations; EPA-SWMM analyzed stormwater runoff by capturing surface saturation and drainage interactions; Rhino–Grasshopper with Ladybug Tools was used to estimate solar energy potential based on panel geometry and site conditions; and OpenStudio–EnergyPlus simulated annual building energy loads influenced by near-roof temperature dynamics. While each platform operates independently and was used in isolation, together they can provide a multi-perspective analysis of how biosolar roofs perform compared to PV, green, and concrete roof typologies. The following sections detail the modeling logic, assumptions, and parameters applied within each tool.

2.1 ENVI-met Simulation for Evaluating Cooling Performance

2.1.1 Model Creation and Basic Simulation Settings

I created four rooftop typologies—biosolar, green, PV, and concrete roof modules—using Space 5.7.1, a sub-modeling tool within the ENVI-met simulation suite. Each model consists of a high-resolution voxel grid (0.5 × 0.5 × 0.5 m), and shares the same domain size: 25 × 25 × 6 m (x-grids: 50, y-grids: 50, z-grids: 12). The only differences among the models lie in the inclusion of vegetation, photovoltaic arrays, or both.

Based on the review in Chapter 1, I selected four key design parameters for biosolar roofs: PV height, PV density, PV configuration, and planting density. To minimize variability, I standardized the plant species as perennial ryegrass (25 cm height) over a 50 cm soil substrate for both green and biosolar roof models, and used dark concrete pavement for the PV and concrete roof models. I also applied idealized PV configuration settings informed by earlier findings: 50% PV coverage and a PV height of 1.5 meters. Due to software limitations, PV tilt angles could not be adjusted in the ENVI-met models used for cooling

performance analysis but validated by field measurement with tilted angle in Chapter 4. In contrast, tilt is considered in the solar energy yield and building energy simulations, both of which are detailed later in this chapter.

To compare the environmental performance of the biosolar roof with the other three typologies, I developed separate 3D models for each: biosolar, green, PV, and concrete roofs. All models were constructed using the same base domain and material settings to ensure consistency. Detailed configuration parameters for each typology are provided in **Table 3.1**.

Table 3.1 ENVI-met 3D model configurations

	Base surface	Vegetation	PV height	PV configuration	PV density
Concrete roof	Dark concrete surface	N/A	N/A	N/A	N/A
Green roof	Dark concrete surface	25cm Ryegrass with 50cm substrate	N/A	N/A	N/A
PV roof	Dark concrete surface	N/A	1.5m	Checkerboard pattern	PV array with 50% density
Biosolar roof	Dark concrete surface	25cm Ryegrass with 50cm substrate	1.5m	Checkerboard pattern	PV array with 50% density

2.1.2 ENVI-met Simulation Setting

Regarding the four roof typologies—concrete, green, PV, and biosolar—the simulations were conducted across four key seasonal reference points: spring equinox, the summer solstice, fall equinox, and winter solstice of 2021. For each case, simulations were run during a representative clear-sky day from 9:00 a.m. to 6:00 p.m., covering a full 12-hour daytime period. I specifically selected representative dates near each equinox and solstice in 2021, ensuring that each corresponded to a clear-sky day. If the target date showed overcast conditions, I chose the nearest adjacent day with sunny weather based on local climate data. While this approach may not capture interannual variability, it enables a controlled comparison across roof types under idealized conditions. Future studies should adopt multi-year EPW datasets to more accurately reflect long-term climate patterns and avoid potential issues associated with single-year

weather data.

Eugene, Oregon (marine), Tucson, Arizona (hot and dry), and Buffalo, New York (cold and humid) were chosen to evaluate the environmental performance of each roof typology under distinct climatic conditions and to identify where biosolar roofs demonstrate the most significant benefits. To reflect these climate conditions in the simulations, I used EPW (EnergyPlus Weather) data specific to each location. EPW is a standardized weather file format developed and maintained by the U.S. Department of Energy's EnergyPlus program, containing hourly meteorological data such as temperature, humidity, wind speed, solar radiation, and other key parameters (Crawley et al., 2001).

2.1.3 Interpreting ENVI-met Simulation Results

Envi-met results are composed of multiple stacked 2D layers at each z-profile (height), representing the top view of the 3D model. The z-profile is determined by the spatial voxel resolution of the input 3D model. Leonardo software allows users to explore these 2D layers across different z-profiles, providing an intuitive way to visualize data distribution. This capability not only enhances users' understanding of microclimate variations but also facilitates the identification of specific environmental conditions. Each 2D layer is defined by (x, y) coordinates, with each coordinate containing detailed microclimate information, including wind vectors and temperature. Accordingly, I extracted temperature data from selected z-profiles: 0.25 m to represent the vegetation surface layer, and 1.75 m to represent the near-surface air temperature above the PV array. I then calculated the mean air temperature at each height to assess vertical thermal gradients and evaluate rooftop microclimate conditions.

2.2 SWMM Simulation for Evaluating Stormwater Management

2.2.1 Introduction to EPA-SWMM

The EPA Storm Water Management Model (SWMM) is a widely used computational tool developed by the United States Environmental Protection Agency. It supports integrated hydrologic and hydraulic modeling for urban stormwater systems, enabling detailed analysis of surface runoff, drainage networks, and water quality (Hörnschemeyer et al., 2023; Huber et al., 1975; Jeffers et al., 2022). SWMM is particularly suited for evaluating the performance of green infrastructure strategies—including bioswales, retention basins, green roofs, and permeable pavements—within comprehensive stormwater management frameworks (Huber et al., 1975; Tolderlund, 2010). Its flexible structure allows users to simulate various rainfall events and land cover conditions, making it a robust platform for assessing both conventional and sustainable stormwater solutions (Huber et al., 1975; Jeffers et al., 2022; Tolderlund, 2010).

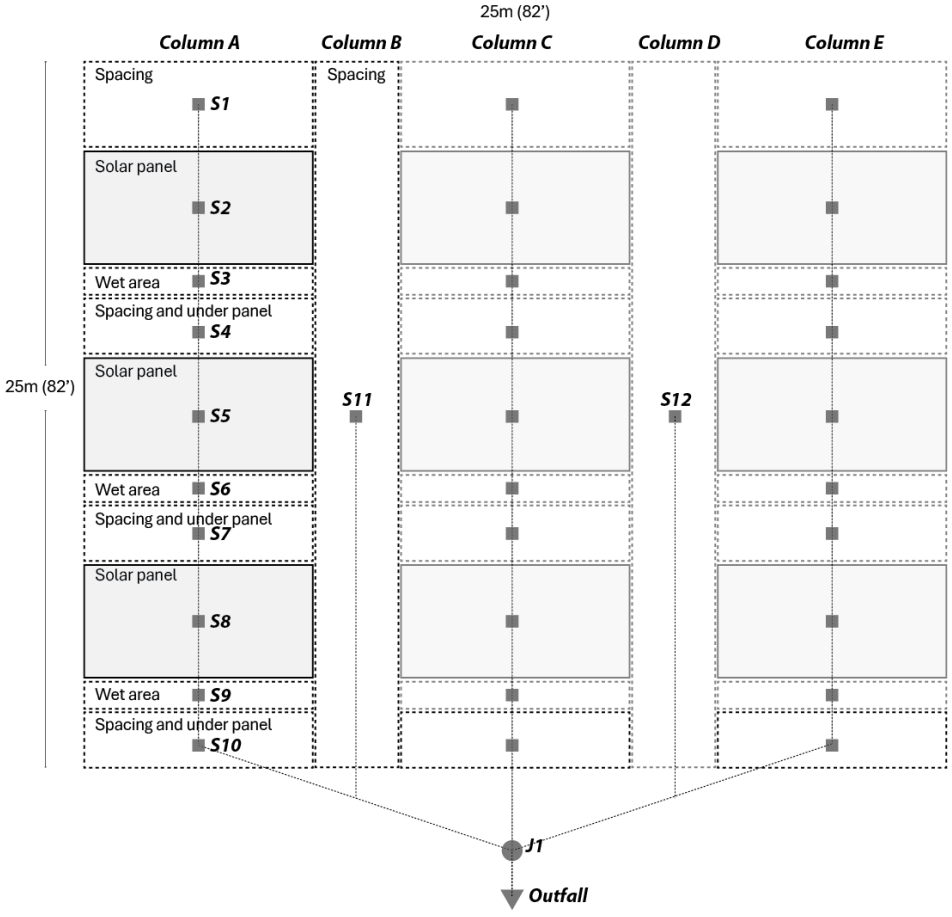
2.2.2 Stormwater Run-off Performance Analysis

Table 3.2 and **Figure 3.3** summarize the SWMM configuration used in this study. A key modeling limitation is that EPA-SWMM cannot explicitly simulate a floating PV canopy that intercepts rainfall and concentrates it onto the substrate below via drip-line discharge. This mechanism, however, plays a critical role in the hydrological performance of biosolar roofs.

To approximate this behavior, I refer to empirical findings from Jahanfar et al. (2019), who observed that 40% panel coverage over green roof modules reduced annual retention by approximately 30%, compared to uncovered green roofs. This reduction was attributed to the panel-induced interception–funneling effect: rain falling onto the PV surface is funneled toward a narrow drip line, which rapidly saturates the underlying substrate and exceeds its storage capacity and increases runoff. In real-world design applications, features such as shallow infiltration trays, gravel beds, or perforated underlayment systems may help retain this concentrated runoff and gradually distribute it into the substrate, thereby improving

water retention performance.

To reflect this dynamic in SWMM, the model was structured around a site layout divided into five vertical columns (north–south), with each PV-covered column further subdivided into ten subcatchments (see **Figure 3.3**). These subcatchments captured three key micro-conditions commonly found in biosolar roof installations: (1) vegetated spaces between PV rows; (2) shaded zones beneath PV panels; and (3) runoff-concentrated “wet areas” at the panel edges. This spatial differentiation enabled a more refined simulation of rainfall redistribution, interception, and vegetation exposure across the rooftop. All subcatchments were defined as 100% impervious in the model; however, vegetated zones were represented using the Green Roof module under SWMM's Low Impact Development (LID) controls. This reflects the rooftop isolation from natural soil, where no infiltration to ground is possible. LID unit parameters were defined in Table 3.3.



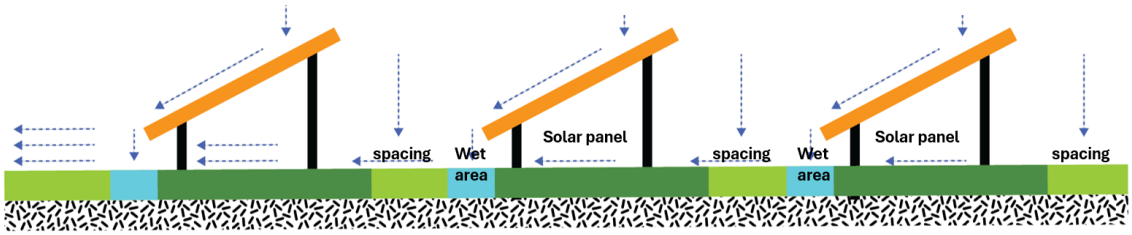


Figure 3.3 Subcatchment Configuration for Biosolar Roof in SWMM Simulation; Adopted from (Nair et al., 2024) and Revised

I applied this modeling framework across three contrasting U.S. climate zones—Eugene, OR (marine), Tucson, AZ (hot and arid), and Buffalo, NY (cold and humid)—using EPW weather datasets to simulate localized hourly precipitation. In each city, I modeled three rooftop types: a fully impervious concrete roof (100% imperviousness; single large subcatchment), a green roof (100% imperviousness; LID applied; single large subcatchment), and a biosolar roof (100% imperviousness; LID applied; specified subcatchments mimicking biosolar geomtery). Each was assigned to a standardized 25 × 25 m subcatchment. I also established another modeling assumption: concrete roofs represent both conventional concrete rooftops and PV rooftops. Since each rooftop is treated as an independent subcatchment (Gullotta et al., 2023; Nair et al., 2024) . Both concrete and PV roofs consist of impervious hard surfaces with no vegetation to retain water, and their hydrological behavior can be considered equivalent in this context. In this model, PV panels are also assumed to behave as fully impervious surfaces, contributing directly to surface runoff without any infiltration (Nair et al., 2024).

I employed the Green-Ampt infiltration method to estimate soil-water movement, with rooftop-scale flow routed via kinematic wave simulation. Each subcatchment was paired with a single inlet–outlet node and conduit to represent its drainage path. In the green roof scenarios, a Low Impact Development (LID) – green roof was applied across 100% of the subcatchment area (see **Table 3.3**).

Table 3.2 EPA-SWMM analysis process at each model

Stage	Contents	Concrete & PV roof	Green roof & Biosolar roof
1. Climate & Weather Data input	Input meteorological data; set rainfall event pattern	Eugene, Tuscon, Buffalo (EPW) data was used	
2. Subcatchment composition	Define Subcatchment layout	Subcatchment (25m x 25m), the same size of other simulation models - concrete: a single subcatchment - green roof: a single subcatchment with LID - biosolar: divided mulitple subcatchments within 25 × 25 m area to reflect biosolar runoff dynamic	
3. Hydrologic Process setting	Hydrological model selection for simulation; Greem-Ampt allow soil parameter input	Green-Ampt; Impervious: 100%	
4. Hydrological network assembly	Define inlet and outlet nodes with a conduit to represent flow paths	Kinematic wave routing was chosen for short conduit simulation	
5. LID integration	Integrate green infrastructure: Green roof applied as LID unit (see Table 3.3 for details)	N/A	Green Roof (fullly and partially)
6. Run simulation	-	-	

Table 3.3 EPA-SWMM green roof configuration: input settings and simulation parameters (Hörnschemeyer et al., 2023; Huber et al., 1975; Jeffers et al., 2022; Tolderlund, 2010)

Layer & field (units)	Input value	description
Surface		
Berm Height (mm)	30 mm	Depth that can temporarily retain on the roof before it spilling. (Higher berms can increase retention but add weight)
Vegetation Volume Fraction	0.75	Fraction of the surface layer occupied by vegetation
Surface Roughness (Manning n)	0.2	Controls flow velocity over the vegetation surface; dense sedum short grass (0.15-0.25)
Surface Slope (%)	0.5 %	Mean rooftop surface pitch;
Soil (growing medium)		
Thickness (mm)	300 mm	Depth of engineered substrate (thicker media can store more water but more weight)
Porosity (vol frac)	0.30	Total void space at saturation (default)
Field Capacity (vol frac)	0.25	Moisture retained after gravity drainage (deftult)
Wilting Point (vol frac)	0.08	minimum amount of water in the soil that the plant requires not to wilt

Saturated Conductivity (mm h^{-1})	100 mm h^{-1}	water permeability under saturated soil conditions
Conductivity Slope (HCO)	20	How quickly the soil's ability to conduct water decreases as it dries (default).
Surface Head (mm)	5 mm	Capillary suction at the wetting front; help infiltration realistic for shallow media (default).
Drainage Mat		
Thickness (mm)	25 mm	The thickness of drainage layer
Void Fraction	0.80	Proportion of empty spaces in the mat; (default)
Roughness (Manning n)	0.20	Hydraulic roughness inside the mat (default)

2.3 Solar Energy Potential Evaluation

2.3.1. Overview of Modeling Requirements for Biosolar Roofs

Accurately assessing the energy performance of biosolar roofs requires simulation tools that can go beyond conventional PV system modeling. Unlike standard PV installations, biosolar roofs have evaporative cooling and altered airflow—directly beneath the PV arrays. These localized factors can influence module temperature and, consequently, solar conversion efficiency. To account for these interactions, the selected tool must be able to incorporate not only PV system parameters but also 3D rooftop geometry and temperature-sensitive effects.

For this study, Rhinoceros 7 was used in combination with Grasshopper, its parametric design plugin. Grasshopper's flexible visual programming environment allowed for detailed rooftop configurations and dynamic adjustment of PV-related parameters. Environmental simulation was conducted using Ladybug and Honeybee, two open-source plugins that operate within Grasshopper and are widely used in architectural environmental analysis.

2.3.2 Comparison and Rationale for Selecting Rhino-Grasshopper

A reason for choosing tools for biosolar roof's energy yield lies in the capability of elaborate 3D geometry modeling and supports temperature sensitive variation in PV yields. **Table 3.4** shows the key differences in terms of geometric flexibility, temperature sensitivity, mounting configuration, and analysis objectives, among the major PV yields modeling tools, such as PVSyst, PV*SOL, and ArcGIS Solar Analyst. While PVSyst and PV*SOL are highly capable for system sizing and economic feasibility analysis, they lack fine-grained control over geometry and environmental detail (Anang et al., 2021; Baqir & Channi, 2021; Choi et al., 2011; Dondariya et al., 2018; Kavitha et al., 2021; Singh & Banerjee, 2015). For instance, they model temperature influence through simplified coefficients but do not simulate vegetation-induced microclimate cooling. Similarly, ArcGIS Solar Analyst excels in regional-scale

irradiation analysis but is not equipped for performance modeling at the module or rooftop level. However, Rhino-grasshopper (by LadyBug and HoneyBee plugins) supports detailed 3D geometry for building rooftop and PV layouts (Chang et al., 2019; Qingsong & Fukuda, 2016); temperature-sensitive simulation that reflects microclimatic feedbacks[2]; user-defined PV module parameters, including tilt, height, orientation, and mounting type; integration of EPW (EnergyPlus Weather) files, allowing realistic, location-specific solar and temperature inputs. Given these capabilities, Rhino-Grasshopper was determined to be the most appropriate platform for simulating biosolar roofs, where the interaction between vegetation, PV hardware, and rooftop microclimate is central to system performance.

Table 3.4 Comparison of Solar Potential Estimation Software

Comparison Criteria	Rhino-Grasshopper (Ladybug & Honeybee) (Chang et al., 2019; Qingsong & Fukuda, 2016)	PVSyst (Anang et al., 2021; Baqir & Channi, 2021; Singh & Banerjee, 2015)	PV*SOL (Dondariya et al., 2018; Kavitha et al., 2021)	ArcGIS (Solar Analyst) (Choi et al., 2011; Kausika & van Sark, 2021)
Purpose	3D modeling, parametric design, environmental performance analysis	PV system technical and economic analysis	PV system technical and economic analysis	GIS-based solar radiation analysis for urban/regional scale
Strengths	Temperature-sensitive estimation and flexible geometry modeling	Comprehensive technical design and feasibility	User-friendly interface, quick PV system analysis	solar potential analysis over large geographic areas
Geometry Modeling	Highly detailed, flexible 3D modeling	Simplified, limited geometric modeling	Limited geometric modeling (PV panel placement focus)	GIS-based spatial modeling using DEM, buildings, and urban features
Temperature & Efficiency	Temperature sensitive	Simplified consideration	Simplified consideration	NA
Weather Data	EPW	EPW	EPW	Uses weather data integrated in GIS
PV Module Library	Limited database, (custom-defined modules)	Extensive PV module database	Extensive PV module database	NA
Mounting & Cooling Type	Detailed mounting type and airflow considerations	Simplified mounting options only	Simplified mounting options only	NA
Typical Applications	Early-stage architectural/urban design analysis	Detailed PV system engineering and design stages	Professional PV system design, installation planning	Urban or regional-scale solar resource mapping and planning

[2] Rhino supports solar yield simulations that account for temperature-sensitive PV panel efficiency; however, it cannot incorporate the cooling effects of vegetation through evapotranspiration on the microclimate.

2.3.3 Solar Energy Potential Estimation in Rhino-Grasshopper

In Rhino-Grasshopper, solar energy potential was estimated using the Ladybug Tools suite within Grasshopper. The simulation workflow involved several key steps and input parameters. First, EPW weather data files were imported to ensure accurate solar radiation and temperature inputs corresponding to each study location (Eugene, Tucson, Buffalo). I used a series of PV modeling components in Ladybug—such as *SimplifiedPhotovoltaicsModule*, *PhotovoltaicSurfaces*, *SunPathShading*, and *DCtoACderateFactor*—and customized the relevant input variables. For example, the mounting type was set to Open Rack to account for elevated panels with high airflow potential. The technical PV efficiency was set at 15%, assuming crystalline silicon panels, and the temperature coefficient was set to –0.5%/°C, representing performance losses under heat accumulation. The module active area was defined as 90%, excluding frames and inactive zones, and albedo was set to 0.2 to reflect typical surface reflectivity. These settings allowed for detailed estimation of both hourly and annual solar yields across different rooftop configurations—including biosolar systems. Importantly, however, the rhino-grasshopper was limited to capture how vegetation-induced cooling can reduce PV panel temperatures and relevant enhance PV efficiency.

2.4 OpenStudio-EnergyPlus for Evaluating the Impact on Building Energy Load

2.4.1 Introduction to OpenStudio-EnergyPlus

I used OpenStudio–EnergyPlus to evaluate how each four roof type—concrete, PV, green, and biosolar roof—influences annual heating and cooling energy loads, by considering the dynamic interactions between rooftop surface conditions. OpenStudio is an open-source building energy modeling platform developed by the National Renewable Energy Laboratory (NREL) in collaboration with the U.S. Department of Energy (DOE) (Guglielmetti et al., 2011). It is designed to streamline the energy modeling process by providing a user-friendly interface and integration tools for EnergyPlus, a powerful simulation

engine for building energy and environmental performance (Barber & Krarti, 2022; Guglielmetti et al., 2011). While EnergyPlus conducts detailed thermodynamic simulations—including factors such as solar radiation, thermal mass, HVAC systems, and internal loads—OpenStudio acts as a flexible interface that supports model construction, visualization, and workflow automation. This integration enables researchers and practitioners to assess the impacts of different architectural and environmental design choices, such as roofing typologies, on a building's energy demand throughout the year (Barber & Krarti, 2022; Guglielmetti et al., 2011).

2.4.2 Analysis Process of OpenStudio-EnergyPlus

To analyze the impact of rooftop typologies on building energy performance, I simulated four different roof types—biosolar roof, green roof, PV roof, and concrete roof—using the OpenStudio–EnergyPlus platform (see **Figure 3.4**). First, the base building was modeled in SketchUp to reflect the general form and dimensions of Pacific Hall at the University of Oregon, a typical mid-sized institutional building with a flat roof. Each rooftop condition was then individually implemented and modified according to its respective typology, while all other architectural and occupancy parameters were kept constant to isolate the effect of the roofing system.

After creating the 3D geometry in SketchUp, the models were imported into OpenStudio, where the simulation environment was configured. All four models share the same building footprint, orientation, and internal zone layout. The rooftop occupancy rate—defined as the portion of the roof that directly influences indoor thermal zones—was standardized across all typologies to ensure consistency.

The key inputs in OpenStudio include Schedules, Construction Layers, and Internal Loads—such as occupant density and associated heat gains, lighting and equipment loads, ventilation rates, and HVAC settings. The HVAC configuration defines heating and cooling airflow based on preset indoor temperature ranges and operational schedules.

OpenStudio – EnergyPlus

Modeling is based on the ASHRAE 90.1-2010 'Large Office' prototype, representing a typical mid-2010s North American office building

Parameter	Concrete	PV Roof	Green Roof	Biosolar Roof
Roof construction ID	RRR-ConcreteRoof-IEAD CZ 2-5	RRR-ConcreteRoof-IEAD CZ 2-5	RRR-ConcreteRoof-IEAD CZ 2-5 *(Vegetation cover applied)*	RRR-ConcreteRoof-IEAD CZ 2-5 *(Vegetation cover applied)*
Effective R-value ($ft^2 \cdot h \cdot °F/Btu$)	24.73	24.73	32.84	32.84
PV shade structure	N/A	PV-canopy shade structure	N/A	PV-canopy shade structure

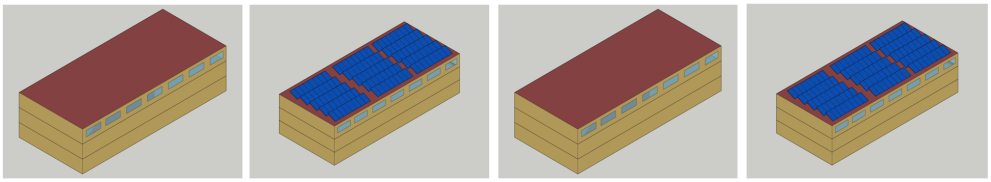


Figure 3.4 Four modules' settings in OpenStudio

Table 3.5 The common parameter settings in OpenStudio across four modules

Category	Key input parameter	Model setting (unit)
Prototype	90.1-2010 Large-Office	Closed-office, whole-building zoning
People density	Occupants	0.005 people / ft^2
Lighting load	LPD	0.90 W / ft^2
Equipment load	Plug/Process	0.54 W / ft^2
Infiltration	Air leakage	0.0446 cfm / ext-surf-ft^2
Ventilation	Outdoor air	5 cfm / person
Thermostat set-points	Heating / Cooling	70 °F / 75 °F
HVAC system	System type	VAV w/ reheat (prototype default)
Simulation control	Timestep / RunPeriod	6 timesteps h^{-1}, full-year

Table 3.6 Additional parameter settings for green roof and biosolar roof in OpenStudio

Parameter (Unit)	Value
Height of plants (m)	0.5
Leaf Area Index	1
Leaf reflectivity	0.22
Leaf emissivity	0.95
Minimum stomatal resistance ($s \cdot m^{-1}$)	180
— Soil layer: *Green Roof Soil* —	
Roughness (categorical)	Rough
Thickness (m)	0.5
Thermal conductivity, dry ($W \cdot m^{-1} \cdot K^{-1}$)	0.35
Density, dry ($kg \cdot m^{-3}$)	1 100
Specific heat, dry ($J \cdot kg^{-1} \cdot K^{-1}$)	1 200

Thermal absorptance	0.9
Solar absorptance	0.7
Visible absorptance	0.75
Saturation volumetric moisture content ($m^3 \cdot m^{-3}$)	0.3
Residual volumetric moisture content ($m^3 \cdot m^{-3}$)	0.01
Initial volumetric moisture content ($m^3 \cdot m^{-3}$)	0.1

3. Results

3.1 Impact on Cooling Performance (ENVI-met Results)

Figure 3.3 shows the annual average differences in potential air temperature (ΔT, °C) for PV, green, and biosolar roofs compared to the concrete roof baseline, measured at two heights: 0.25 m (near-vegetation air temperature) and 1.75 m (air temperature above the PV panel). Positive values indicate a cooler microclimate than the concrete roof, while negative values indicate warming.

At 0.25 m (near-vegetation air temperature), all three climate zones demonstrated clear cooling effects from vegetated systems, especially from the biosolar roof. In particular, biosolar roofs showed the greatest median cooling performance across all climates, averaging approximately 1.5 °C cooler than the concrete roof. In Tucson, the maximum cooling benefit reached nearly 3.5 °C, indicating that the biosolar roof can deliver substantial microclimate mitigation in hot-dry climates. By contrast, the PV roof alone showed minimal cooling effects, with temperature reductions generally below 0.5 °C—highlighting the importance of vegetation-driven evapotranspiration in cooling effect.

At 1.75 m (air temperature above the PV panel), the magnitude of cooling was substantially reduced. Temperature differences across all roof types narrowed, and median values approached zero in all three location. However, biosolar and green roofs still retained a slight cooling advantage, while PV roofs continued to show negligible or inconsistent effects. This suggests that the cooling benefits of vegetation and shading are concentrated near the surface, with diminishing influence at higher elevations.

These results confirm that biosolar roofs are most effective in cooling near-surface microclimates, especially in hot and dry climate where their structural configuration may help mitigate intense solar gain and surface heat accumulation. While their cooling influence becomes less distinctive above the PV canopy, their role in improving rooftop thermal environments remains significant in all three climates. Importantly, modeled performance assumes healthy vegetation coverage, which in practice may require supplemental irrigation in hot and arid regions to prevent grass dryness and maintain evapotranspiration-

driven cooling. Thus, the sustained cooling benefit of biosolar roofs in such climates may depend on water availability or drought-adapted planting strategies.

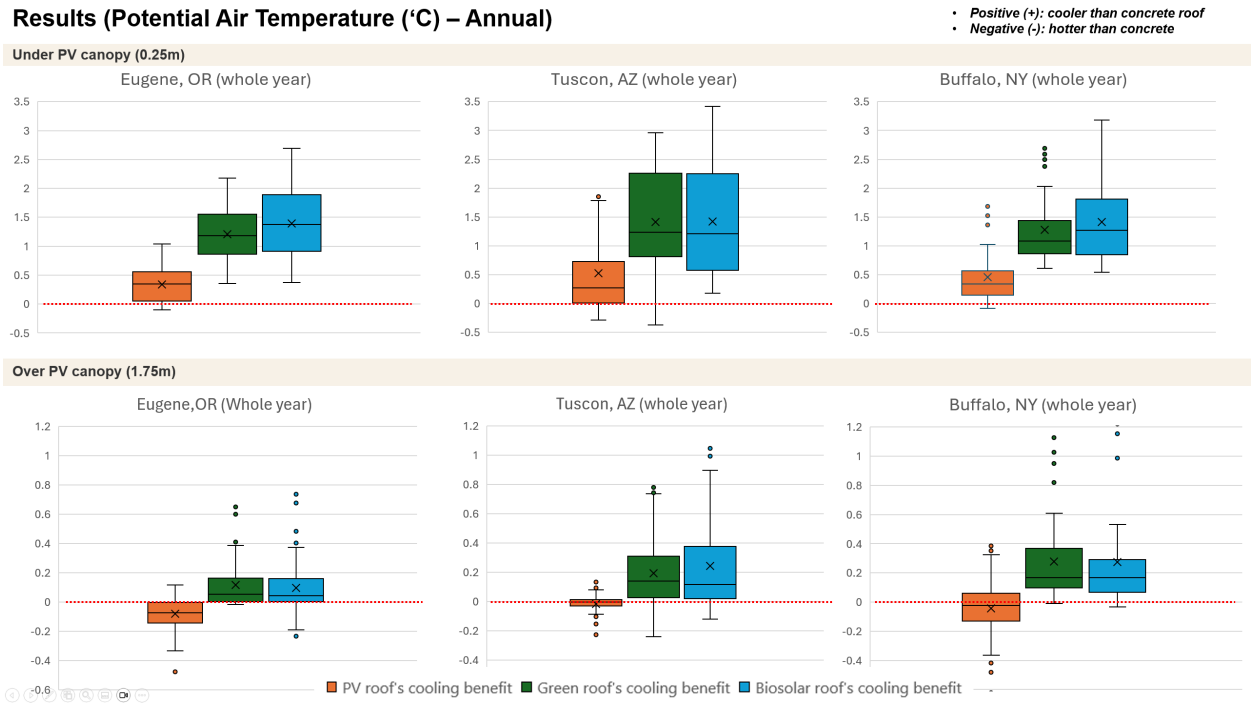


Figure 3.5 Annual Average of Potential Air Temperature Differences (°C) at Two Heights by Roof Typology and Climate Zone; positive value means cooler than concrete roof; negative value means hotter than concrete roof

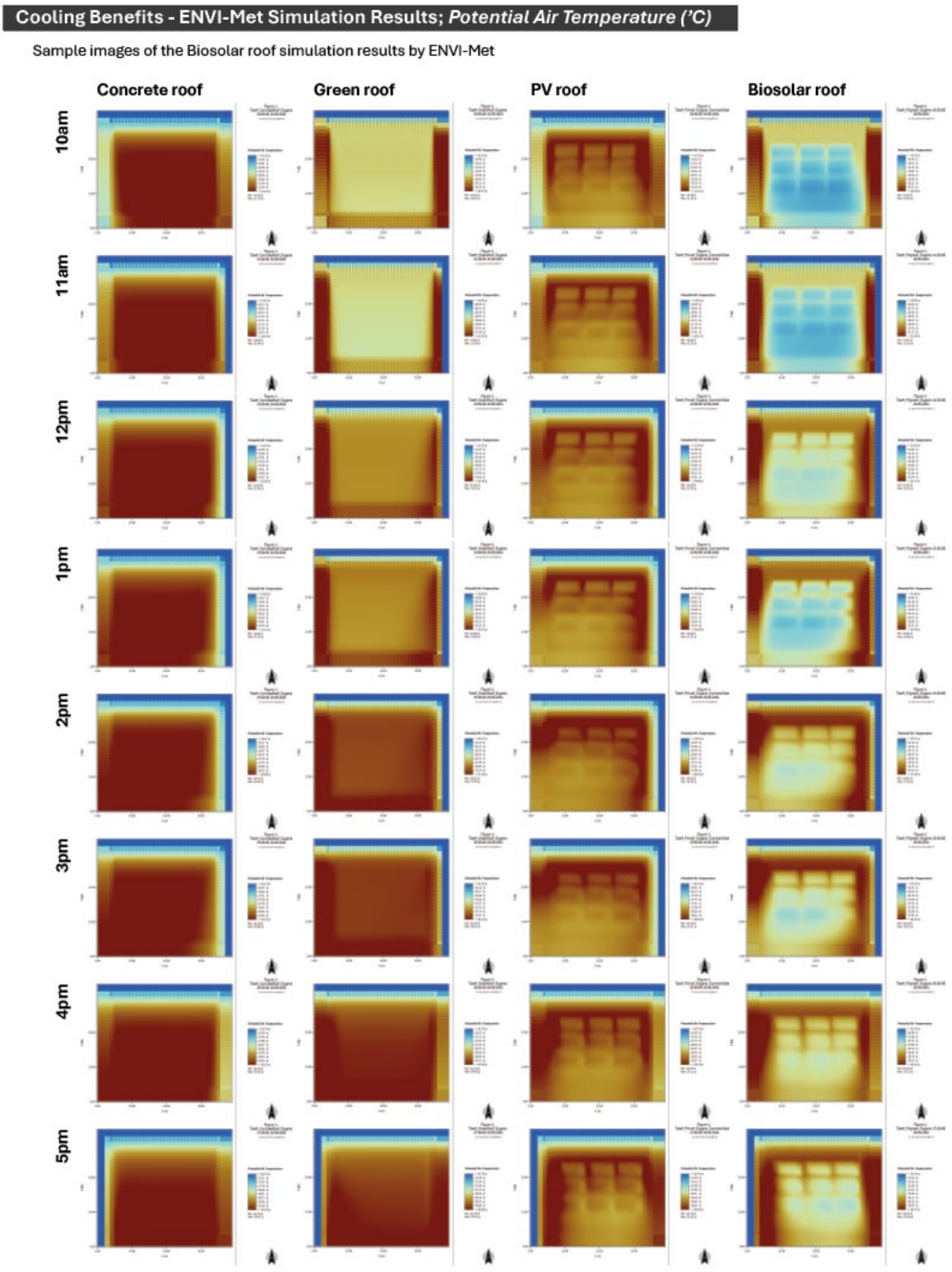


Figure 3.6 Example snapshots of ENVI-met simulations at near-vegetation level in Eugene, OR (z=0.25m)

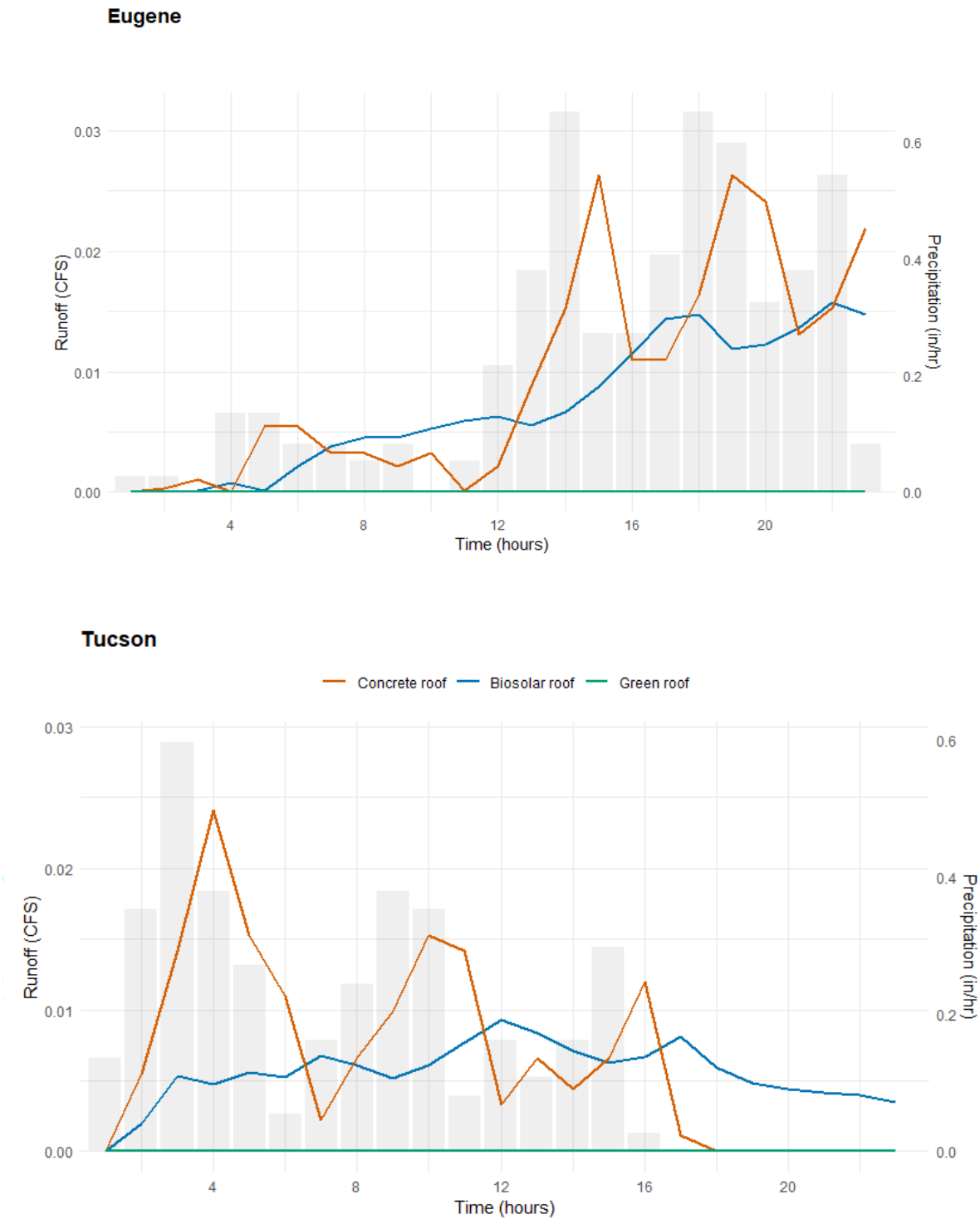
3.2 Impact on Stormwater Management (SWMM Results)

A 24-hour storm event was simulated in EPA SWMM for three representative U.S. climates: Eugene, OR (marine), Tucson, AZ (hot and dry), and Buffalo, NY (cold and humid). The simulation used 60-minute interval precipitation data from 2013, during which significant rainfall events occurred. Although I replicated the geometry of the biosolar roof using multiple subcatchments to reflect the hydrologic dynamics associated with its design (Jahanfar et al., 2019; Nair et al., 2024), it should be recognized that the absence of natural subsoil beneath rooftop systems may limit deeper infiltration and increase surface runoff compared to ground-level vegetated areas.

Across all three cities—Eugene, Tucson, and Buffalo—the biosolar roof consistently produced less runoff than the concrete roof, while the green roof outperformed concrete and biosolar roof, generating virtually no surface runoff (**Figure 3.7**). This pattern highlights the critical role of vegetation in regulating rooftop stormwater. Green roofs, with full and unobstructed vegetation coverage, maximize rainfall retention by allowing uniform infiltration and storage across the substrate layer. However, in biosolar roofs, PV panels redirect rainfall toward narrow drip-line zones, forming concentrated "wet areas"—typically along panel edges—which can exceed the local retention capacity of the underlying soil, causing quicker saturation and increased runoff. This simulation result is consistent with empirical findings that PV coverage on green roofs resulted in a 30% reduced retention due to the funneling effect of panels (Jahanfar et al., 2019). They also showed the concentrated discharge at panel edges can diminish the benefits of vegetation, especially when drainage infrastructure is not adapted to handle localized saturation (Jahanfar et al., 2019). Similarly, in the biosolar roof simulations, while vegetation contributed to peak flow reduction and discharge delay, the PV structure introduced spatial imbalances in water distribution, reinforcing the need for design solutions that mitigate edge runoff.

Despite these limitations, biosolar roofs contribute to regulating stormwater peaks more effectively than bare concrete roofs where all rainfall becomes immediate runoff without delay or absorption. Taken together, these results highlight that while green roofs deliver the highest level of stormwater retention,

biosolar roofs still contribute meaningfully to rooftop stormwater regulation—particularly during heavier or prolonged rainfall events.



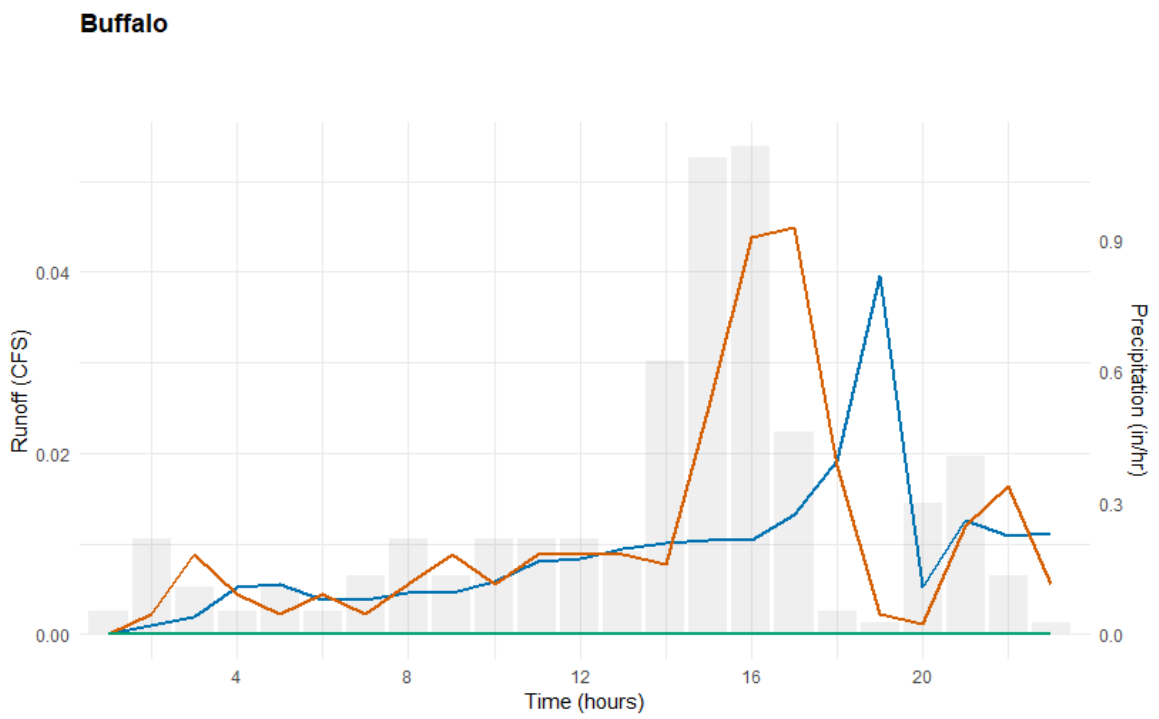


Figure 3.7 Simulated stormwater runoff reduction by vegetated roofs (green/biosolar) under 24-hour rain events in Eugene, Tucson, and Buffalo.

3.3 Impact on Solar Energy Yields (Rhino-Grasshopper Analysis Results)

Figure 3.8 presents the annual AC energy yield for two rooftops—half-density coverage of PV roof and biosolar roof—across Eugene (OR), Tucson (AZ), and Buffalo (NY). The "half-density" term refers to PV installations covering 50% of the available rooftop footprint, respectively, while the biosolar roof scenario incorporates vegetation beneath a half-density PV array. Because no existing simulation software directly accounts for the evaporative cooling effects of rooftop vegetation, the biosolar yield was calculated by manually increasing the half-density yield by 3%, a value supported by earlier studies on plant-mediated cooling (Alshayeb & Chang, 2018; Chemisana & Lamnatou, 2014; Hui & Chan, 2011; Irga et al., 2021; Nagengast et al., 2013; Talwar et al., 2023).

When the rooftop footprint[3] is fully covered by (20kW) biosolar roof systems with half PV density and vegetation, the simulated yields reach 22.6 MWh/$_{yr}$ in Eugene, 32.1 MWh/$_{yr}$ in Tucson, and 22.9 MWh/$_{yr}$ in Buffalo—enough electricity to supply roughly 3 average U.S. households in Tucson (based on the data that The average U.S. household consumes:10,500 kWh (EIA.gov.com). The slight increase in energy production compared to the PV roof can be considered a meaningful gain over long-term operation—especially when biosolar roof installations and system capacity scale up with higher adoption rates across a city.

Notably, Tucson's high insolation levels yielded the largest absolute energy production in all scenarios. In contrast, more temperate climates like Eugene and Buffalo produced lower overall yields, but still displayed clear distinctions among the biosolar and PV roofs. These results highlight both the influence of local climatic conditions and the potential for biosolar roofs to improve efficiency through vegetation-driven cooling—a synergy that may be particularly beneficial in regions with abundant solar resources and elevated summertime temperatures.

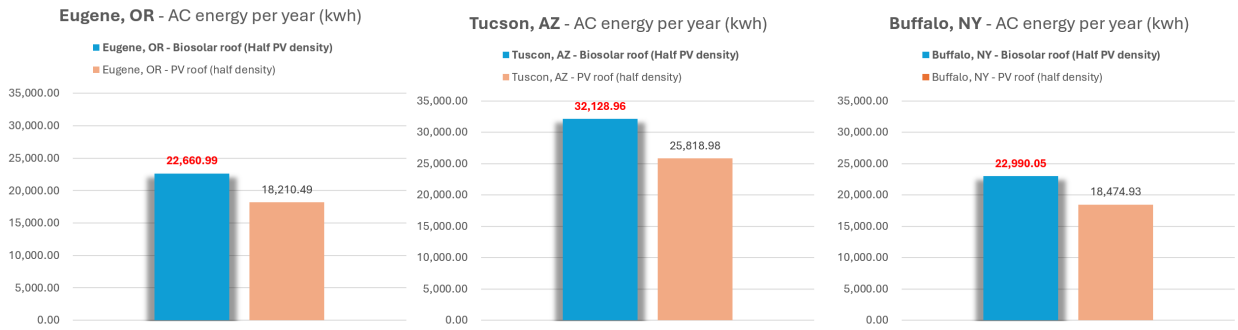


Figure 3.8 Annual simulated AC energy yield (kWh) for half PV density of Biosolar roof and PV roof across climatic zones (Full PV density is added for the comparison with Half density)

[3] Assuming a rooftop size of 25 × 25 m for the Pacific Hall building at the University of Oregon, with 100 panels rated at 400 W each.

3.4 Impact on Building Energy Load (OpenStudio Results)

The OpenStudio results, **Table 3.7**, showed that the biosolar roof recorded the lowest energy demand for both cooling and heating, among the four modules, across all three climate zones. This outcome highlights the synergistic effect of the vegetation and its soil substrate and photovoltaic canopy in reducing rooftop surface heat gain. Not just because of the vegetation's evaporative cooling and thermal insulation, it seems that the additional shading by PV arrays contributes to reducing solar heat gain on the roof surface. Under peak seasonal conditions (peak design load periods for cooling and heating), the biosolar roof effectively lowered both cooling and heating design loads compared to the concrete roof. Cooling demand decreased by up to 5.22% in Eugene, 0.89% in Tucson, and 0.66% in Buffalo, while heating demand dropped by 3.4%, 4.7%, and 2.2%, respectively, across the same locations. This relatively greater cooling load reduction observed in Eugene may be attributed to its mild, moderately sunny summer climate, where evapotranspiration remains effective and the baseline cooling demand is high enough to make vegetation and PV shading more impactful. Also, biosolar roof's reduced heating load may suggest the insulation benefit of the vegetation during winter season.

The PV roof also performed better than the conventional concrete roof in all climate conditions except in Buffalo during summer. This may indicate that PV shade contributes to reducing both cooling and heating loads. However, since PV roofs do not include soil or vegetation, their performance in reducing heating demand was noticeably weaker compared to the green and biosolar roofs, especially in colder climates. On the other hand, the difference between the green roof and biosolar roof was minimal, regarding heating load. For example, in Eugene, the heating design load for the green roof was 272.6 kBtu/h, while the biosolar roof was slightly lower at 266.25 kBtu/h—only a 2.3% difference.

The tendency of cooling and heating loads varies depending on local climate. For example, in Tucson (hot-arid), all roof types recorded higher cooling loads, and the relative benefits of vegetation appeared to be comparatively minimal. This may be due to the limitations of evapotranspiration under hot, dry conditions, where limited water availability and intense solar radiation can overwhelm the cooling

potential of the vegetation layer. In this case, the shading effect—rather than vegetation—may play a more significant role in reducing cooling loads because shade is more effectively reduce the intense solar gain and heat accumulation on rooftop surface. Therefore, in dry climates, the overall effectiveness of vegetated roofs may remain limited unless consistent irrigation is provided. In contrast, Buffalo (cold and humid) showed the highest heating loads among the three cities, and the thermal buffering effect of vegetation—especially the green and biosolar roofs—was more noticeable. Compared to the concrete roof, heating design loads were reduced by 0.92% with the green roof and by 2.2% with the biosolar roof, highlighting the added insulating benefit of vegetation and PV shading in colder climates.

Table 3.7 Cooling and heating design loads and reduction rates (%) of alternative roof types under peak design conditions compared to conventional concrete roof sacross three climate zones (Eugene, OR; Tucson, AZ; Buffalo, NY)

Climate	Scenario	Cooling Design Load (ton)	Cooling Load Reduction vs. Concrete Roof (%)	Heating Design Load (kBtu/h)	Heating Load Reduction vs. Concrete Roof (%)
Eugene, OR	Concrete Roof	40.6	0	275.61	0
Eugene, OR	Green Roof	40.39	0.52	272.6	1.09
Eugene, OR	PV Roof	38.5	5.17	268.62	2.54
Eugene, OR	Biosolar Roof	38.48	5.22	266.25	3.4
Tuscon, AZ	Concrete Roof	41.49	0	217.49	0
Tuscon, AZ	Green Roof	41.49	0	214.62	1.32
Tuscon, AZ	PV Roof	41.13	0.87	209.36	3.74
Tuscon, AZ	Biosolar Roof	41.12	0.89	207.27	4.7
Buffalo, NY	Concrete Roof	39.55	0	386.71	0
Buffalo, NY	Green Roof	39.56	0.03	383.14	0.92
Buffalo, NY	PV Roof	39.81	0.66	381.32	1.39
Buffalo, NY	Biosolar Roof	39.81	0.66	378.22	2.2

Table 3.8 presents the monthly variation and overall distribution of cooling loads by roof type across the three locations. **Figure 3.9** shows additional clarity on the temporal dynamics and statistical spread of the

load values throughout the year. Across three climates, cooling demand was concentrated in the summer months, with July and August emerging as the peak cooling periods. In Tucson, cooling loads remained high for an extended period—from April through September—however the differences among roof types were marginal. This reinforces that climate conditions dominate roof performance in a hot-dry climate.

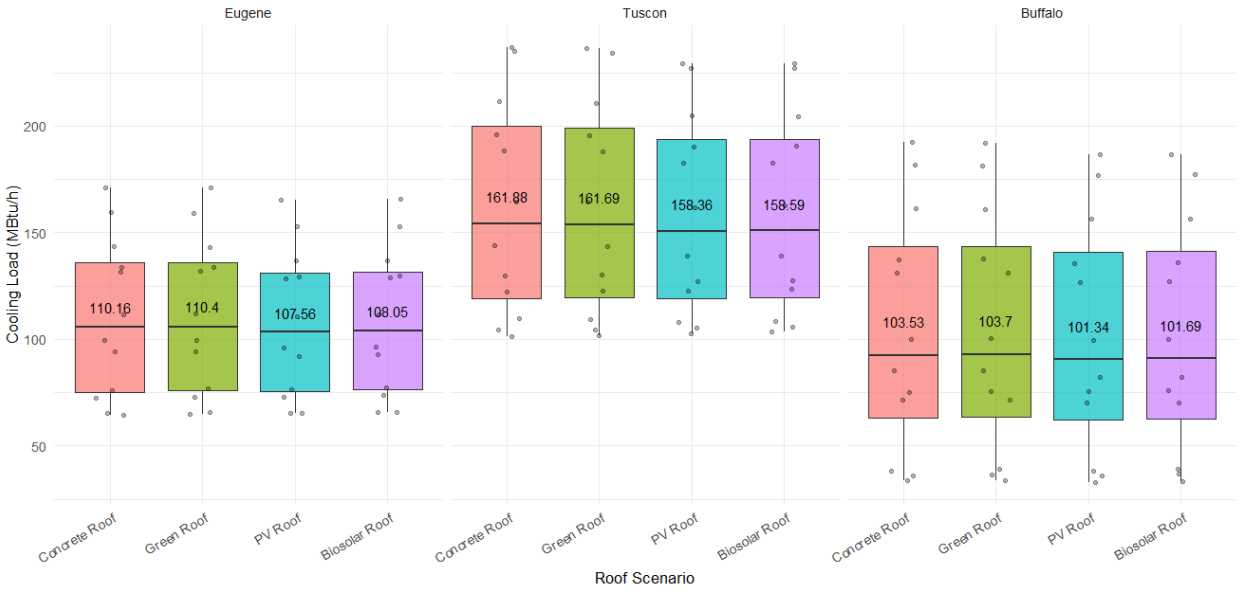


Figure 3.9 The boxplot of cooling load (kBtu/h) by roof typology across three climate zones

Table 3.8 Monthly cooling load trends and distribution by roof typology across three climate zones

Cooling load (kBtu/h)	Scenario	Jan	Feb	Mar	Apr	May	Jun	Jul	Aug	Sep	Oct	Nov	Dec
Eugene	Concrete Roof	72.25	65.4	93.94	99.59	133.55	143.3	159.38	171.05	131.63	111.41	76.08	64.34
Eugene	Green Roof	72.9	65.83	94.25	99.67	133.68	143	159.04	171.01	131.91	111.9	76.69	64.93
Eugene	PV Roof	72.93	65.27	92.12	95.94	128.42	136.62	152.66	165.07	129.13	110.66	76.57	65.36
Eugene	Biosolar Roof	73.6	65.74	92.62	96.27	128.89	136.86	152.9	165.6	129.7	111.31	77.22	65.91
Tuscon	Concrete Roof	101.3	109.56	129.91	143.72	188.4	211.3	237.01	234.96	195.85	164.22	122.23	104.14
Tuscon	Green Roof	101.85	109.4	130.15	143.39	187.71	210.37	236.19	234.14	195.44	164.44	122.72	104.46
Tuscon	PV Roof	102.71	108.02	126.93	139.02	182.58	204.7	229.39	227.11	190.14	161.78	122.77	105.13
Tuscon	Biosolar Roof	103.38	108.2	127.51	139.17	182.43	204.37	229.18	226.96	190.38	162.46	123.43	105.63

Buffalo	Concrete Roof	35.74	33.5	71.37	85.26	130.89	161.19	192.47	181.56	137.4	99.84	74.88	38.2
Buffalo	Green Roof	36.39	33.85	71.5	85.33	130.84	160.72	191.95	181.41	137.73	100.42	75.38	38.86
Buffalo	PV Roof	35.94	32.94	70.01	82	126.69	156.44	186.57	177	135.42	99.4	75.28	38.35
Buffalo	Biosolar Roof	36.59	33.32	70.25	82.35	126.87	156.35	186.57	177.28	135.93	100	75.8	38.99

Figure 3.10 and **Table 3.9** show the monthly heating load patterns for each roof typology across the three study locations. This shows how roof configurations influence on thermal performance throughout the season. Buffalo demonstrated the longest and most intensive heating load during in winter season, with significant demand from October through April. The concrete roof showed the highest heating loads in general, on the other hand, the biosolar and green roofs showed comparably lower values during the winter. For example, in Buffalo, the biosolar roof reduced heating demand by up to 5.05% in December and 4.87% in March compared to the concrete roof, while the green roof showed reductions of up to 3.56% and 3.23% during the same months. This supports the earlier finding that vegetation can function as insulation thermal mass in cold-humid climates. In Eugene, the seasonal heating load profile was similar to Buffalo's but milder in magnitude. Although the differences of Eugene’s heating load among roof typologies were smaller than in Buffalo, the biosolar roof still maintained the lowest monthly heating loads in January and February. Conversely, Tucson displayed minimal heating demand throughout the year. This result confirms that heating-related design interventions has less relevance in hot-arid climates, and performance optimization in such regions should focus instead on cooling load reduction.

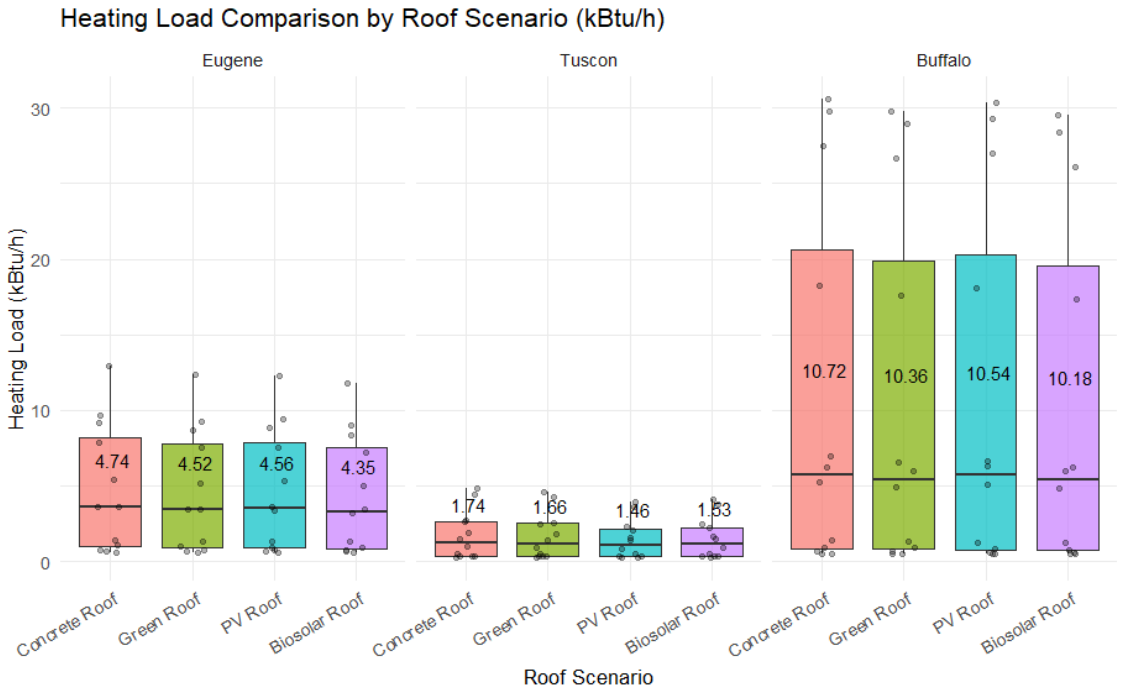


Figure 3.10 The boxplot of heating load (kBtu/h) by roof typology across three climate zones

Table 3.9 Monthly heating load trends and distribution by roof typology across three climate zones

Heating load (kBTU/h)	Scenario	Jan	Feb	Mar	Apr	May	Jun	Jul	Aug	Sep	Oct	Nov	Dec
Eugene, OR	Concrete Roof	9.19	9.68	5.43	3.65	1.4	0.79	0.6	0.71	1.08	3.6	7.9	12.9
Eugene, OR	Green Roof	8.69	9.28	5.16	3.46	1.34	0.77	0.59	0.69	1.02	3.43	7.51	12.34
Eugene, OR	PV Roof	8.84	9.41	5.31	3.65	1.35	0.75	0.59	0.69	0.94	3.37	7.58	12.26
Eugene, OR	Biosolar Roof	8.38	9.02	5.03	3.45	1.29	0.73	0.59	0.67	0.9	3.21	7.21	11.76
Tuscon, AZ	Concrete Roof	4.85	2.73	1.94	1.47	0.53	0.32	0.26	0.34	0.38	1	2.62	4.47
Tuscon, AZ	Green Roof	4.6	2.59	1.83	1.39	0.53	0.31	0.26	0.33	0.38	0.95	2.49	4.24
Tuscon, AZ	PV Roof	3.92	2.3	1.58	1.38	0.51	0.3	0.26	0.33	0.37	0.86	2.09	3.62
Tuscon, AZ	Biosolar Roof	4.13	2.45	1.68	1.46	0.52	0.31	0.26	0.33	0.37	0.9	2.19	3.82
Buffalo, NY	Concrete Roof	29.81	30.58	18.28	6.21	1.38	0.66	0.48	0.53	0.93	5.27	6.97	27.52
Buffalo, NY	Green Roof	28.95	29.79	17.63	5.95	1.32	0.64	0.48	0.53	0.89	4.94	6.56	26.63
Buffalo, NY	PV Roof	29.28	30.35	18.06	6.31	1.28	0.62	0.48	0.53	0.82	5.12	6.63	27
Buffalo, NY	Biosolar Roof	28.42	29.55	17.39	6.03	1.23	0.61	0.48	0.53	0.79	4.81	6.24	26.13

4. Discussion

In chapter 3, the simulation results collectively demonstrate the multifunctional performance of biosolar roofs across diverse environmental performance—microclimate cooling, stormwater management, and solar energy potential, and building energy load decrease. Among the four rooftop typologies tested, biosolar roofs consistently demonstrated strong and well-balanced performance across multiple environmental criteria across all climate zones.

Suitability of Biosolar Roofs in Hot and Dry Climate

The findings in this chapter support the view that biosolar roofs are particularly well-suited to hot and dry climates—not despite the heat, but because of it. biosolar roofs can mitigate extreme rooftop temperatures, conserve water through shading-induced soil moisture retention, and maintain sufficient solar potential and energy yields—all of which are critically important in arid urban settings. ENVI-met results showed that biosolar roofs achieved up to 3.5 °C lower near-vegetation air temperatures compared to concrete roofs, outperforming both green and PV-only systems in Tucson, AZ. This substantial cooling benefit suggests that PV shading plays a critical role in heat mitigation, in addition to the cooling effect from plant evapotranspiration. SWMM simulations further confirmed the hydrological relevance of biosolar roofs in dry climates. Due to Tucson's typically dry soil conditions, the vegetated substrate was able to absorb a significant portion of the initial rainfall, reducing the first runoff peak by 46% and delaying the peak by nearly three hours. These effects contribute to stormwater buffering and help prevent drainage system overload during short but intense rain events. Additionally, Tucson is among the regions with the highest solar irradiance, offering excellent conditions for solar energy generation. Finally, OpenStudio-EnergyPlus results indicated that the biosolar roof showed the lowest cooling energy load among all typologies in Tucson. While the benefits of vegetation alone may be limited under water stress, the combination of PV shading and substrate insulation led to measurable reductions in thermal load on the building envelope. Therefore, biosolar roofs may offer a climate-responsive and resource-efficient

strategy for hot and dry climate regions like Tucson.

Limitations

One significant technical limitation of this study is the lack of integrated simulation software that can model the complex thermodynamics of biosolar roof systems. Specifically, existing tools do not provide a unified framework that can comprehensively account for the synergistic effects of plant evapotranspiration, wind flows, ambient humidity, and air temperature on PV efficiency improvement. Consequently, each analysis was performed separately with model domains matched in scale rather than through a standardized setting, making it impossible to isolate and simulate the precise mechanisms behind PV efficiency improvements induced by vegetation and wind effects. Given that the co-benefits of a biosolar roof stem from microclimatic alterations—primarily the cooling effects of evapotranspiration and the modulation of wind dynamics—it is crucial to develop comprehensive analytic techniques based on the empirical studies that can systematically evaluate these interactions.

Additional limitations of Envi-met software were the limitation in modeling. Its inability to adjust PV tilt angles, which only allow two configurations: perpendicular or parallel to the ground. The highest achievable spatial resolution was 0.5 × 0.5 × 0.5 meters, a scale that, while regarded as adequate for neighborhood-scale simulations, is insufficient for detailed analyses at the single-rooftop level. This spatial resolution sometimes caused sporadic errors in wind speed processing at the voxel level occasionally resulted in anomalously high velocities, further complicating the accurate simulation of PV performance. Moreover, the simulation did not account for varying soil depths, despite varying plant heights being considered. Given the significant impact of substrate depth on plant health, soil moisture retention, and overall rooftop hydrology, future research should incorporate simulations with varied soil depths corresponding to plant species and climate conditions. Also, this study did not consider PV self-shading effects. Given that PV panels arranged in certain configurations can partially shade one another—leading to subtle changes in performance—future studies should explicitly consider the impact of PV self-

shading in biosolar roof simulations. These technical constraints highlight the need for enhanced modeling frameworks capable of integrating complex thermodynamic processes and refined spatial resolutions to better capture the nuances of biosolar roof efficiency improvements.

Although EPA-SWMM is a proven program for city-wide storm-water studies, it is built for ground-level landscapes, not rooftops. To model each roof in SWMM, I had to treat the roof surface as a simple sub-catchment and give it uniform values for slope, roughness, and depression storage. This approach can only approximate the more complicated conditions that exist on an elevated deck. Because SWMM cannot place structures above a catchment, it also cannot simulate a photovoltaic canopy or the unique water movement that occurs on a biosolar roof. Likewise, the program's soil routine is meant for natural soil layers and does not reflect the shallow growth media, drainage mats, and filter fabrics used in green roof systems. Even with these limits, I chose SWMM for the early phase of this study because my goal was to understand near-surface runoff, not deep soil processes. Idealizing the roof as a sub-catchment gave a reasonable first estimate of runoff while letting me use SWMM's well-tested routing tools and keep the model consistent with the city-scale drainage work presented elsewhere in the dissertation. Future research should consider integrating more advanced modeling approaches to address SWMM's structural limitations. For example, recent studies have shown the potential of coupling SWMM with HEC-RAS to overcome SWMM's inability to simulate in-depth soil vertical profiles and its water movement (Bragg et al., 2025; Khatooni et al., 2025).

Another limitation involves the choice of perennial ryegrass used uniformly across simulations. While ryegrass was used as a standardized vegetation baseline in this research for comparison, it may not be ideal for all climates, particularly in hot and dry regions such as Tucson, where drought-tolerant species could provide more robust and sustainable performance. Therefore, future research should explore climate-specific vegetation selections and corresponding soil depths to enhance biosolar roofs performance across varied regional environments.

Finally, building-energy simulations in this study utilized the ASHRAE 90.1-2010 Large Office prototype

for Climate Zone 4 (Eugene) and applied it uniformly for Tucson and Buffalo as well. Given that ASHRAE standards provide distinct prototypes tailored specifically to different climate zones, future research should utilize the correct ASHRAE prototypes corresponding precisely to each studied location—such as ASHRAE 90.1-2010 Large Office CZ 4 for Eugene, CZ 6 for Buffalo, and CZ 2 for Tucson. Employing these climate-specific prototypes will enhance the accuracy and generalizability of the energy modeling results.

5. Conclusion

This chapter comprehensively evaluated the multiple environmental performances of biosolar roofs and demonstrated their promising potential as a multifunctional strategy for enhancing climate-adaptive rooftop solutions. Through a combination of systematic analyses, biosolar roofs were shown to reduce near-surface air temperatures, manage stormwater runoff, lower building energy loads, and maintain strong solar energy yields. In hot and dry regions like Tucson, AZ, the synergy between vegetation and photovoltaic panels is expected significant. PV shade also contributed to meaningful reductions in thermal load and surface runoff. While green roofs alone showed limited performance in water-scarce contexts, biosolar roofs overcame such constraints by integrating energy generation and microclimatic regulation.

This study primarily addresses the performance of biosolar roofs at the single-rooftop scale. However, scaling the research to examine the impacts across dense urban environments and remains critical. Future investigations should focus on how the widespread implementation of biosolar roofs influences urban microclimates at neighborhood and city scales. Such scaling-up research is essential to provide quantitative estimations that can support urban planners and policy makers in advocating for sustainable roofing strategies. In particular, understanding the transformation of rooftop surfaces—from conventional empty concrete to incorporating PV panels, vegetation, or a combination thereof—could yield valuable insights into mitigating the Urban Heat Island Effect (UHIE). Therefore, a comprehensive analysis employing advanced analytic approaches may be necessary to elucidate the complex thermodynamic interactions that occur with such transitions. A more integrated modeling framework that captures the nuanced interplay between surface albedo, energy balance modifications, and microclimate dynamics would be particularly valuable. This expanded research could pave the way for evidence-based urban planning policies aimed at promoting sustainable urban design, thereby bolstering the wide-scale adoption of biosolar roofing strategies across metropolitan regions.

An additional limitation is the lack of an integrated analysis among dependent variables evaluated in this chapter, including cooling performance, stormwater reduction, building energy load, and solar energy

yield. Even though each simulation provided valuable insights respectively, differences in simulation timing, methods, spatial resolution, and assumptions constrained the possibility to analyze interactions or their cumulative effects systematically. This limited connectivity may result from difficulties in standardizing modeling conditions of diverse software platforms—ENVI-met, SWMM, Rhino-Grasshopper, and OpenStudio-EnergyPlus. Given that changes in one (e.g., increased cooling from vegetation) can directly influence others (e.g., solar panel efficiency and building energy consumption), recognizing these complex interactions is important. Therefore, future research should aim for integrated approaches that can rigorously evaluate these interdependencies, providing more holistic insights into the multifunctional performance of biosolar roof systems.

This chapter highlights the necessity of context-sensitive design that can leverage both natural and technological systems. As cities seek adaptive, resource-efficient approaches to address climate risks, biosolar roofs can offer a resilient pathway toward more sustainable urban environments. However, for the widespread adoption of biosolar roof, future studies should incorporate economic analyses, assessing lifecycle costs of biosolar systems, compared to conventional green or PV roofs. These economic evaluations would guide policy incentives and investment decisions effectively, ensuring both environmental sustainability and economic feasibility in urban areas.

References

Abdalazeem, M. E., Hassan, H., Asawa, T., & Mahmoud, H. (2022). Review on integrated photovoltaic-green roof solutions on urban and energy-efficient buildings in hot climate. *Sustainable Cities and Society*, *82*(April), 103919. https://doi.org/10.1016/j.scs.2022.103919

Alshayeb, M. J., & Chang, J. D. (2018). Variations of PV panel performance installed over a vegetated roof and a conventional black roof. *Energies*, *11*(5). https://doi.org/10.3390/en11051110

Anang, N., Syd Nur Azman, S. N. A., Muda, W. M. W., Dagang, A. N., & Daud, M. Z. (2021). Performance analysis of a grid-connected rooftop solar PV system in Kuala Terengganu, Malaysia. *Energy and Buildings*, *248*. https://doi.org/10.1016/J.ENBUILD.2021.111182

Baqir, M., & Channi, H. K. (2021). Analysis and design of solar PV system using Pvsyst software. *Materials Today: Proceedings*, *48*, 1332–1338. https://doi.org/10.1016/j.matpr.2021.09.029

Barber, K. A., & Krarti, M. (2022). A review of optimization based tools for design and control of building energy systems. *Renewable and Sustainable Energy Reviews*, *160*(February), 112359. https://doi.org/10.1016/j.rser.2022.112359

Bragg, M. A., Poudel, A., & Vasconcelos, J. G. (2025). *Comparing SWMM and HEC-RAS Hydrological Modeling Performance in Semi-Urbanized Watershed*.

Chang, S., Saha, N., Castro-Lacouture, D., & Yang, P. P. J. (2019). Generative design and performance modeling for relationships between urban built forms, sky opening, solar radiation and energy. *Energy Procedia*, *158*(August), 3994–4002. https://doi.org/10.1016/j.egypro.2019.01.841

Chemisana, D., & Lamnatou, C. (2014). Photovoltaic-green roofs: An experimental evaluation of system performance. *Applied Energy*, *119*, 246–256. https://doi.org/10.1016/j.apenergy.2013.12.027

Choi, Y., Rayl, J., Tammineedi, C., & Brownson, J. R. S. (2011). PV Analyst: Coupling ArcGIS with TRNSYS to assess distributed photovoltaic potential in urban areas. *Solar Energy*, *85*(11), 2924–2939. https://doi.org/10.1016/j.solener.2011.08.034

Dondariya, C., Porwal, D., Awasthi, A., Shukla, A. K., Sudhakar, K., Murali, M. M., & Bhimte, A. (2018). Performance simulation of grid-connected rooftop solar PV system for small households: A case study of Ujjain, India. *Energy Reports*, *4*, 546–553. https://doi.org/10.1016/J.EGYR.2018.08.002

Fleck, R., Gill, R., Pettit, T. J., Torpy, F. R., & Irga, P. J. (2022). Bio-solar green roofs increase solar energy output: The sunny side of integrating sustainable technologies. *Building and Environment*, *226*(August), 109703. https://doi.org/10.1016/j.buildenv.2022.109703

Guglielmetti, R., Macumber, D., & Long, N. (2011). OpenStudio : An Open Source Integrated Analysis Platform Rob Guglielmetti , Dan Macumber , and Nicholas Long. *Building Simulation 2011: 12th Conference of International Building Performance Simulation Association*, 442–449.

Gullotta, A., Aschale, T. M., Peres, D. J., Sciuto, G., & Cancelliere, A. (2023). Modelling Stormwater Runoff Changes Induced by Ground-Mounted Photovoltaic Solar Parks: A Conceptualization in EPA-SWMM. *Water Resources Management*, *37*(11), 4507–4520. https://doi.org/10.1007/s11269-023-03572-3

Hörnschemeyer, B., Henrichs, M., Dittmer, U., & Uhl, M. (2023). Parameterization for Modeling Blue–Green Infrastructures in Urban Settings Using SWMM-UrbanEVA. *Water (Switzerland)*, *15*(15). https://doi.org/10.3390/w15152840

Huber, W. C., Heaney, J. P., Medina, M. A., Peltz, W. A., Sheikh, H., & Smith, G. F. (1975). Storm Water Management Model User'S Manuel. Version Ii. *Environ Prot Technol Ser EPA*, *670 /2-75–017*.

Hui, S. C. M., & Chan, S.-C. (2011). Integration of green roof and solar photovoltaic systems. *Joint Symposium*, 1–12.

Irga, P., Fleck, R., Wooster, E., Torpy, F., Pettit, T., Gill, R., & Ball, J. (2021). *Green Roof & Solar Array Comparative Research Project Final Report July 2021*. City of Sydney Council.

Jahanfar, A., Drake, J., Sleep, B., & Margolis, L. (2019). Evaluating the shading effect of photovoltaic panels on green roof discharge reduction and plant growth. *Journal of Hydrology*, *568*(October 2018), 919–928. https://doi.org/10.1016/j.jhydrol.2018.11.019

Jahanfar, A., Sleep, B., & Drake, J. (2018). Energy and carbon-emission analysis of integrated green-roof photovoltaic systems: probabilistic approach. *Journal of Infrastructure Systems*, *24*(1), 4017044.

Jeffers, S., Garner, B., Hidalgo, D., Daoularis, D., & Warmerdam, O. (2022). Insights into green roof modeling using SWMM LID controls for detention-based designs. *Journal of Water Management Modeling*, *30*(March). https://doi.org/10.14796/JWMM.C484

Kausika, B. B., & van Sark, W. G. J. H. M. (2021). Calibration and validation of ArcGIS solar radiation tool for photovoltaic potential determination in the Netherlands. *Energies*, *14*(7). https://doi.org/10.3390/en14071865

Kavitha, M., Immanuel, D. G., Rex, C. R. E. S., Meenakshi, V., Pushpavalli, M., Singari, S., & Baskaran, V. (2021). Energy Forecasting of Grid Connected Roof Mounted Solar PV Using PVSOL. *Proceedings of the 2021 IEEE International Conference on Innovative Computing, Intelligent Communication and Smart Electrical Systems, ICSES 2021*, 1–6. https://doi.org/10.1109/ICSES52305.2021.9633888

Kelly, C., Sen, B., & Tatari, O. (2020). A system dynamics analysis of the alternative roofing market and its potential impacts on urban environmental problems: A case study in Orlando, Florida. *Resources, Conservation and Recycling*, *153*. https://doi.org/10.1016/J.RESCONREC.2019.104556

Khatooni, K., Hooshyaripor, F., MalekMohammadi, B., & Noori, R. (2025). A new approach for urban flood risk assessment using coupled SWMM–HEC-RAS-2D model. *Journal of Environmental Management*, *374*(January), 123849. https://doi.org/10.1016/j.jenvman.2024.123849

Lamnatou, C., & Chemisana, D. (2015). A critical analysis of factors affecting photovoltaic-green roof performance. *Renewable and Sustainable Energy Reviews*, *43*, 264–280. https://doi.org/10.1016/j.rser.2014.11.048

Nagengast, A., Hendrickson, C., & Scott Matthews, H. (2013). Variations in photovoltaic performance due to climate and low-slope roof choice. *Energy and Buildings*, *64*, 493–502. https://doi.org/10.1016/j.enbuild.2013.05.009

Nair, A. A., Rohith, A. N., Cibin, R., & McPhillips, L. E. (2024). A Framework to Model the Hydrology of Solar Farms Using EPA SWMM. *Environmental Modeling and Assessment*, *29*(1), 91–100. https://doi.org/10.1007/s10666-023-09922-0

Ogaili, H., & Sailor, D. J. (2016). Measuring the effect of vegetated roofs on the performance of photovoltaic panels in a combined system. *Journal of Solar Energy Engineering*, *138*(6), 61009.

Pan, Z., Wang, C., Yu, B., Chen, Z., Yuan, Y., Li, G., Zhang, J., & Xiao, T. (2024). Assessing multifunctional retrofit potential of urban roof areas and evaluating the power and carbon benefits under efficient retrofit scenarios. *Journal of Cleaner Production*, *444*(October 2023), 141270. https://doi.org/10.1016/j.jclepro.2024.141270

Qingsong, M., & Fukuda, H. (2016). Parametric Office Building for Daylight and Energy Analysis in the Early Design Stages. *Procedia - Social and Behavioral Sciences*, *216*, 818–828. https://doi.org/10.1016/j.sbspro.2015.12.079

Sailor, D. J. (2008). A green roof model for building energy simulation programs. *Energy and Buildings*, *40*(8), 1466–1478. https://doi.org/10.1016/j.enbuild.2008.02.001

Sattler, S., Zluwa, I., & Österreicher, D. (2020). The “PV rooftop garden”: providing recreational green roofs and renewable energy as a multifunctional system within one surface area. *Applied Sciences*, *10*(5), 1791.

Scherba, A., Sailor, D. J., Rosenstiel, T. N., & Wamser, C. C. (2011). Modeling impacts of roof reflectivity, integrated photovoltaic panels and green roof systems on sensible heat flux into the urban environment.

Building and Environment, *46*(12), 2542–2551. https://doi.org/10.1016/j.buildenv.2011.06.012

Shafique, M., Luo, X., & Zuo, J. (2020). Photovoltaic-green roofs: A review of benefits, limitations, and trends. *Solar Energy*, *202*(February), 485–497. https://doi.org/10.1016/j.solener.2020.02.101

Singh, R., & Banerjee, R. (2015). Estimation of rooftop solar photovoltaic potential of a city. *Solar Energy*, *115*, 589–602. https://doi.org/10.1016/J.SOLENER.2015.03.016

Talwar, P., Verma, N., Khatri, H., Ahire, P. D., Chaudhary, G., Lindenberger, C., & Vivekanand, V. (2023). A systematic review of photovoltaic-green roof systems in different climatic conditions focusing on sustainable cities and societies. *Sustainable Cities and Society*, *98*(July), 104813. https://doi.org/10.1016/j.scs.2023.104813

Tolderlund, L. (2010). Design Guidelines and Maintenance Manual for Green Roofs in the Semi-Arid and Arid West. *University of Colorado Denver*, 59. http://www.epa.gov/region8/greenroof/pdf/GreenRoofsSemiAridAridWest.pdf

CHAPTER 4

EMPIRICAL AND COMPARATIVE PERFORMANCE ASSESSMENT FOR BIOSOLAR ROOF

1. Introduction

Building upon the simulation-based analyses presented in the previous chapters, this chapter introduces a reduced-scale rooftop experiment to empirically evaluate the environmental performance of biosolar roofs. While Chapters 2 and 3 explored how design parameters and climatic conditions shape performance through simulation tools, the applicability of those results ultimately depends on validation against real-world data. Without such empirical verification, the theoretical advantages of biosolar systems remain speculative and difficult to translate into practical design or policy recommendations.

Although prior studies have examined specific benefits of biosolar roofs—such as improved PV efficiency or microclimate cooling—most were conducted in independent contexts, often comparing only two roof types at a time (e.g., PV vs. biosolar) (Abdalazeem et al., 2022; Talwar et al., 2023). As a result, there remains a notable lack of side-by-side, multi-typology field evaluations conducted under identical environmental conditions. To address this gap, this chapter addresses a field experiment designed to monitor the environmental behavior of concrete, green, PV, and biosolar roof modules installed under the same rooftop setting.

This chapter focuses on detecting empirical patterns of interaction that can be observed through real-world monitoring. These include how vegetation shading influences soil moisture, how thermal behavior shifts under PV canopies, and how PV orientation and ground treatments affect solar energy production. The biosolar module itself was internally divided into shaded and unshaded areas, allowing micro-scale thermal comparisons within the same module footprint.

Additionally, this chapter explores how east- and west-facing bifacial PV arrays, in combination with a high-reflective film[4], may mitigate the challenge of energy supply and demand imbalance, especially during morning and evening time. This investigation is particularly relevant for biosolar designs in cloudy or snow-prone climates.

This chapter addresses the following five research questions:

1. *How much more (or less) solar energy does the biosolar roof generate compared to the PV roof, when both lie in the same PV configuration*
2. *How does shade affect soil moisture on the biosolar roof, and how does that compare to the green roof?*
3. *How does the air temperature near the vegetation differ across shaded and unshaded parts of the biosolar roof—and compared to the air temperature on PV, green, and concrete roof?*
4. *How do surface temperatures vary between the five roof types: biosolar, green, PV, concrete, and the one with reflective film?*
5. *Can bifacial solar panels facing east and west help produce more energy during the early morning and late afternoon? And does covering reflective film under the model improve that effect?*

By integrating empirical monitoring with prior simulations, this chapter aims to validate key assumptions, clarify biosolar roof performance under real conditions, and contribute design-relevant evidence for broader implementation in diverse climate contexts.

[4] A high-reflective film (albedo 0.95) was installed to contrast with the low-albedo concrete surface and examine how surface reflectivity influences microclimate conditions and bifacial PV solar yield. The aim was to assess the effect of increased diffuse radiation on bifacial PV performance and near-surface thermal behavior.

2. Method

2.1 Field Experiment Design and Installation

A field experiment was established on the rooftop of Pacific Hall at the University of Oregon in Eugene, Oregon. The experiment spans from September 2024 to August 31, 2025, and incorporates four scaled modules: biosolar roof, green roof, PV roof, and concrete roof. Each module is constructed at a 1.8m × 1.8m (6 ft × 6 ft) scale, reflecting practical constraints including a 6.8 kg (15 lbs) / ft² load limit and a budget of $5,000.

2.2 Experiment Modules Description

Four experimental rooftop modules, each measuring 1.8m × 1.8m (6′ × 6′), were constructed to evaluate the environmental performance of different roof typologies under controlled conditions. Each module was installed on a rubber membrane and waterproof vinyl to prevent damage. A raised planter box was placed on top and filled with a lightweight growing medium—a 7:3 soil-to-perlite mix—to meet the 6.8 kg (15 lbs)/ft² structural load limit of the Pacific Hall rooftop. A 4.5-foot French drain—consisting of a perforated polystyrene pipe covered with polyrocks—was embedded within the garden bed and then covered with the soil substrate. The module size was chosen to balance structural safety, material availability, construction feasibility, and a total budget constraint. Table 1 contains specific model configuration.

As **Table 4.1** and **Figure 4.1** show, the four roof types include: (1) a biosolar roof, consisting of an extensive green roof overlaid with two southern facing 130 W photovoltaic panels mounted at a height of 1 meter; (2) a PV roof, with the same PV configuration but without vegetation; (3) a green roof, using the same soil and vegetation as the biosolar module but without PV panels; and (4) a concrete roof, represented by a nearby exposed rooftop section without added treatments. The 1-meter PV height was selected based on previous simulation findings, optimizing both indirect light availability for vegetation

and cooling benefits from plant-driven evapotranspiration. Additionally, both the biosolar and PV roof modules include two types of PV systems installed in alternating positions: a south-facing PV array tilted at 30 degrees, and a vertically mounted bifacial PV facing east and west.

To support proper drainage in the vegetated modules, a French-drain-style perforated PVC pipe was embedded within the planter beds to prevent water accumulation from storms or irrigation. Vegetation was composed of perennial ryegrass (*Lolium perenne L.*) for its shade-tolerant and their hardiness and ability to survive rooftop microclimatic conditions (Cool et al., 2004; Koehler, 2023).

Table 4.1 Summary of experimental module configurations

	Size	Layering	PV panel	Surface type	Drainage	PV orientation
Biosolar roof	6’ x 6’	10” Soilmix (Soilmix 70% Perlite 30%)	Two 130W solar PV panels	Vegetation (Ryegrass sod)	French drainage (perforated pipe)	South facing
			Two 120W Bifacial solar PV panels			West and East facing
PV roof	6’ x 6’	N/A	Two 130W solar PV panels	Gravel surface	N/A	South facing
			Two 120W Bifacial solar PV panels			West and East facing
Green roof	6’ x 6’	10” Soilmix (Soilmix 70% Perlite 30%)	N/A	Vegetation (Ryegrass sod)	French drainage (perforated pipe)	N/A
Concrete roof	6’ x 6’	N/A	N/A	Gravel surface	N/A	N/A



Figure 4.1 Top: experimental setup on the rooftop (south-facing biosolar roof, PV roof, and green roof modules); bottom: East-West facing bifacial biosolar and PV roof setup on the rooftops

2.3 Environmental Sensors Installations and Data Collection

To evaluate the environmental performance of each rooftop module, I installed HOBO environmental sensors and data loggers to monitor air temperature, surface temperature, relative humidity, soil moisture, wind speed, and solar yield. These specific parameters were selected based on conjecture from previous studies, which suggest that cooling effects and corresponding PV efficiency gains can be linked to the interplay among air temperature, wind, and plant evapotranspiration beneath a PV array (Bousselot et al., 2017; Jahanfar et al., 2019; Talwar et al., 2023; Zluwa & Pitha, 2021). Accordingly, in the biosolar roof module, supplementary sensors were placed in both shaded and non-shaded areas to capture the nuanced impacts of partial PV coverage on thermal and moisture conditions. Data was recorded every 10 seconds and logged every 30 seconds, with manual data exports occurring approximately every 18 days.

Figure 4.2 illustrates the sensor placements and the overall monitoring setup. Data collection began in early October 2024 and continue through August 2025 to capture a full year of seasonal variation.

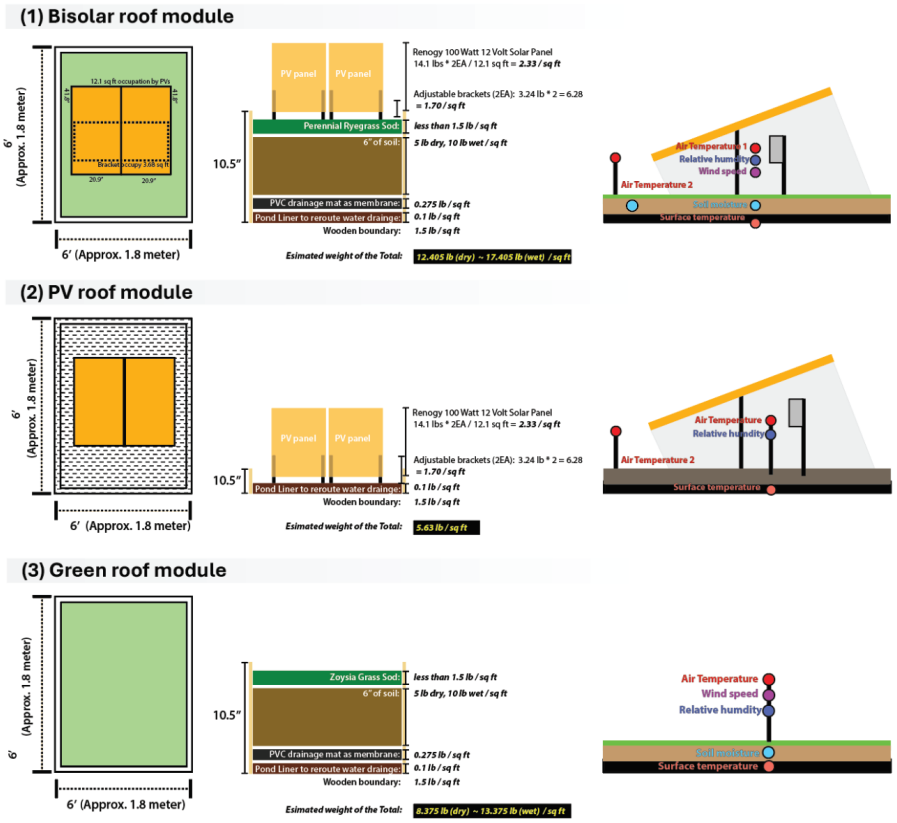


Figure 4.2 Weight estimation and environmental sensor installation scheme (air temperature sensors at 0.25m)

2.4 Off-grid Solar PV System and Real-time Solar PV Yield Monitoring System

I installed two sets of approximately 500 W of off-grid solar PV capacity on the rooftop as shown in **Figure 4.3**. One system consists of a 250 W unit made up of two 130 W monofacial PV panels, while the other consists of a 240 W unit comprising two 120 W bifacial PV panels. These were integrated into the PV roof and the biosolar roof modules, respectively. Each system was paired with a separate Battery Management System (BMS), forming independent off-grid setups. The BMS is an electronic controller that monitors and regulates rechargeable batteries, ensuring safe operation, prolonging battery life, and maintaining optimal performance (Cao et al., 2024). Through built-in Bluetooth functionality, the BMS wirelessly communicates with a Raspberry Pi microcomputer, allowing for real-time solar yield data to be processed and logged (Cao et al., 2024; Hindi et al., 2024; Kishore Kumar et al., 2021). The Raspberry Pi—a small, affordable single-board computer—has seen widespread adoption in research for low-cost environmental monitoring, prototyping, and data collection (Kishore Kumar et al., 2021; Upton & Halfacree, 2012) . By leveraging this integrated network of hardware, I was able to capture solar power generation metrics on a second-by-second basis, providing a robust dataset for analyzing off-grid PV system performance and comparing the efficiency of various rooftop configurations.

The architecture of real-time monitoring system in Raspberry Pi consists of the major four steps shown in **Figure 4.4**, from raw data acquisition to final visualization (Hindi et al., 2024). First, Mosquitto (an MQTT broker) receives raw data from the BMS and send it to a subscriber—Telegraf—which helps to aggregate and format the data (Hindi et al., 2024). Next, Telegraf writes the processed outputs and sends them to InfluxDB, which helps construct a time-series database for high-frequency sensor data (Hindi et al., 2024). Finally, Grafana queries InfluxDB and renders the results on an online dashboard, enabling users to view real-time solar yield and environmental metrics through a standard web interface (Hindi et al., 2024).

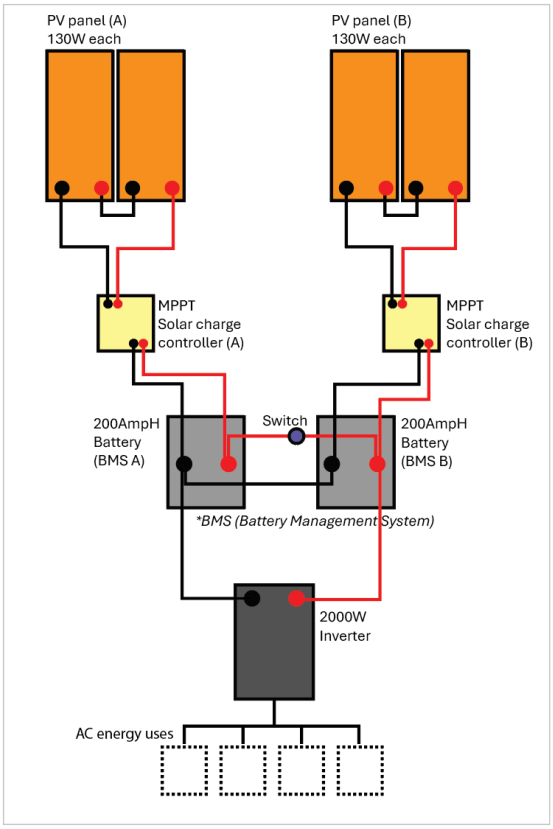


Figure 4.3 Off-grid solar PV system composition

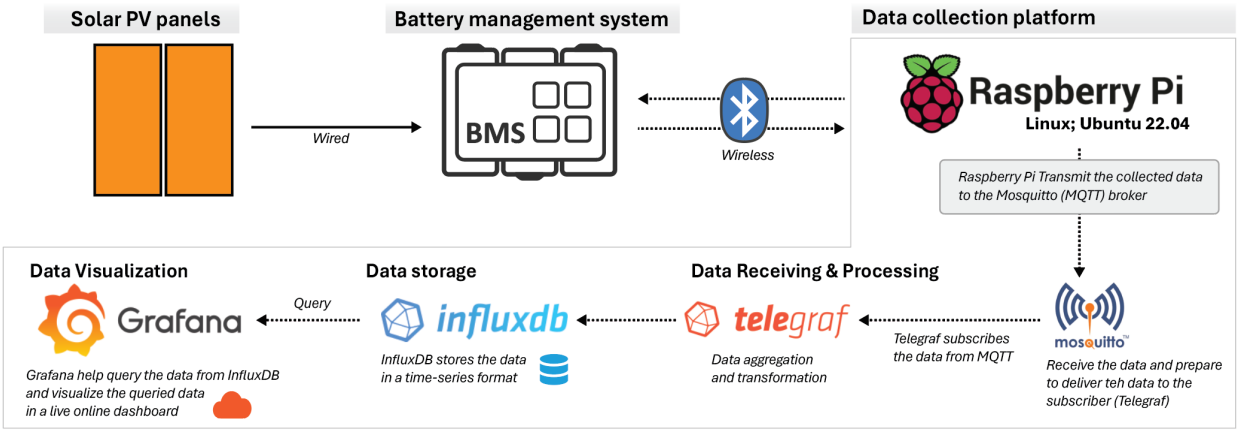


Figure 4.4 Internet of Things (IoT) Realtime monitoring system with Raspberry Pi and BMS

2.5 Bifacial East-West Facing Solar PV Installations

To investigate whether bifacial PV modules can help reduce the mismatch between solar energy supply and demand during early morning and late afternoon hours, I designed a supplemental rotational experimental setup that alternately tested two PV configurations under different rooftop surface conditions. The first configuration involved a conventional monofacial PV system, with panels tilted at 30 degrees and south facing—representing a standard PV or biosolar roof layout. The second configuration used a vertically mounted bifacial PV system facing east and west, intended to capture reflected sunlight during low-angle hours of the day. These two PV types were alternately installed over a raised vegetation bed to simulate two versions of biosolar roofs: the standard biosolar roof (with tilted monofacial PV) and the bifacial biosolar roof (with vertical bifacial PV).



Figure 4.5 Bifacial East-West facing solar PV experiment setup over vegetation (Left) and high-albedo reflective film (Right)

Both configurations were tested under the same location and structural conditions, with only the PV array swapped to isolate the effect of panel type and orientation. The same alternating approach was applied to a bare concrete surface to simulate PV roof conditions. This allowed for side-by-side comparison between

standard PV roofs and bifacial PV roofs under non-vegetated conditions. In addition, as a third setup, a high-albedo reflective film was laid to assess the effect of surface reflectivity on bifacial PV performance (**Figure 4.5**). In this configuration, the bifacial PV array was mounted above a high-albedo reflective film placed directly on the rooftop, simulating the conditions of a cool roof. All systems used identical Battery Management Systems (BMS) and sensor arrays to continuously monitor solar yield, air temperature, surface temperature, and soil moisture where applicable. This consistent monitoring framework ensured that performance differences could be attributed to PV configuration and surface treatment rather than external variability.

3. Results

3.1 Near-Surface Air Temperature Comparisons in Autumn

Figure 4.6 presents boxplots of air temperature (near-surface) measurements collected during autumn across four rooftop modules—biosolar (shaded and non-shaded), green, PV, and concrete. The concrete roof consistently showed higher temperatures, with the widest range and highest upper quartile values. In contrast, the shaded area of the biosolar roof showed the lowest average temperature (11.5 °C) and the lowest maximum temperature (28.1 °C), compared to the concrete roof's average of 13.2 °C and peak of 35 °C. This contrast highlights the synergetic cooling effects of vegetation and PV shading, which together lower near-vegetation air temperatures. Notably, the shaded area of the biosolar roof and the PV

roof (under PV shade) showed greater cooling than, the biosolar's non-shaded area and the standalone green roofs. This supports the simulation results in Chapters 2 and 3, which found that PV shading reduces near-vegetation air temperatures more effectively than vegetation alone. Although the simulated cooling effect was relatively modest—around 0.5 °C on average—the observed difference of approximately 2 °C between the concrete and biosolar roofs emphasizes the importance of identifying optimal design configurations to maximize the cooling benefits of biosolar systems.

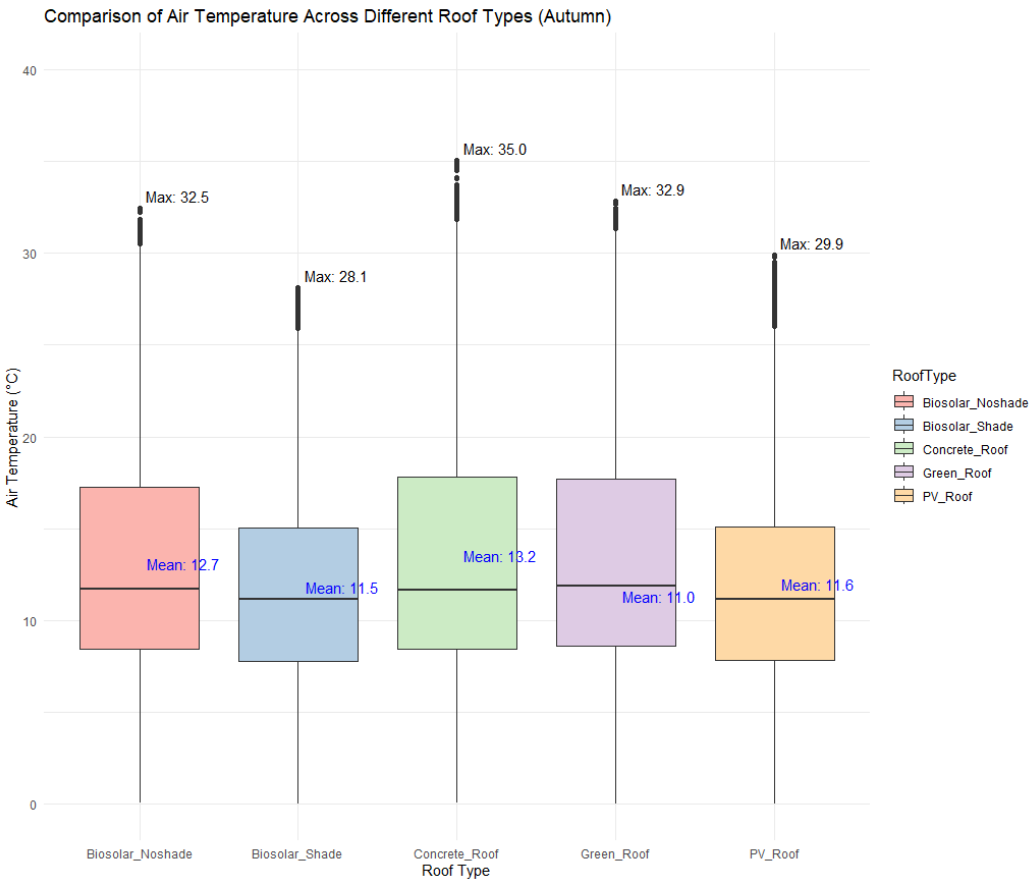


Figure 4.6 Comparison of air temperature across different roof types (autumn); Colored boxes represent the inter-quartile range (IQR, 25th–75th percentiles)[5].

[5] The black line inside each box marks the median. Whiskers extend to ± 1.5 × IQR (Interquartile Range), and points beyond them are statistical outliers. Blue text gives the mean for each roof, while black "Max:" labels mark the absolute peak temperature recorded. Shaded biosolar plots register the lowest mean (11.5 °C) and the narrowest IQR, indicating the roof type with the least temperature variation. Concrete roofs reach both the highest mean (13.2 °C) and the hottest single event (35 °C), highlighting rapid daytime heating. Biosolar roofs without shade and PV roofs fall between these extremes, whereas the vegetated green roof moderates peak temperatures but still shows a broad middle-50 % spread.

3.2 Near-Surface Air Temperature Comparisons in Spring

Figure 4.7 shows the same near-surface air temperature measurements but collected during Spring (March 8 to March 11, 2025). Despite the seasonal shift, the results closely mirrored the autumn trends. The biosolar's shaded area consistently recorded lower near-surface air temperatures than the concrete, green and PV roofs. Also, the cooling effect of PV shading appeared stronger than that of vegetation alone, as seen in the comparison between the average and peak temperatures of the green and PV roofs—though still less effective than the biosolar roof.

Notably, the average air temperature difference between the coolest (biosolar) and hottest (concrete) roofs narrowed from 2.3 °C in Autumn to 1.4 °C in Spring. This reduction may suggest that the biosolar roof's relative cooling benefit becomes more significant under hotter conditions, as observed during Eugene's 2024 Autumn season was warmer than 2025 Spring, based on recorded temperature peaks.

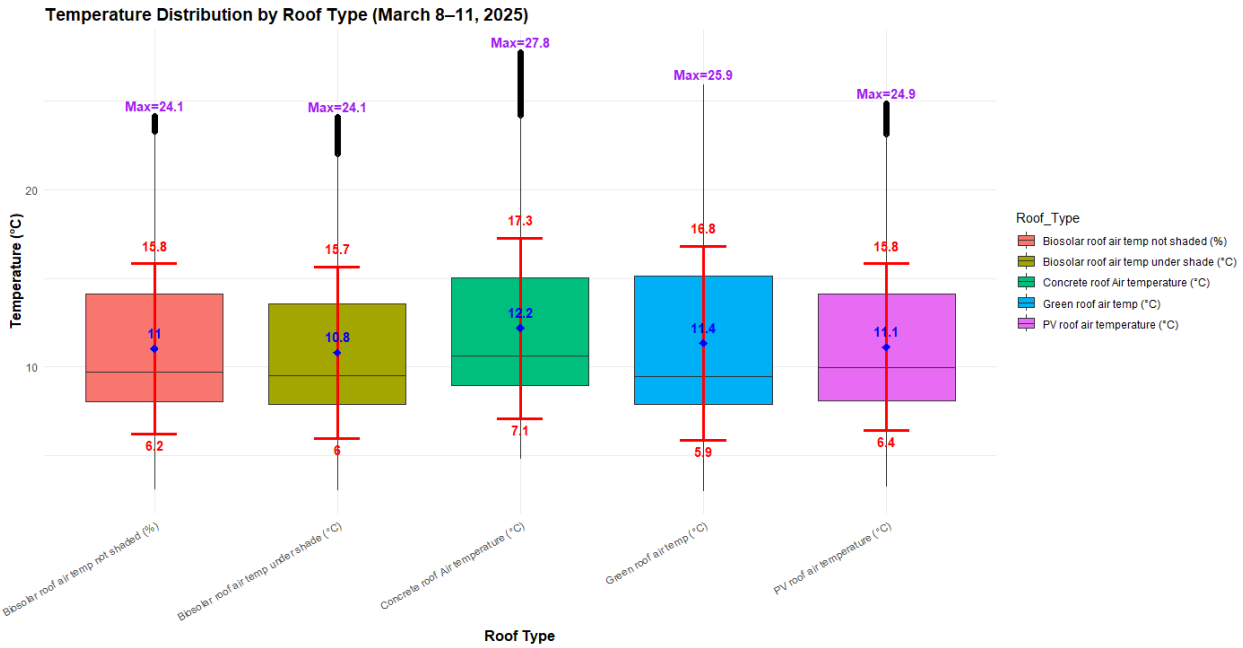
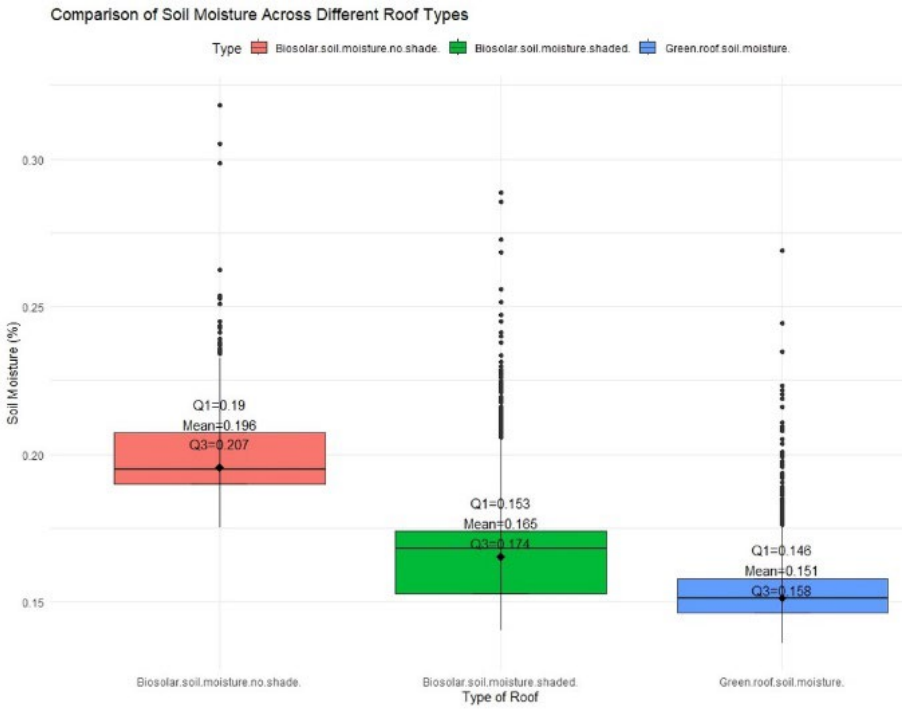


Figure 4.7 Near-surface air temperature comparisons in spring[6]

[6] Boxes give the IQR with medians, whiskers, and outliers as defined previously. Blue diamonds mark the mean, and the red capped bar shows the range of mean ± standard deviation (SD) (values in red). Compared with the other roofs, the shaded-biosolar roof has the narrowest SD band, revealing the least temperature fluctuation; the green roof exhibits the widest band, indicating larger day-to-day temperature variability.

3.3 Soil Moisture Dynamics Under Dry Conditions and Manual Irrigation

First, **Figure 4.8** shows the measurement during the manual irrigation[7], with clear and sunny days between October 10 to 16, in 2024. In the boxplot of Figure 4.8, the non-shaded area of the biosolar module (red color) was represented as a highest mean soil moisture around 0.196 % among three places, whereas the shaded area of the biosolar configuration and the green roof recorded lower averages (0.165 % and 0.151 %, respectively). Interestingly, this suggests that irrigated water was more concentrated in areas where the tilted PV panels were closest to the vegetation surface. This may be because I cleaned the PV panels during irrigation, and the cleaning water runoff likely accumulated at that point, increasing soil moisture there than shaded area. Also, Figure 4.8 shows that PV shade plays a significant role in sustaining soil moisture over time, especially compared to the green roof, which is fully exposed to direct solar radiation during the measurement periods.



[7] I cleaned the PV panels and irrigated the vegetation simultaneously using a sprinkler hose connected to a water source.

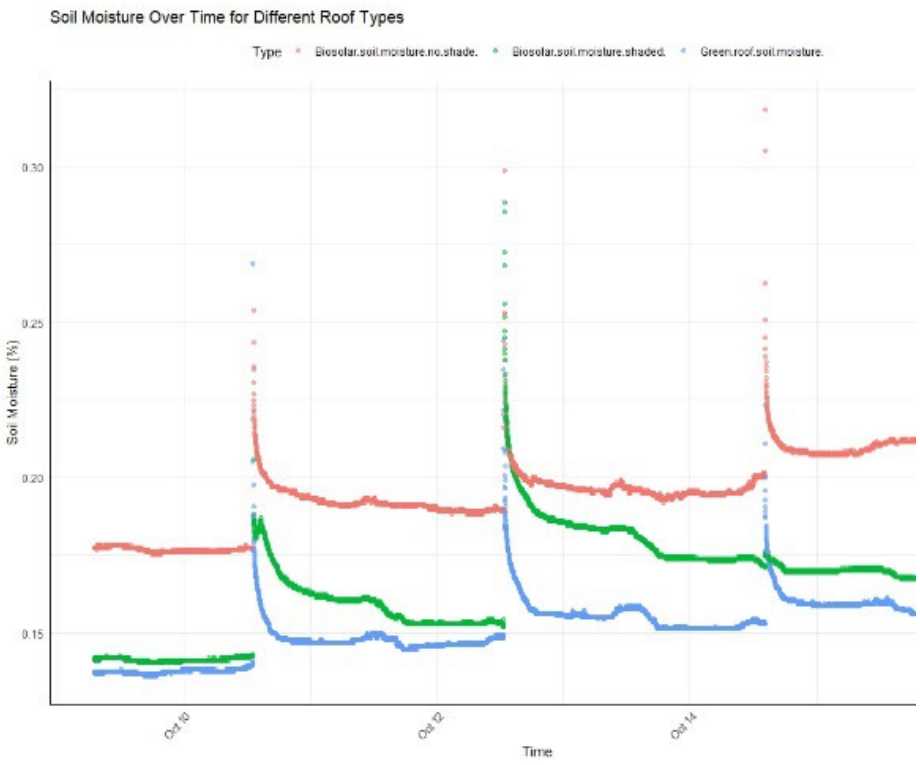


Figure 4.8 (Top) Boxplot comparing soil moisture levels among biosolar shaded, biosolar non-shaded, and green roof modules, during manual irrigation periods. (Bottom) Line graph showing temporal soil moisture dynamics, during manual irrigation periods.

3.4 Soil Moisture Dynamics During Rainy Season

During the rainy period (**Figure 4.9**), soil moisture levels increased noticeably across all roof types. The non-shaded area of the biosolar roof showed a 57% rise, the shaded area increased by approximately 13%, and the green roof showed the largest relative increase of over 76%, compared to the irrigation scenario. The highest mean soil moisture was observed in the non-shaded biosolar area (0.308 m^3/m^3), likely because rainwater runoff from the sloped PV panels accumulated in the lower-pitched area—resulting in higher moisture levels than the green roof (0.266 m^3/m^3). In contrast, the shaded area of the biosolar module recorded the lowest mean value (0.187 m^3/m^3), likely due to partial rainfall interception by the PV panel. Also, the time-series soil moisture plot supports these findings, showing synchronized moisture peaks and gradual declines across all modules in response to rainfall events.



Figure 4.9 (Top) Boxplot comparing soil moisture levels among Biosolar shaded, Biosolar non-shaded, and green roof modules during rainy season. (Bottom) Line graph showing temporal soil moisture dynamics, during rainy season.

3.5 Solar Yield Comparison Between the Biosolar Roof and The PV Roof Modules

Based on **Figure 4.10**, the comparison between biosolar and conventional PV roof modules shows that the biosolar roof yielded 2.29% more electricity (Watts) on average between January 13 and March 15, 2025 (n = 16,757). This result aligns with previous empirical findings that biosolar systems typically improve PV efficiency by up to 5% compared to standard PV roofs due to panel cooling (Abdalazeem et al., 2022; Lamnatou & Chemisana, 2015; Talwar et al., 2023).

I also conducted a paired t-test to statistically assess the differences of PV yields as shown in **Table 4.2**. The results revealed a statistically significant difference in energy generation between the biosolar roof and the PV roof modules ($p < 0.001$). The average yield difference was approximately 1.49 Watts, with a 95% confidence interval ranging from 0.74 Watts to 2.24 Watts. This indicates that the biosolar roof can consistently outperform the PV roof module in terms of energy generation, likely due to microclimatic cooling effects by vegetation.

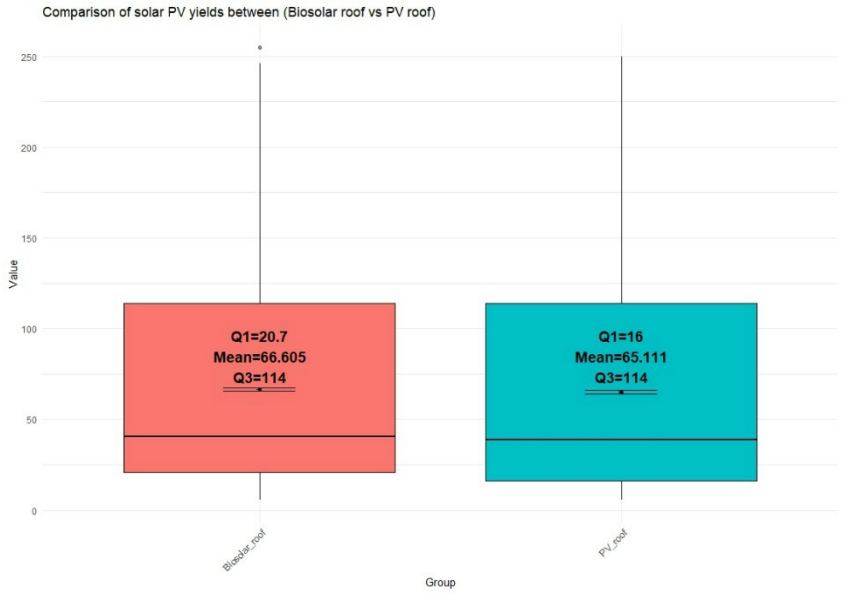


Figure 4.10 A box plot comparing PV energy yield between biosolar and standard PV roofs (unit: Watts)

Table 4.2 Paired t-test results comparing PV energy yield between biosolar and standard PV roofs

Test	t-statistic	Degrees of Freedom (df)	p-value	Mean Difference	95% CI Lower Bound	95% CI Upper Bound
Paired t-test	3.8993	16755	< 0.001	1.493662	0.742817	2.244507

3.6 Bifacial Solar Yield Enhancement on Reflective Film

Figure 4.11 compares the electrical yield of the bifacial PV module when it was installed above a conventional concrete roof and when the same module was repositioned above a high-reflective polymer film. The box whisker plots reveal a systematic upward shift in the entire yield distribution when the Bifacial PV is placed on reflective film. Daily mean solar yield increased from 68.1 W on concrete to 78.2 W on the reflective film, which is equivalent to an enhancement of 14.8 %, between April 12 and 15 2025[8] (n = 2,457). This aligns with previous findings that installing bifacial PV modules over reflective surfaces can increase energy yields by 15–30%, primarily due to enhanced irradiance from the high-albedo surface (Katsikogiannis et al., 2022; Yusufoglu et al., 2014).

Both quartiles moved upward: the first quartile rose from 13.6 W to 24.7 W and the third quartile from 135 W to 152 W. The inter-quartile range widened only marginally, indicating that the improvement is not driven by extreme values but by a broad-based elevation of yields measurement every second. The maximum instantaneous output likewise increased, from 170 W to 184 W, confirming that the reflective surface can sustain higher peak currents under identical irradiance conditions.

The scatter plot of Figure 4.11 clarifies the overall PV yield improvement over the reflective film during the day (April 12 – 15, 2025). In the morning hours (08:00–10:30), the reflective configuration already delivers ~35 W while the concrete reference remains below 25 W, consistent with enhanced ground-reflected irradiance at low sun angles. Between 11:30 and 15:30 the advantage peaks: the

[8] Four consecutive perfectly clear-sky days were selected: April 12–13 for the bifacial PV without reflective film, and April 14–15 with the reflective film.

reflective module plateaus near 180 W, exceeding the concrete case by roughly 20 W, which corresponds to a relative gain of 12–15 %. After 16:00 both curves converge, yet the film maintains a residual benefit of 5–8 W until sunset. The diurnal signature therefore corroborates the albedo-driven bifacial-gain mechanism proposed in Chapter 3. **Table 4.3** presents the results of a paired t-test, confirming the statistical significance of PV yield improvements under reflective film conditions ($p < 0.001$).

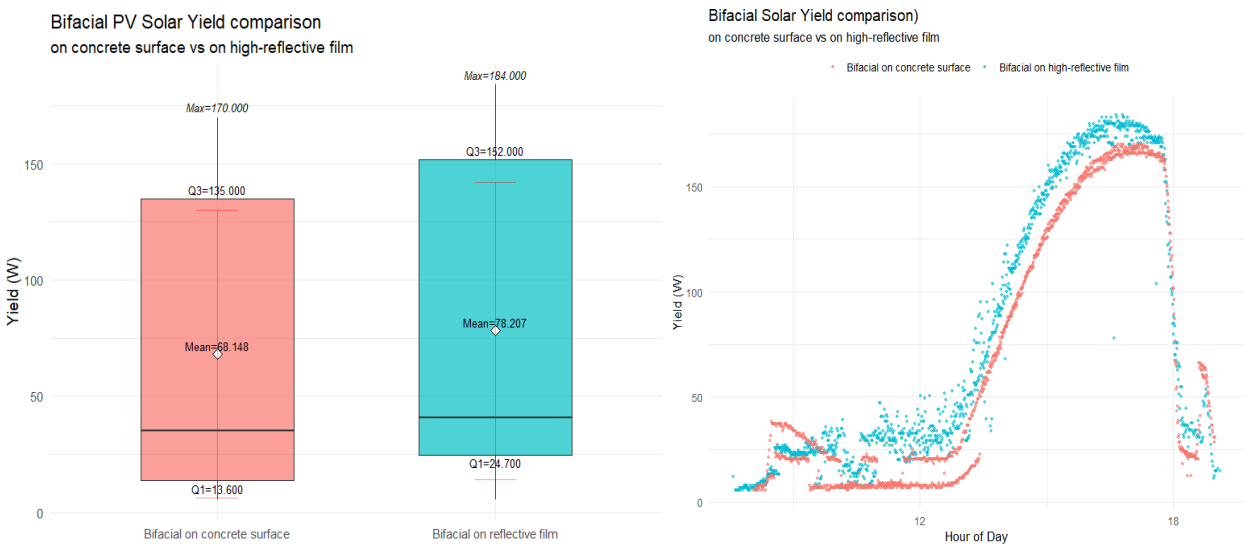


Figure 4.11 Left: Boxplot showing higher mean yield for bifacial PV on reflective film (78.2 W) than on concrete (68.1 W). Right**:** Diurnal yield curve indicating consistently greater performance on reflective film, especially during early and late hours

Table 4.3 Comparison of bifacial PV solar yield on concrete vs high-reflective film surfaces

Test	t-statistic	Degrees of Freedom	p-value	Mean Difference	95% CI Lower Bound	95% CI Upper Bound
Paired t-test	3.8993	16,755	< 0.001	1.494	0.743	2.245

3.7 Comparison of Surface Temperature Across the Modules

Figure 4.12 presents surface temperature measurements from April 14 to 17 across different roof types. The concrete roof showed the highest peaks, rising from around 15 °C in the morning to over 50 °C at midday. In contrast, the reflective film stayed much cooler, between ~18 °C and 28 °C due to its high albedo that reflects sunlight. Green and biosolar roofs showed similar daily patterns, but with noticeable differences in peak temperature. The green roof warmed from ~16 °C to ~30 °C, while the biosolar roof reached nearly 40 °C. This difference may be due to sensor-placement and edge effects, considering their vegetation beds sizes are the same. To be more specific, the sensor for the green roof was mounted on the northern face of its raised bed underneath, benefiting from partial shade cast by the bed's height and cooler rooftop edges. In contrast, the biosolar sensor was placed in the southern face of its bed underneath, which exposed to more radiated heat from the surrounding bare concrete surfaces, limiting lateral cooling. Therefore, considering the small size of the module (6'*6'), proximity to contrasting surface conditions exaggerates microclimate effects. This sensor placement issue, which may have led to locally elevated temperatures in the biosolar module, should be corrected in future research by standardizing sensor locations across modules or incorporating spatial averaging to reduce edge-effect bias.

These surface temperature patterns provide strong physical evidence that supports the building cooling load results discussed in Chapter 3. Roofs with higher surface temperatures—such as the concrete roof, which peaked above 50 °C and recorded the highest daily mean (26.6 °C)—conduct more heat into the building. This aligns with the Chapter 3 simulation findings, which showed that concrete roofs imposed the greatest cooling energy demand.

In contrast, the green roof and reflective film surface maintained lower and more stable temperatures (around 14 °C), which also corresponds with their better performance in reducing cooling loads in Chapter 3. Interestingly, the near-surface air temperature beneath the shaded area of the PV roof was higher than the surface temperatures beneath both the reflective and green roofs. This further highlights

the importance of high-albedo surfaces in cooling rooftop microclimates.

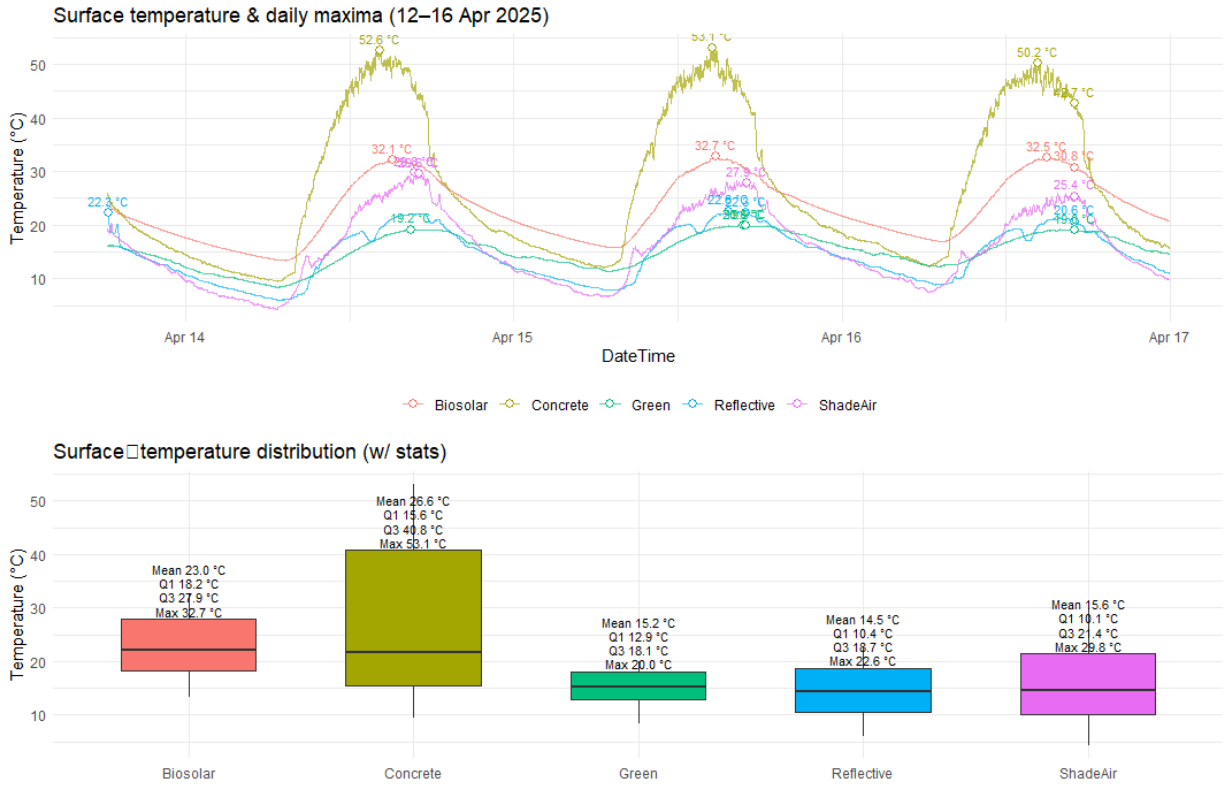


Figure 4.12 (Top) Diurnal surface temperature patterns and daily maxima across five roof types (Apr 12–16, 2025), and (Bottom) Box plot comparison of surface temperature distributions.

4. Discussion

This chapter presents an empirical comparison of the environmental and energy performance of four rooftop types: concrete, green, PV, and biosolar modules. In response to the five research questions, the key findings are summarized as follows:

1. How much more (or less) solar energy does the biosolar roof generate compared to the PV roof, when both lie in the same PV configuration?

The field measurement showed that biosolar roof module produced approximately 2.29% more electricity on average compared to a conventional PV roof module in the identical PV configurations during January 13 and March 15, 2025, with statistical significance (paired t-test; $p < 0.001$). This aligns with previous studies suggesting biosolar roofs can enhance up to 5% of PV efficiency through cooling effect by vegetation.

2. How does shade affect soil moisture on the biosolar roof, and how does that compare to the green roof?

PV shade notably enhanced soil moisture retention compared to the unshaded areas of the green roof module. Under manual irrigation (dry season), although water concentration was higher in the non-shaded area of the biosolar roof due to runoff from PV panel cleaning, the shaded area of the biosolar roof retained soil moisture for a longer duration than the green roof that was fully exposed to solar radiation. During the rainy season, the shaded biosolar area showed the lowest average soil moisture because the PV canopy partially intercepted precipitation. In contrast, the fully exposed green roof, without any overhead structure, recorded higher soil moisture levels—an observation consistent with Jahanfar et al., (2019). This suggests that while PV shading enhances soil moisture persistence during dry periods, it may hinder evenly distributed soil moisture recharge during rainfall. Although all modules had identical French drain systems, the presence of PV structure may have affected more on how rainwater was retributed within each bed. These findings highlight the need for adaptive design strategies, such as adopting a checkerboard PV pattern or integrating shallow trays to help distribute rainwater more evenly beneath the

panels.

3. How does the air temperature near the vegetation differ across shaded and unshaded parts of the biosolar roof—and compared to the air temperature on PV, green, and concrete roof?

Air temperature measurements clearly showed that the shaded areas of the biosolar roof consistently maintained 1–2 °C lower temperatures than the unshaded areas. The biosolar roof's shaded area recorded the lowest near-surface air temperature among all roof types. In contrast, the concrete roof consistently showed the highest temperatures. The PV roof also showed notable cooling performance, emphasizing that PV shade plays a significant role in cooling the near-surface microclimate. This trend—where shading provides a greater cooling effect than vegetation alone—aligns with the ENVI-met simulation results presented in Chapters 2 and 3.

4. How do surface temperatures vary between the five roof types: biosolar, green, PV, concrete, and the one with reflective film?

Surface temperature data revealed distinct thermal behaviors across the five roofs. Concrete surfaces showed the highest peak temperatures and largest fluctuations, supporting their contribution to increased building cooling loads in Chapter 3. The green roof module and Reflective film roofs maintained the stable fluctuations of surface temperatures due to high albedo. Biosolar roofs had slightly elevated temperatures probably due to disparity in sensor location and exposure to adjacent hotter concrete surfaces, highlighting the influence of micro-site conditions on thermal performance.

5. Can bifacial solar panels facing east and west help produce more energy during the early morning and late afternoon? And does covering reflective film under the module improve that effect?

The analysis conclusively showed bifacial PV panels positioned over reflective films significantly improved solar energy production, especially. Specifically, average daily yields improved by approximately 14.8%, between April 12 and 15, 2025, with increased gains during morning and afternoon hours. This proves that reflective surfaces under bifacial modules can enhance albedo-driven irradiance,

which aligns with the previous empirical findings by Katsikogiannis et al., (2022).

Rethinking Solar PV Panel Orientation for Grid Balance and Seasonal Stability

This study revealed that East–West facing bifacial PV panels can serve as a promising strategy to flatten solar generation curves and address the so-called “duck curve,” where electricity supply peaks at midday but dips during high-demand morning and evening hours, as shown in the scatter plot in Figure 4.13. Unlike conventional south-facing arrays, east–west bifacial modules distribute energy production more evenly throughout the day, especially improving yield during early morning and late afternoon hours when standard panels underperform. Prior findings from Germany support this pattern (Katsikogiannis et al., 2022), confirming that east–west bifacial installations can match south-facing performance during these critical off-peak windows.

These modules are also particularly well-suited for higher-latitude regions where low solar angles and snowfall challenge conventional PV systems as Figure 4.13. By capturing sunlight on both front and rear surfaces, bifacial designs reduce shading and snow accumulation impacts, offering greater seasonal consistency in output. Together, these benefits suggest east–west facing bifacial PVs as a climate-responsive alternative for rooftop solar, particularly in cities facing winter performance constraints or growing demands for grid resilience.

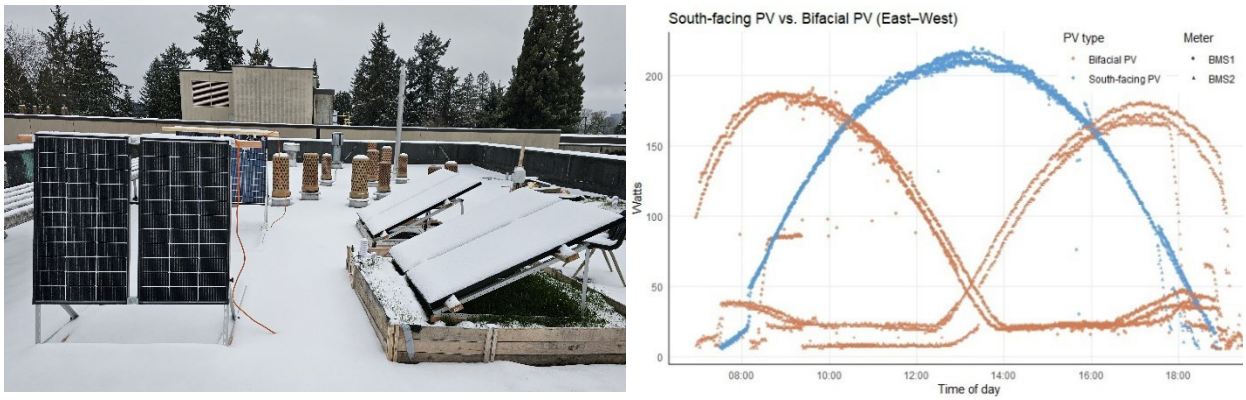


Figure 4.13 (Right) Advantage of bifacial panels in mitigating snow accumulation compared to tilted modules, and (Left) Scatter plot showing daily accumulated solar yield for bifacial PV panels (east–west facing) and conventional PV panels (south-facing tilt)

However, this study utilized a single configuration of bifacial modules in terms of height, tilt angle, and spacing. Given the significant impact these variables can have on solar yield, microclimate conditions, and overall biosolar roof performance, future investigations should systematically vary these parameters to identify optimal design configurations tailored to specific climatic conditions.

Biosolar Roof's Multiple Benefits in Improving Rooftop Microclimates

Despite the lack of strong statistical correlations between PV efficiency and environmental variables such as wind speed or humidity, the field data consistently demonstrated that biosolar roofs reduced rooftop temperatures more effectively than standalone green or PV roofs. This performance advantage was most apparent in the shaded area of the biosolar modules, where PV shade and vegetation-driven evapotranspiration happen together. This combined cooling effect was especially represented under hot and dry climatic conditions, as shown in Chapter 3, suggesting potential that biosolar roofs can effectively mitigate rooftop heat in cities facing severe Urban Heat Island Effect challenges. Although this experiment was conducted during a relatively moderate season and did not fully cover extreme hot-weather conditions, the biosolar roof is still expected to deliver strong and spatially consistent cooling effects across different rooftop areas. Also, the result of surface temperature measurements suggests that integrating high-albedo materials into urban roofing strategies could play a pivotal role in mitigating urban heat islands, consequently decreasing cooling energy demands and enhancing urban resilience during extreme heat events.

Another notable finding from this chapter is the significant influence of PV panel geometry on soil moisture distribution. During manual irrigation and panel cleaning, runoff from the PV panels tended to concentrate in areas directly beneath the lower edges of PV panel—specifically, the non-shaded areas of the biosolar module in this study. This uneven redistribution highlights the importance of considering how PV geometry affects soil moisture patterns. Future biosolar roof designs should integrate runoff management strategies in relation to vegetation patterns that address this spatial variability to optimize irrigation efficiency and promote water conservation. For example, adopting a checkerboard PV pattern

may help distribute runoff more evenly by allowing water to fall between panel rows rather than concentrating along continuous edges. Additionally, incorporating shallow trays or zigzag runoff guides beneath the panels could help diffuse concentrated flows and enhance irrigation efficiency.

Limitations and Future Research Directions

The field experiment in this chapter were constrained by their relatively small scale and seasonal context[9]. Future studies should consider these experimental frameworks across seasons and diverse climatic zones to better understand local meteorological influences on biosolar roof performance. In particular, scaling up vegetation plot size under PV panels would enable more realistic simulation of large-scale rooftop systems and improve the accuracy of energy and moisture performance assessments. Comprehensive, full-rooftop scale comparative assessments could further validate and extend current findings, ultimately guiding robust and data-driven strategies for sustainable rooftop design.

The small size of the modules was also limited to monitoring the biodiversity and habitat values of biosolar roofs. The close adjacency of modules—not as each independent rooftop scale—may have restricted reliable comparisons regarding plant species diversity, insect and bird presence frequency. Therefore, future research should implement larger-scale biosolar roof experiments to comprehensively evaluate their potential contributions to urban biodiversity and habitat quality.

Sensor Placement and Experimental Controls: Methodological Insights

The observed differences between surface temperature measurements on biosolar and green roofs emphasized the critical importance of precise sensor placement and controlled experimental conditions. Even minor variations in sensor location significantly impacted temperature readings, illustrating

[9] Although October is not as hot as summer, there were a couple of relatively hot days in early October.

microclimatic variability within small rooftop areas. Future research should implement rigorous sensor positioning protocols, using more sensors, and consider larger-scale setups to mitigate localized microclimate biases and improve result reliability and generalizability.

Microclimatic and Diffuse Radiation Influences on PV Yield Variability

Irregular patterns in PV yield measurements were represented, and it seems that substantial complexities are associated with outdoor experimental conditions, notably driven by indirect (diffuse) solar radiation influenced by surrounding structures. The persistence of unexplained fluctuations despite module repositioning highlights the need for systematically accounting for diffuse contextual radiation in future experimental designs. Incorporating advanced radiation measurement equipment or additional diffuse irradiance sensors could enhance the accuracy of PV yield predictions. This would ensure more reliable data interpretation and improved understanding of environmental influences on PV performance.

5. Conclusion

In conclusion, this chapter demonstrates the transformative potential of biosolar roofs as multifunctional urban infrastructure. By integrating energy generation, microclimate regulation, and water management within a single rooftop, biosolar roofs can offer a compelling pathway toward climate-adaptive, resource-efficient cities. As urban populations grow and climate extremes intensify, rooftops—once passive, underutilized surfaces—can be reimagined as a place for climate resilience. Moving forward, scaling up such integrated solutions will require not only refined technical design but also stronger policy frameworks and interdisciplinary collaboration. Biosolar roofs are not just a design intervention, they could be a paradigm shift in how cities harness underutilized space for a more sustainable future.

References

Abdalazeem, M. E., Hassan, H., Asawa, T., & Mahmoud, H. (2022). Review on integrated photovoltaic-green roof solutions on urban and energy-efficient buildings in hot climate. *Sustainable Cities and Society*, *82*(April), 103919. https://doi.org/10.1016/j.scs.2022.103919

Bousselot, J., Slabe, T., Klett, J., & Koski, R. (2017). Photovoltaic Array Influences the Growth of Green Roof Plants. *Journal of Living Architecture*, *4*(3), 9–18. https://doi.org/10.46534/jliv.2017.04.03.009

Cao, Z., Gao, W., Fu, Y., & Mi, C. (2024). Wireless Battery Management Systems: Innovations, Challenges, and Future Perspectives. *Energies* , *17*(13). https://doi.org/10.3390/en17133277

Cool, M., Hannaway, D. B., Larson, C., & Myers, D. (2004). Perennial ryegrass (Lolium perenne L.). *Forage Fact Sheet. Oregon, USA: Oregon State University*.

Hindi, I., Alyaman, M., AboZenah, A., Zaid, A., & Shrara, M. (2024). Smart Alarm IoT System: Monitoring Elevator Traffic and Meteorological Data on Job Sites Using MQTT and InfluxDB integrated with Grafana. *2024 15th International Conference on Information and Communication Systems, ICICS 2024*, 1–6. https://doi.org/10.1109/ICICS63486.2024.10638309

Jahanfar, A., Drake, J., Sleep, B., & Margolis, L. (2019). Evaluating the shading effect of photovoltaic panels on green roof discharge reduction and plant growth. *Journal of Hydrology*, *568*(October 2018), 919–928. https://doi.org/10.1016/j.jhydrol.2018.11.019

Katsikogiannis, O. A., Ziar, H., & Isabella, O. (2022). Integration of bifacial photovoltaics in agrivoltaic systems: A synergistic design approach. *Applied Energy*, *309*(January), 118475. https://doi.org/10.1016/j.apenergy.2021.118475

Kishore Kumar, K., Rishi Kanth, N., Rasidhar, L., & Srinath, A. (2021). Design of real time efficient sun tracking system for smart irrigation using raspberry pi. *International Journal of Systems Assurance Engineering and Management*. https://doi.org/10.1007/s13198-021-01383-6

Koehler, M. (2023). Extensive Green Roof Study on a Retrofit Building in Berlin, Germany: Report After 34 Years of Monitoring. *Journal of Living Architecture*, *10*(1), 1–12. https://doi.org/10.46534/jliv.2023.10.01.001

Lamnatou, C., & Chemisana, D. (2015). A critical analysis of factors affecting photovoltaic-green roof performance. *Renewable and Sustainable Energy Reviews*, *43*, 264–280. https://doi.org/10.1016/j.rser.2014.11.048

Talwar, P., Verma, N., Khatri, H., Ahire, P. D., Chaudhary, G., Lindenberger, C., & Vivekanand, V. (2023). A systematic review of photovoltaic-green roof systems in different climatic conditions focusing on sustainable cities and societies. *Sustainable Cities and Society*, *98*(July), 104813. https://doi.org/10.1016/j.scs.2023.104813

Upton, E., & Halfacree, G. (2012). *Meet the raspberry Pi*. John Wiley & Sons.

Yusufoglu, U. A., Lee, T. H., Pletzer, T. M., Halm, A., Koduvelikulathu, L. J., Comparotto, C., Kopecek, R., & Kurz, H. (2014). Simulation of energy production by bifacial modules with revision of ground reflection. *Energy Procedia*, *55*, 389–395. https://doi.org/10.1016/j.egypro.2014.08.111

Zluwa, I., & Pitha, U. (2021). The combination of building greenery and photovoltaic energy production—a discussion of challenges and opportunities in design. *Sustainability (Switzerland)*, *13*(3), 1–29. https://doi.org/10.3390/su13031537

DISSERTATION CONCLUSION

This dissertation comprehensively investigated the environmental performance of biosolar roofs through a combination of simulation, parametric modeling, and field validation. By integrating vegetation and photovoltaic systems within the same rooftop footprint, biosolar roofs offer promising multifunctional benefits—ranging from microclimate cooling and stormwater retention to solar energy generation and building energy savings.

Chapter 1 presented a comprehensive review of the multifunctional benefits, practical challenges, and key design parameters of biosolar roofs. It also highlighted the fragmented nature of existing research and the lack of standardized design or planning guidelines of biosolar roofs. This chapter also highlighted the fragmented nature of current research and the lack of standardized design or planning guidelines. Chapter 2 explored how different combinations of design parameters—PV height, density, configuration, and planting density—affect rooftop cooling performance. Simulation results, supported by field validation, emphasized the complex interplay between PV shade, evapotranspiration, and airflow. Chapter 3 expanded the evaluation across three climate zones—Eugene (marine), Tucson (hot and arid), and Buffalo (cold and humid)—and demonstrated how biosolar roof performance varies depending on environmental context. The findings showed that vegetation-driven cooling is most effective in humid climates, while PV shading plays a larger role in dry regions. Stormwater retention was also shaped by PV-induced drip-line runoff dynamics. Chapter 4 validated these findings through a field experiment, confirming that carefully optimized biosolar designs can reduce rooftop temperatures, improve soil moisture persistence and solar yields under real-world conditions.

From a performance-centric design perspective, biosolar roofs do not passively deliver multifunctional benefits; rather, their multifunctional benefits hinges on how deliberately the system is designed in response to local environmental conditions and functional goals. A key insight from this study is that

trade-offs are inherently tied to climate context. For example, in temperate, marine climates like Eugene where solar availability is moderate and rainfall is relatively consistent throughout the winter, biosolar roofs benefit from a balanced design approach. Moderate PV coverage can provide sufficient shading to support microclimate cooling without overly limiting solar access for vegetation. Given the region's milder winters and less extreme sun angles, PV systems facing south may perform adequately, while maintaining good plant health under partial shade. Additionally, selecting plant species adapted to persistent moisture and moderate light levels can further enhance stormwater retention and vegetation resilience throughout the seasons.

In hot, arid climates like Tucson, where intense solar radiation and minimal precipitation dominate, the cooling and water-retention functions of biosolar roofs face critical limitations. Vegetation under these conditions is more vulnerable to desiccation due to low humidity and high evapotranspiration demand. Therefore, biosolar roof designs in Tucson may prioritize maximizing PV shading to reduce direct solar exposure on planting beds, using dense panel arrays and taller mounting structures. Pairing PV arrays with drought-tolerant, shade-adapted species—especially those capable of surviving under limited irrigation and shade—can help maintain vegetation health while reinforcing passive cooling. Additionally, integrated irrigation systems or runoff redistribution (underneath PV) strategies may be essential to compensate for the lack of natural moisture input and to ensure long-term system viability.

In contrast, cold-humid cities like Buffalo experience long winters, frequent precipitation, and low sun angles due to their higher latitude. Under these conditions, vegetation-driven insulation becomes a crucial asset for reducing building heat loss. At the same time, rooftops must be capable of managing substantial snowmelt and rainfall. To ensure sufficient solar exposure for vegetation during short, low-sunlight days, designs may require reduced PV density and strategic spacing. In such contexts, bifacial PV panels facing east–west may be particularly well suited, as they can capture diffuse and reflected light during off-peak hours, helping maintain energy production despite seasonal variation in solar intensity.

At a broader planning scale, a more context-driven framework is essential—one that accommodates site-specific conditions and balances multiple priorities. Urban rooftops today are demanded to serve many roles: providing ecological value, energy generation, spaces for socializing, and resilience to climate stress—while all of them complying with structural limitations and safety codes. Therefore, the most effective biosolar roof may be not a fixed typology, but a flexible system configured around place-based goals, environmental conditions, and end-user needs.

A useful first step in strategic biosolar design is to distinguish whether a rooftop is accessible to people. Human access can serve as a clear indicator estimating the functional context and spatial expectations placed on the rooftop. First, publicly accessible rooftops—such as residential or semi-public spaces—may prioritize social interaction, visual quality or what residents demand. Several real-world examples feature pergolas with PV modules installed overhead while supporting climbing vegetation on vertical trellises. These configurations can offer co-benefits, such as ecosystem services and on-site energy production. However, the physical separation between panels and planting beds may limit the synergistic gains in soil moisture retention and PV efficiency. In contrast, service-only rooftops—those accessed primarily for maintenance—may allow for more performance-driven layouts, where design strategies can be optimized based on specific climatic conditions. This rooftop distinction would offer a practical lens for tailoring biosolar roof applications—not only to meet the environmental performance goals of individual rooftops, but also to inform broader, place-based planning at the urban scale.

In conclusion, this dissertation contributes a performance-based, climate-responsive framework for biosolar roof design—bridging environmental simulation, empirical validation, and rooftop programming to support adaptable, resilient strategies for sustainable urban futures.